Modification of Novel Portland Based Cement For Orthopaedic Application

by

Amirpasha Moetazedian

A thesis submitted to the University of Birmingham

for the degree of Master of Science by Research

Biomaterials Units

School of Dentistry

University of Birmingham

May 2018

Abstract

Portland cement (PC) is a ceramic hydraulic cement which has been used in construction for decades and more recently for dental applications. PCs possess high durability and compressive strength and demonstrate good biological responses, that are generating interest as a potential material for orthopaedic applications. The present study investigated the addition of porogens to induce large macropores e.g. >100 μm to promote potential bone ingrowth, whilst retaining appropriate mechanical and physical properties for vertebroplasty used to stabilise fractured vertebral bodies.

The cements containing 20 wt% bismuth oxide (radiopacifying agent) and 5 wt% calcium chloride (setting accelerant) were prepared using a range of powder-to-liquid ratios and porogens (including mannitol, sucrose and sodium bicarbonate or foaming agents) were added from 1-20 wt% to induce macroporosity either after or during setting of the cement. Increasing the concentration of sugars increased the initial setting time 3-fold, whilst causing the cement paste to behave as a liquid. The compressive strengths of modified cements were reduced by up to 90 % after 7 days of storage through increasing flaws and porosity. The macrostructural analysis using scanning electron microscopy (SEM) showed no major difference between the modified cements and controls.

10 wt% foamed gelatine (FG) was found to improve the viscosity of the paste so that it was readily injectable, and demonstrated sufficient cohesion after injection. FG

doubled the setting time approximately and generated large interconnected pores ranging from 100-400 μm in diameter according to SEM images. The compressive strengths of foamed cements were sufficiently high after 7 and 30 days of storage to stabilise fractured vertebral bodies.

The addition of 10 wt% FG has shown the potential to modify PC by inducing large pores, whilst maintaining high injectability and compressive strength, which warrants further testing for clinical application in verterbroplasty.

Acknowledgments

Foremost I would like to thank my incredible supervisors, Dr. Mike Hofmann and Dr. Dick Shelton for all their valuable guidance, support and patience throughout this invaluable experience.

I would like to show my appreciation to Patricia Andreu Cabedo at School of Chemical Engineering, University of Birmingham for her assistance with mercury intrusion porosimetry. I would like to particularly thank Behnam Dashtbozorg, James Alexander and Yana Liang at School of Metallurgy and Materials, University of Birmingham with their support.

My heartfelt gratitude to all my colleagues at School of Dentistry, especially Dr. Nina Vyas, Cleo White, Samir Hamidi and Naveed Saeed for their help. I would like to acknowledge all the lab technician at School of Dentistry.

I am truly grateful to my family and friends for their comfort, encouragement and love, particularly my brother Dr. Reza Moetazedian for his support and motivation throughout my life.

Abbreviations

ATR **A**ttenuated **T**otal **R**eflectance

BMD **B**one **M**ineral **D**ensity

C-A-H **C**alcium **A**luminate **H**ydrate

CMC **C**ritical **M**icelle **C**oncentration

CPCs **C**alcium **P**hosphate **C**ements

C-S-H **C**alcium **S**ilicte **H**ydrate

DW **D**istilled **W**ater

EDS **E**nergy **D**ispersive X-ray **S**pectroscopy

FCS **F**oetal **C**alf **S**erum

FDA **F**ederal **D**rug **A**dministration

FG **F**oamed **G**elatine

FP **F**oamed **P**olysorbate 80

FTIR **F**ourier **T**ransform **I**nfrared spectroscopy

FWHM **F**ull **W**idth **H**alf **M**aximum

HA **H**ydroxyapatite

KP **K**yphoplasty

MIP **M**ercury **I**ntrusion **P**orosimetry

MMA **M**ethyl **M**ethacrylate

MW **M**olecular **W**eight

NS **N**on **S**ignificant

OP **O**steoporosis

OVCFs **O**steoporotic **V**ertebral body **C**ompression **F**ractures

PBS **P**hosphate **B**uffer **S**aline

PC **P**ortland cement

PLR **P**owder to **L**iquid **R**atio

PMMA **P**oly **M**ethyl **M**ethacrylate

PVP **P**ercutaneous **V**ertebroplasty

SBF **S**imulated **B**ody **F**luids

SD **S**tandard **D**eviation

VCFs **V**ertebral **C**ompression **F**ractures

WPC **W**hite **P**ortland **C**ement

Wt **W**eight

XRD **X**-**R**ay **D**iffraction

Contents

List of Figures

List of Tables

Chapter 1

Introduction

1.1 Project background

Biomaterials play an important role in medicine due to the limitations of allografts and autografts including the requirement for a secondary surgery, limited supply, morbidity risk, infection and disease transmission [1, 2]. A biomaterial has been defined as "a non-viable material which is used and intended to interact with biological system in medical devices for augmentation or replacement of any tissue, organ or function of the body" [1, 2].

Bone is a composite living tissue which serves as a mechanical support for the body [3, 4]. Throughout its life, bone undergoes constant remodelling as it is subjected to physiological and mechanical stresses [3, 4]. Bone defects may still occur as a result of trauma, or bone disease e.g. osteoporosis (OP) or cancer. This can give rise to a loss of normal bone function and ultimately bone fracture, which in the spine can cause vertebral compression fractures (VCFs) [5, 6]. VCFs are the most common fractures experienced by patients with OP and the highest annual incidence of fractures is reported to be 700,000 and 120,000 in the USA and UK respectively [7, 8, 9].

Percutaneous vertebroplasty (PVP) is a common minimally invasive surgical technique used to treat patients with fractured vertebral bodies [6, 7, 8]. The main goal of PVP is to stabilise the bone defect by injection of a bone cement [6, 10]. Therefore, the ideal bone cement should possess high injectability for insertion, generate an appropriate biological response, adequate mechanical properties and a reasonably short setting time which facilitates placement but does not require extended operating theatre time [6, 10].

A common bone cement used for PVP is based on an acrylic cement known as polymethylmethacrylate (PMMA), which is the most widely used biomaterial for fixation of prostheses and filling bony cavities [6, 10]. However, PMMA has various limitations including thermal tissue necrosis due to its exothermic polymerisation reaction, lack of bone anchorage and monomer toxicity [10, 11]. Another cement of interest is calcium phosphate cements (CPCs) that have demonstrated excellent biological properties but poor mechanical properties, limiting potential use for PVP [6].

Portland cement (PC) is a ceramic cement which has been used extensively in the construction industry [12, 6]. While in dentistry, PC is the major component of mineral trioxide aggregate (MTA) which is an endodontic cement [12]. There is great interest in using PC-based cements for PVP applications due to good durability, high compressive strength and are capable of setting in *in vivo* environment and have exhibited appropriate biological responses [5, 6].

In a recent study, a novel PC was developed by the addition of liquefying agents and accelerants to PC, so that it was injectable, set within 20 min and possessed sufficient

compressive strength [13, 14]. There are still challenges which need to be addressed to make this novel PC a viable substitute to PMMA. It would be desirable to have a porous interconnected structure to allow cell infiltration and a framework for the subsequent bone ingrowth, whilst providing sufficient strength for the vertebral body [15, 16]. Hence, a range of available techniques to introduce porosity was selected from the literature for the present study.

1.2 Overview of the skeletal system

The skeletal system is composed of 206 bones along with joints and cartilages which has several essential functions such as [3, 6, 17]:

- **Support:** serves as a structural framework and supporting soft tissues.
- **Protection:** protects internal organs such as the spinal cord.
- **Locomotion:** the majority of skeletal muscles are connected to bone to assist in movement.
- **Homeostasis:** reservoir for calcium to improve the strength of bone.

Bone is composed of 50-70 wt% mineral phase, 20-40 wt% organic phase and the remaining is water and lipids [3, 4, 18]. The main constituent of the organic phase is type I collagen fibres positioned in different orientations to form a lamellar structure [3, 4]. The mineral phase is hydroxyapatite (HA) which is found within the framework formed

by collagen fibres and ground substance [3, 4]. As the mineral crystals deposit within the organic collagen matrix there is substitution over time with other salts and ions such as calcium carbonate, magnesium and potassium [3, 17, 19]. Therefore, the combination of the mineral and organic phases are responsible for the properties of bone [3, 4, 18].

Two types of bone either cortical or cancellous define the function and structure present [4]. Approximately 90 % of cortical bone is mineralised providing sufficient resistance to various stresses arising from support of weight and movement [3, 4, 17, 19]. In contrast, cancellous bone contains a honeycomb-like arrangement of rods and trabecular plates with only 20 % mineralised tissue, which reduces the overall weight of bone [3, 4, 17, 19]. At the same time, this porous structure gives cancellous bone eight times greater surface-to-volume ratio compared with cortical bone as shown in Figure 1.1 [3, 4, 17, 19].

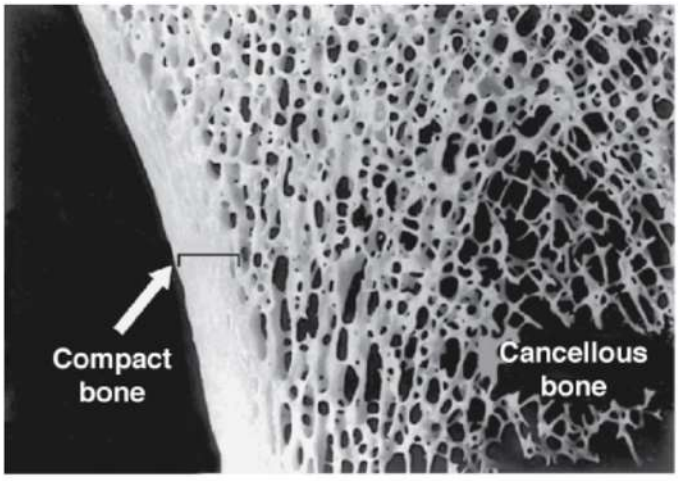

Figure 1.1: Cross section of dried bone indicating the cortical and porous cancellous bone [20].

1.2.1 Mechanical properties of bone

The structure of bone is complex and anisotropic, hence determining the exact values for the mechanical properties of bone is difficult [3, 21]. Nevertheless, a wide range of values have been presented in the literature (Table 1.1) [6, 15, 22]. It is crucial to note that the strength of bone is dependent on bone type, composition, age and gender etc [3, 19].

Table 1.1: General mechanical properties of cortical and cancellous bones [3].

Bone property	**Range**
• **Cortical bone**	
Compressive strength (MPa)	130-230
Elastic modulus (GPa)	15-35
Tensile strength (MPa)	90-190
• **Cancellous bone**	
Compressive strength (MPa)	2-9
Elastic modulus (GPa)	0.1-3.5

1.3 Vertebral column

The vertebral column consists of 26 structural units called vertebra which protect the spinal cord and provide support of the head whilst also allowing a range of movements [4, 5]. The vertebrae typically consist of 75 % cancellous bone and 25 % cortical bone

[4]. The vertebral column is divided into five regions: cervical, thoracic, lumbar, sacrum and coccyx as shown in Figure 1.2 [4, 19]. Although vertebrae vary in shape, size and function, there are a number of shared features, including a vertebral body and arch, processes and pedicles (Figure 1.2 b) [4]. One of the most important parts of the vertebra is the vertebral body which is the disc-shaped anterior portion, made of a thick cancellous bone and a thin layer of cortical bone to form a porous, yet strong structure to withstand loading [15, 23, 19].

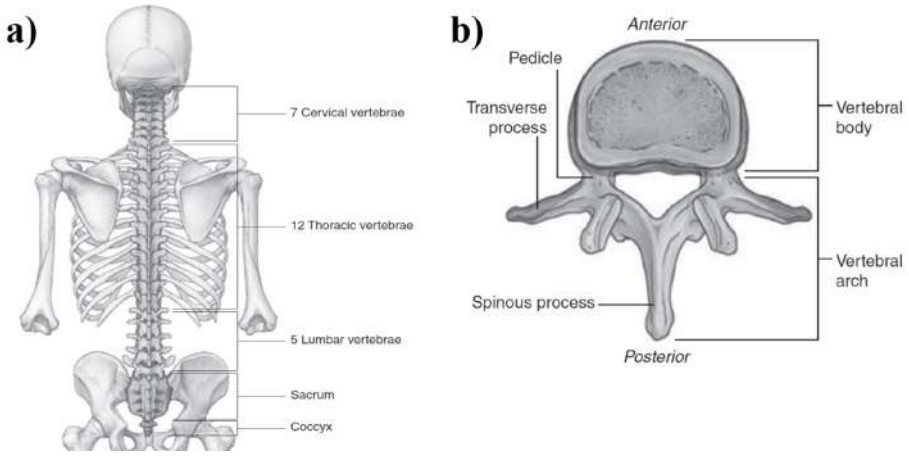

Figure 1.2: a) Posterior view of the body showing vertebral column divisions. **b)** the typical features of a vertebra [23].

1.3.1 Vertebral compression fractures

Impairment of bone function may occur from trauma caused by an accident or bone disease, which is now emerging as one of the main public health issues especially within

the elderly [8, 24, 25, 26]. The result of bone disease is bone structure deterioration, which leads to fracture. The most common aetiology of VCFs has been reported as age related osteoporotic vertebral compression fractures (OVCFs), which are associated with sudden back pain [7, 8].

OP is "an ongoing systemic skeletal disease associated with diminished bone mineral density (BMD) and alteration of bone microarchitecture" [7, 21, 18]. The main result of OP is a substantial reduction in bone strength as the weakened bone cannot withstand the mechanical demands placed upon it [6, 7]. OP affects a large proportion of women (4 out of 10) due to oestrogen deficiency and it has been estimated that by 2020, the prevalence of OVCFs will be increased by 50 % [26, 27]. The incidence of VCFs is generally higher for women than men as shown in the Figure 1.3 [26, 28, 29].

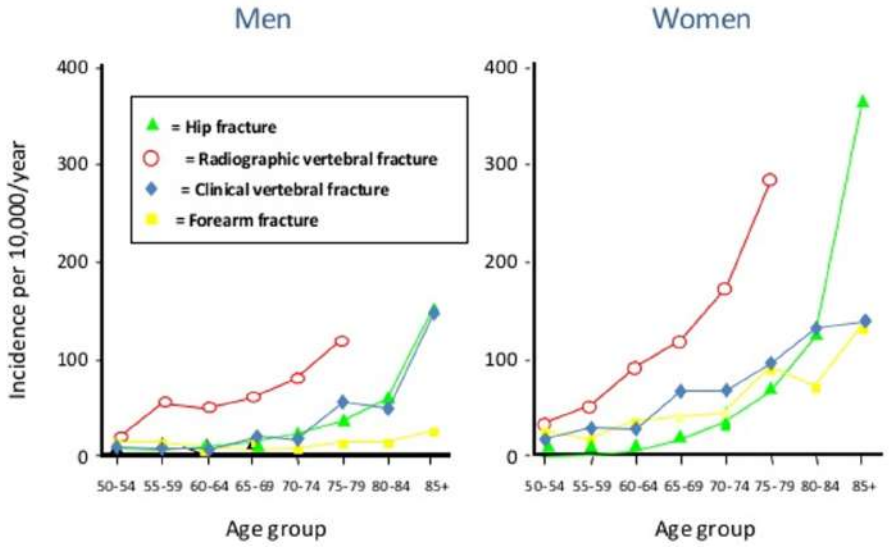

Figure 1.3: Vertebral fracture incidence is relatively higher for women more than 60 years old compared with men [30].

1.4 Percutaneous vertebroplasty (PVP) and kyphoplasty (KP)

The typical treatment for VFCs is bed-rest, while in severe cases; plaster casts, back braces and spinal fusion are all available options [28, 29]. There are a number of complications associated with these methods including expensive procedures, risk of infection and high blood loss etc [27, 28, 29].

In 1987, Galibert *et al.* introduced a new minimally invasive technique called PVP as an alternative treatment for those with VCFs [6, 31]. It was shown that PVP improves a patient's quality of life by stabilising the weakened vertebral bodies as much as possible to the functional vertebra [10]. Whilst, KP restores the height lost by resorbing vertebrae by inflating a balloon within the vertebral column followed by stabilisation of the vertebral body with bone cement [6, 10, 27].

The PVP procedure is generally performed under imaging guidance such as C-arm fluoroscopy or in combination with computational tomography guidance to obtain fine images [6]. During the surgery, the patient will be asked to lie in a prone position on the X-ray table whilst sedated. Administration of local anaesthetic would reduce the possible pain during the time of surgery [6, 32, 33]. It is generally preferred to assess needle insertion and cement injection via anterioposterior and lateral radiographic guidance, while the patient is stationary. The vertebral body is held in place by the insertion of Kirschner wires through paraspinal muscle and pedicles [26, 32, 34, 35]. Afterwards, the surgeon

inserts a bore needle (10-15-gauge) in the anterior third of the vertebral body up to the mid-line. The bone cement is mixed and prepared to be injected immediately whilst using live fluoroscopy to avoid any damage to the spinal column as shown in Figure 1.4 [26, 32]. The PVP procedure typically takes 1 h, but it may take longer if there are multiple fractures. Patients will be required to stay in hospital for 6 h to be monitored before being discharged [6, 10, 36].

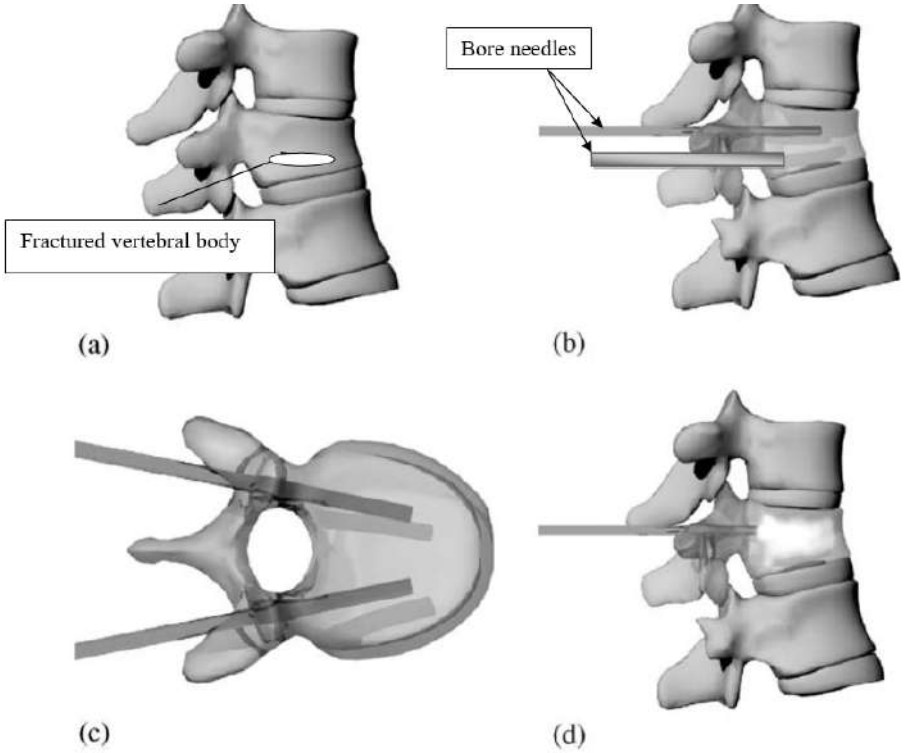

Figure 1.4: Diagram summarising the vertebroplasty procedure: **a)** fractured vertebral body, **b)** insertion of bore needle into the target site, **c)** and **d)** injection of bone cement [6, 37].

1.5 Ideal bone cement for PVP

Bone cements play a key role in the clinical outcome of PVP and there has been widespread research and developments to exploit different types of biomaterials for PVP. The most crucial physical and mechanical characteristics of bone cements are summarised as below [10, 38, 39, 40]:

(i) **Mechanical properties**: bone cement should ideally possess high durability and mechanical properties as close as possible to that of healthy bone for example, compressive strength [10].

(ii) **Setting time**: the optimum setting time for PVP is normally stated to be approximately 20 min [10].

(iii) **Injectability**: if cement cannot be injected to the target site, it will have a significant impact on the clinical outcome of PVP. The materials consistency should not lead to a phenomenon called phase-separation during the injection period. Phase-separation occurs when the liquid phase is extruded and leaves the majority of the solid phase inside the syringe during the injection, affecting cement integrity [38].

(iv) **High radiopacity**: during surgery, live imaging is always used to allow the surgeon to correctly insert the needle into the target site, while preventing any cement from leaking into the surrounding tissues. It is highly desirable for bone cement to contain a radiopacifying agent [6, 10].

In addition to the requirements for physical properties, the ideal bone cement should also fulfil biological properties to prevent the occurrence of complications during tissue-biomaterials interactions which involves a cascade of inflammatory and wound healing responses [10, 38].

(i) **Bioactivity**: this property is stated as "demonstrating a particular biological response by the formation of a direct chemical bond between tissue and material" [1, 2]. Illustrating this property would allow a faster bone integration at the surface of the biomaterial [2].

(ii) **Osteoinductivity**: "capability of inducing pluripotent stem cell differentiation into osteoblastic phenotype" [41].

(iii) **Osteoconductivity**: "providing a receptive scaffold for bone growth on its surface" [41].

(iv) **Porosity**: a porous cement with sufficient interconnectivity would provide the suitable framework for fluid transport and bone ingrowth [3].

1.6 Current orthopaedic bone cements

1.6.1 Poly methylmethacrylate (PMMA) cement

PMMA has been used as the filler material for many orthopaedic applications. PMMA was first used for cranioplasty in monkeys in late 1930s [6, 42]. This material is generated

by mixing the powder and liquid phases together to initiate the polymerisation reactions [42]. The powder phase consists of pre-polymers, methylmethacrylate (MMA) copolymers, barium sulphate as a radiopacifying agent and benzoyl peroxide to generate free radicals for the polymerisation reaction [38]. The liquid phase contains MMA, hydroquinone as a stabiliser and N,N-dimethyl-p-toluidine as an accelerator to allow polymerisation at room temperature [43].

One of the main reasons for choosing PMMA for PVP applications, was its successful history in total hip replacement performed by Sir John Charnley in 1960, through demonstrating desirable properties including: high injectability, ease of handling, low cost, high radiopacity and high strength of 80 MPa, which enables early stabilisation of the fractured vertebral body which leads to immediate pain relief for the patient [43, 44].

1.6.1.1 Possible complications associated with PMMA

The exothermic polymerisation reaction of PMMA has been reported to reach up to 75 ^{o}C after injecting within human cadavers and could lead to thermal tissue necrosis [45, 46]. The high temperature of polymerisation could also limit the incorporation of antibiotics and growth factors, due to the risk of denaturation [6, 10, 45, 46]. Leaking of MMA monomer into surrounding tissues has been shown to cause osteoblast necrosis, osteocyte damage and blockage of blood arteries e.g. pulmonary embolisms which are highly undesirable [42, 47, 48].

PMMA has been demonstrated to be an inert material with no bone integration on its

surface [6, 45]. Alternatively, a fibrous tissue is formed around the material, isolating it from the surrounding tissue which may result in bone cement fracture [6, 45]. There is a great risk of cracks and dislodging of PMMA for younger patients due to a higher elastic modulus of the PMMA compared with healthy bone which results in a secondary fracture [49].

1.6.2 Calcium phosphate cement (CPCs)

CPCs are another type of bone cement which have been used for bone defect repair since the 1920s [3, 50]. Brown and Chow developed the first self-setting CPC system from tetracalcium phosphate and dicalcium phosphate dihydrate, which was injectable and hardened *in vivo* [22, 50]. After CPCs were approved by the FDA for medical use, widespread research on this material was carried out to produce other calcium phosphate containing compounds [50, 51]. The setting chemistry of CPC is based on dissolution-precipitation. However, the end-product primarily depends on the setting pH; thus, CPCs are separated into two groups of hydroxyapatite for pH > 4.2, and acidic CPC i.e. brushite when pH is < 4.2 [52, 53].

CPCs have a similar chemical composition to the mineral phase of bone, demonstrate osteoconductivity, have sufficient porosity and set isothermally [54]. However, CPCs are resorbable and do not possess high durability [52, 53]. Additionally, acidic CPCs have poor mechanical strength and injectability, which limits their application for PVP [53, 55, 56].

1.7 Introduction of Portland cement (PC)

PC has the potential to replace PMMA for load-bearing applications and it is classified as a hydraulic cement; which means that water is required to start the setting reaction and hardening mechanisms [5, 12]. The main raw materials of PC consist of 60-75 wt% calcium oxide (CaO), 10-25 wt% silicon dioxide (SiO_2), 2-10 wt% of alumina (Al_2O_3) and 3-8 wt% iron (III) oxide (Fe_2O_3) [57, 58]. The raw materials are crushed and fired together in a rotary kiln at 1500-1600 ^oC causing fusion and forming nodules (clinker) [12, 59]. Calcium sulphate dihydrate (gypsum) will be then added at 5 wt% for controlling the reactivity of clinkers [5]. Depending on the final constituents and the fineness of PC powder, it can be divided into different types: I, II, III, IV, V and white PC (WPC) [12, 60, 59].

1.7.1 Hydration of PC-based cements

PC is predominately composed of four anhydrous clinkers: 50-75 wt% tricalcium silicate or alite, 4-30 wt% dicalcium silicate or belite, 7-10 wt% of tricalcium aluminate and 5-15 wt% tetracalcium aluminoferrite [13, 58]. The dissolution of clinkers occurs at different times and rates according to the reactivity of the individual phase, therefore, a better understanding of PC hydration can be achieved by characterising the roles of each clinker in the hydration mechanism [59, 61].

1.7.1.1 Hydration of alite and belite

On contact of water with the powder phase, the alite and aluminate will immediately begin to hydrate due to their higher reactivities compared with the other clinkers [6, 59]. Rapid dissolution of calcium and silicate ions causes a reaction with water to form a porous calcium silicate hydrate (C-S-H) layer (Equation 1.1) with more than 20 polymeric forms [60, 62].

$$2(3CaO.SiO_2) + 11H_2O \rightarrow 3CaO.SiO_2.8H_2O + 3Ca(OH)_2 \quad (1.1)$$

Tricalcium silicate + water $\rightarrow$ calcium silicate hydrate + calcium hydroxide

Formation of C-S-H starts from a few nuclei and progressively grows outward to form bundles of lath-like crystalline material, which forms an internal pores system called gel pores (0.5-10 nm) [63]. The formed C-S-H gel and its internal pores occupy a greater volume than the unhydrated reactants, and interconnects the reactants within 6 h to harden the paste into a solid body [59, 63]. C-S-H is the main phase responsible for the strength and durability of the PC [6, 13, 59]. Production of C-S-H is associated with precipitation of another by-product, known as Portlandite, which is a rhombohedral calcium hydroxide crystal that increases the pH to 11 [60, 59]. Belite is less reactive compared with alite and its hydration starts after 10 days by forming smaller C-S-H bundles which, contribute

towards the long-term strength of cement (Equation 1.2) [5, 6, 59].

$$2(2CaO.SiO_2) + 9H_2O \rightarrow 3CaO.SiO_2.8H_2O + Ca(OH)_2 \quad (1.2)$$

Dicalcium silicate + water $\rightarrow$ calcium silicate hydrate + calcium hydroxide

1.7.1.2 Hydration of aluminate and ferrite phases

Tricalcium aluminate interacts with gypsum and water to form a layer of needle-like crystals of hexacalcium aluminate trisulphate (ettringite) during the first 2 h (Equation 1.3) [6, 59]. Ettringite is responsible for early strength as well as improving workability of the cement by delaying the hydration of the reactants [6, 60].

$$3CaO.Al_2O_3 + 3CaSO_4.2H_2O + 26H_2O \rightarrow 6CaO.Al_2O_3.3SO_3.32H_2O \quad (1.3)$$

Tricalcium aluminate + gypsum + water $\rightarrow$ ettringite

In the absence of gypsum, the aluminate phase will react with Portlandite to form calcium aluminate hydrate (C-A-H) according to Equation 1.4 [6, 60, 64]. Formation of C-A-H is undesirable as it reduces the workability of the cement by causing an early stiffening of the PC [6, 60, 64]. Following the consumption of the gypsum within 2 days, the resultant ettringite crystals react with the remaining aluminate phase to produce calcium monosulphate according to Equation 1.5 [6, 60]. As the hydration continues for several months, the hydrates will be precipitated which will slow down the hydration rate

with the transition into a solid body by shifting from the setting phase to hardening (Figure 1.5) [59, 65, 66].

$$3CaO.Al_2O_3 + Ca(OH)_2 + 12H_2O \rightarrow 4CaO.Al_2O_3.13H_2O \tag{1.4}$$

Tricalcium aluminate + calcium hydroxide + water $\rightarrow$ calcium-aluminate-hydrate

$$6CaO.Al_2O_3.3SO_3.32H_2O + 2(3CaO.Al_2O_3) + H_2O \rightarrow 3(4CaO.Al_2O_3.SO_3.12H_2O) \tag{1.5}$$

Ettringite + tricalcium aluminate + water $\rightarrow$ calcium monosulphate

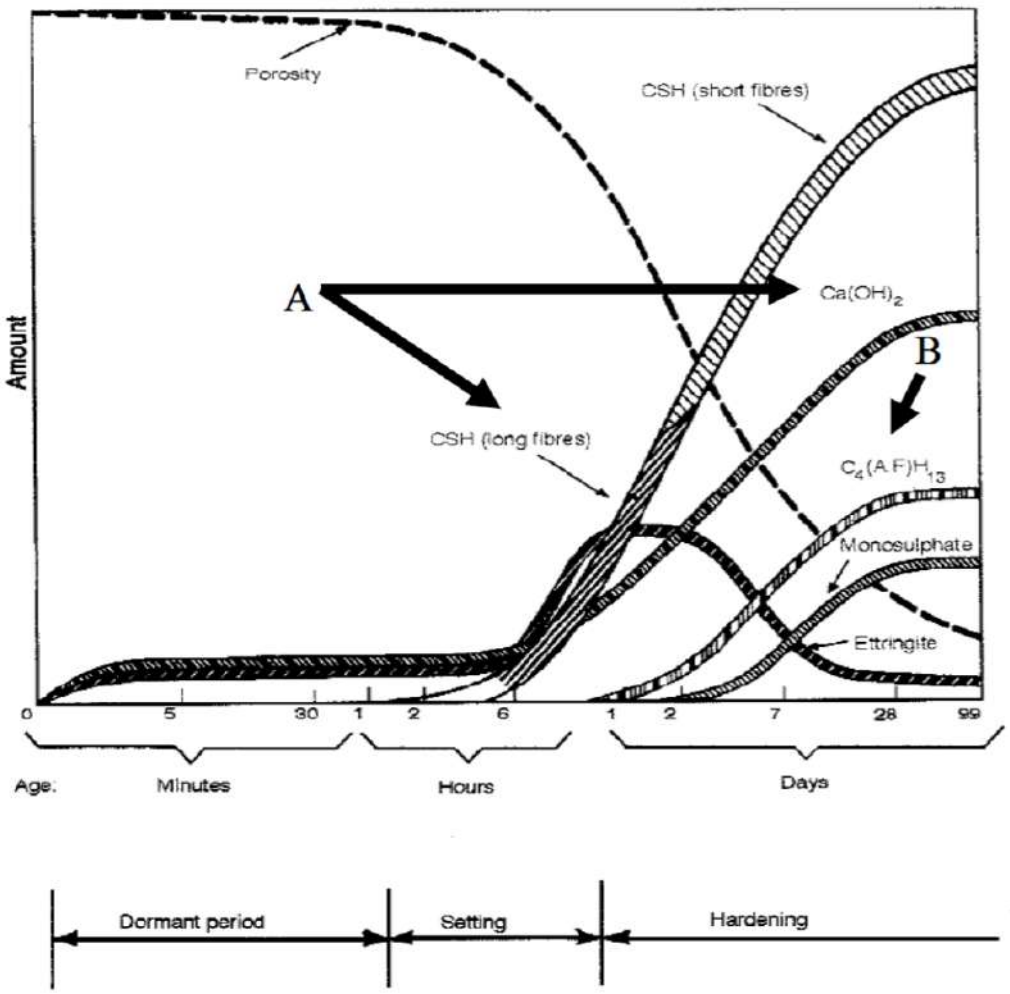

Figure 1.5: The adapted graph showing the steps involves in hydration of PC-based cements as a function of time. **A)** indicates the main hydration phases of PC and **B)** the hydration phase of the aluminate phase [66].

1.7.2 Application of PC-based cement in dentistry

In 1990s, Torabinejad patented a new type of endodontic cement called mineral trioxide aggregate (MTA) which met the criteria for a dental root filling [67]. MTA was based on 80 wt% PC and 20 wt% bismuth oxide (Bi_2O_3) as a radiopacifying agent. In 1997, MTA was FDA approved for dental applications and was commercially available

as ProRoot MTA and MTA Angelus for vital pulp therapy and root perforation repair etc [58, 12, 67]. Following the introduction of MTA, many studies reported good clinical outcomes such as demonstrating an antimicrobial effect [68], dentinogenic properties (dentine bridge formation) [69, 70], calcification [71] and superior sealing abilities etc [72, 73]. These promising results are the driving forces for exploiting and expanding PC 's application in the medical field such as drug delivery system and for load-bearing applications [6, 68].

1.7.3 Biological properties of PC-based cement

1.7.3.1 *In vitro* studies

Biocompatibility is “the ability of the material to perform with an appropriate host response in a particular application”, and is normally assessed via cell growth, gene expression, subcutaneous and direct contact of biomaterial with the body [1, 2, 74]. PCs have been exposed to different cell types including human osteosarcoma cells (MG63) [75, 76], mouse L929 fibroblasts and mouse macrophage [77] and rat osteoblast-like cells [78].

All *in vitro* studies reported that exposure of freshly mixed MTA or PC to all aforementioned cell types resulted in cell death and protein denaturation up to 3 days; whilst, cell growth occurred normally beyond the lysed zone [6, 77, 79, 80]. Therefore, a continuous release of Portlandite during the hydration of the cement into the solution is more likely to damage the cell membranes [66]. As hydration rate slows down, cells can re-

cover from the injury due to dilution of the OH ions from the dynamic fluid flow *in vivo* [77, 79, 80].

Conversely, Camilleri *et al.* reported that cell growth for the set cement after 28 days was significantly lower compared with 1-day [81]. This may have happened due to the change in surface topography of cement after being exposed to extracellular fluid. Therefore, there are multiple factors involved in tissue-biomaterial interactions [81].

PC has been shown to stimulate the formation of HA once immersed in physiological fluids [82]. The interactions that occur between the PC and the storage media can be summarised as below according to [82]:

1. The immediate dissolution of cement permits rapid exchange of Ca^{2+} with OH^- to form a solid-liquid boundary as well as Portlandite which increase the local pH. Other ions such as Fe^{3+} and Al^{3+} may also be released which allow the formation of mineral phases on the outer-surface.

2. The surface of calcium silicate phases are attacked by OH^- which hydrolyse the silicate (SiO_4^{4-}) and forms a porous C-S-H gel on mineral phases. The deprotonation of silanol groups (Si-OH) into negative group SiO^- also occur due to alkaline environment (Equation 1.6).

$$SiOH + H_2O \rightarrow SiO^- + H_3O^+ \tag{1.6}$$

3. The negative group on C-S-H could bond to calcium ions in aqueous solution create

nucleation sites for the heterogeneous nucleation (Equation 1.7).

$$SiO^- + Ca^{2+} \rightarrow SiO - Ca^{2+} \tag{1.7}$$

4. The phosphate ions present in physiological fluid will be hydrolysed into HPO_4^{2-}, which triggers a series of reactions to take place between calcium ions, silanol group and phosphate ions according to Equation 1.8 and 1.9.

$$H_2O + PO_4^{3-} \rightarrow HPO_4^{2-} + OH^- \tag{1.8}$$

$$SiO^- + HPO_4^{2-} \rightarrow SiO - HPO_4^{2-} \tag{1.9}$$

5. The calcium ions continue to be released and cause the dual supersaturation of Ca^{2+} and HPO_4^{2-} thus, precipitation of Ca-P layer on the surface. As the hydration continues and more nucleation sites are formed, the Ca-P rich surface will mature into carbonated apatite since HA is stable at pH $>$ 4.2.

1.7.3.2 *In vivo* studies

Saidon *et al.* implanted MTA and PC in the mandible of guinea pig for periods of 2 and 12 weeks which were then removed for histological analysis. Both materials generated a similar tissue reaction by demonstrating a direct bone integration at the interface, with no

sign of inflammation [79]. Moreover, Holland *et al.* also implanted white and grey MTA in rat connective tissue and observed no difference between these two in terms of tissue reaction [83, 84, 85].

1.7.4 Desirable physiochemical properties of PC for PVP

PC possesses many advantageous properties making it a suitable candidate for load-bearing applications [6, 59, 60]:

- **Setting in aqueous condition**: presence of moisture and extracellular fluid allows the continuous hydration of the PC which will subsequently increase its longevity and strength [6].

- **Less exothermic setting**: the setting reaction of PC is shown to be almost isothermal with a couple of exothermic reactions in the first 10 min. The heat profile of standard PC can reach as high as 29 J/g [13] within 2 h of the setting which is considerably lower than PMMA setting (570 J/g), avoiding the risk of tissue necrosis [86].

- **Durability and compressive strength**: PCs are durable bone cement and as the hydration continues, the compressive strength of cement will increase overtime [59]. The early compressive strength of 54 MPa has been measured for standard PC at a PLR of 4.0 g/ml, which is significantly higher than that of healthy cancellous bone and CPCs [5, 6].

- **Radiopacity**: bismuth oxide has been added successfully to PC-based cement, which is important for monitoring the cement with radiography to prevent any leakage into the surrounding environment [67].

- **Antibacterial effect**: high alkaline setting of the PC has demonstrated an intrinsic antibacterial effect however, the high pH could also result in cell death [87, 88].

1.8 Development of novel PC for PVP

A systematic review on calcium silicate-based cements has indicated that most PCs possess a long setting time of 2-3 h [6, 58]. If used clinically this would require the patient to stay in hospital for a longer time prior to being discharged. The long setting time also implies that the cement is more prone to disintegration, which reduces the longevity and durability of the cement [6, 58]. During the hydration of PC, combination of positive and negative charges cause the agglomeration of cement particles and results in poor handling and a low injectability (25 %). Recent studies have reported that the addition of liquefying and accelerant such as calcium chloride and sodium citrate have improved these limitations [13, 14, 61].

1.8.1 Addition of calcium chloride

The study by Wynn-Jones *et al.* in 2012 was the first research which directly addressed the limitations of PC for PVP [13]. In this study, the addition of 5-10 wt% calcium

chloride to PC at a PLR of 4.5 g/ml reduced the setting time from 120 min to less than 20 min, which was comparable with the setting time of PMMA. Additionally, 10 wt% calcium chloride appeared to act as a liquefying agent by neutralising the surface charge of the cement through a series of reactions between calcium chloride and silanol groups of C-S-H, Portlandite and other salt. These interactions reduced the number of oppositely charged particles, thus created a repulsion force to increase the injectability of this novel PC from 25 to 95 %. Meanwhile, the addition of 5 wt% calcium chloride improved the compressive strength to a level comparable with PMMA, by formation of more ettringite during the first 2 h compared with the control which, contributed toward the early strength of the cement [6, 13].

1.8.2 Addition of sodium citrate

Adding a low concentration of citrate anions to the CPCs has been shown to act as a retardant [22]. At the same time, Wynn-Jones *et al.* demonstrated that the addition of more than 1 wt% citrate to PC acted as both accelerant and liquefying agent [14]. Although the exact mechanism of how citrate anion changes between acting as a retardant and accelerant is not well understood. It was shown that the addition of 2 wt% sodium citrate was enough to improve the injectability to 91 % by creating an electrostatic repulsion between negatively charged particles. The setting time was also reduced to 24 min, and the compressive strength increased to 125 MPa within one day [6, 14]. These studies led to the development of a novel PC which fulfilled the primary requirements for the PVP.

1.9 The significance of porous bone cement

Although studies by Wynn-Jones *et al.* overcame the major issues associated with PCs [13, 14], the bone cement should still provide a suitable framework for cells attachment throughout the bulk structure to allow the bone formation [89]. Thereby, presence of sufficient porosity has emerged as one of the crucial requirements for vertebroplasty (Table 1.1) [90, 91]. Pores are classified as interconnected or non-interconnected [41]. Depending on the composition of bone cement, the amount of intrinsic porosity can be different. Both biological and mechanical properties of cement are highly dependent on the porosity which will be discussed as below [41]:

- **Effect of porosity on biological properties:** the porosity of porous bone cements is often measured, however, no optimal porosity for bone ingrowth has been stated within the literature. Although multiple studies reported that a high porosity (> 50 %) enhanced osteogenesis [41, 92, 93, 94, 95]. In addition to porosity, other relevant parameters of the porous cement including interconnectivity of pores, pore size and pore size distribution must be characterised as well [96, 97]. At the early stage of implantation, the formation of new blood vessels is a prerequisite for bone ingrowth. Studies indicated that presence of open pores with the size of 50 μm provide the path for vascularisation and nutrient transport for survival of cells [41, 92, 98]. Characterisation of pore size is also essential as studies demonstrated that macropores (> 100 μm) provided a higher surface area available for cell attachment and

subsequent differentiation [99, 100]. Meanwhile, micropores (< 100 μm) were involved in higher protein adsorption, ionic exchange and bone cement resorption [15]. CPCs with 20-40 % porosity are considered as a porous bone cement compared with PC which has a porosity of 20 %. In both cement systems, the pores are nano-micron sized and lack the large interconnected pores to enhance bone ingrowth [6, 12, 51, 52].

- **Effect of porosity on mechanical properties:** the porous bone cement should be able to possess sufficient strength to stabilise the vertebral body [10, 38]. Presence of pores and micro-channels allow the hydration and setting of the cement [60]. Takahashi *et al.* showed that during the early stage of cement's hydration, the strength of cement was mostly dependent on the amount of porosity. Likewise, the freshly made paste contains large unfilled spaces with high water content and increasing the porosity results in a loss of the integrity of the material [101, 102]. Apart from induction of pores artificially by additives, porosity may stem from two main sources: i) unconsumed water in the setting reaction and ii) entrapped air in the paste due to dry agglomerates of powder and air bubble [14]. According to Griffith's theory (Equation 1.10) there is a direct relationship between pores and strength for PCs and CPCs systems [102].

$$Compressive\,strength = \sqrt{\frac{E_0.R}{\pi.c}}\, e^{-constant\,RP} \tag{1.10}$$

E_0 = Modulus at zero porosity, R = Fracture's surface energy

c = Critical flaw size, RP = Relative porosity

Porosity exponentially affects the compressive strength of cement, while, the square root of flaw size is inversely proportional to the strength. To favour bone ingrowth and vascularisation, a highly porous bone cement is needed, whereas to ensure early stabilisation of the vertebral body, a strong material would be required.

1.10 Current methods to induce porosity

Various strategies have been developed over the last two decades to induce macroporosity in scaffolds and bone cements [15]. The methods used for self-setting cements are entirely different from those used for ceramic scaffolds, since the porosity in scaffold is introduced during the sintering stage or by toxic chemicals [15]. Therefore, introduction of macroporosity in the self-setting bone cement becomes challenging and limited to two main strategies: i) before and ii) after the cement is set as shown in Table 1.2. Regardless of which process is used, the following requirement should always be fulfilled [15, 103]:

- Minimum interference with cement setting reaction.
- Maintaining the cohesion and injectability of the bone cement.
- Possessing sufficient strength to prevent the collapse of the fractured vertebral body.

Table 1.2: List of the most common techniques to produce a macroporous cement.

Approach	**Technique**	**Type**	**Additive**	**Macroporosity** (%)	**Pore size** (μm)	**Reference**
After setting	Leach-out	Soluble particles	Mannitol, sucrose	17-64	120-270	[104, 105, 106]
		Fibres	Polyglactin 910	25-35	320	[107, 108, 109]
			Aramid, carbon	2-10	10-200	
		Microsphere	Gelatine	45-55	20-37	[110]
	Emulsion	Oil-water	Paraffin/sorbitan	52-65	100-900	[111, 112]
	Template	Positive/negative replica	Polyurethane/resin	25-55	400-1000	[113, 114]
Before setting	Bubbles	soluble powders	Sodium bicarbonate, hydrogen peroxide	13-20 11-36	100-170 210	[106, 115, 116] [117]
	Foams	Foaming agent	Gelatine, polysorbate 80	15-30	30-100	[118, 119, 16]
	Rapid proto-typing	3D printing			12-27	[120, 121]

Of the methods listed in Table 1.2, not all are applicable for the PVP procedure, since some methods require a complex preparation which is undesirable for a self-setting cement [117, 120, 121]. For this reason, the most common and established methods for self-setting bone cement will be discussed in the following sections.

1.10.1 Soluble porogen substance

Various water-soluble porogens including mannitol, sucrose and frozen sodium phosphate particles have been added to CPCs and were subsequently removed by storing in an aqueous environment to induce macropores in the shape that crystals previously occupied [105, 106]. The majority of research focused on using mannitol and sucrose due to suitable solubilities during the setting of the cement (within 5 days) [105, 106]. Markovic *et al.* indicated that the addition of 10 wt% mannitol to CPC at 4.0 g/ml created only 11 % porosity after 20 h of setting [105]. Takagi and Chow showed that by increasing the mannitol content to 40 wt% and lowering the PLR to 3.0 g/ml, the porosity elevated to 70 % with pores of larger than 100 μm [122]. However, the compressive strength was rendered to only 1 MPa which was lower than the healthy cancellous bone [122].

Takagi *et al.* also indicated that the addition of 25 % sucrose to CPCs at 4.0 g/ml successfully induced 50 % porosity with the pores in the range of 100-300 μm after 3 days, however, the diametral tensile strength was 3 MPa [106].

Tang *et al.* investigated the effect of mannitol on the biological responses of the CPCs [123]. It was shown that human umbilical cord stem cells-encapsulated CPCs contain-

ing mannitol significantly elevated mineralisation, alkaline phosphatase and osteocalcin expressions after 14 days compared with control due to the increase in the porosity [123].

The common features in all these studies is that for fabrication of a highly porous bone cement with sufficient interconnectivity, a large amount of porogen is required which significantly reduced the strength of the cement.

1.10.2 Creating porosity by using bubbles

Additions of compounds such as hydrogen peroxide and sodium bicarbonate to CPCs and PMMA have been shown to increase the porosity by generating bubbles during the setting of the cement [117, 124, 125]. Within the engineering literature, there are a few studies that have reported that the addition of 5-8 % hydrogen peroxide to PC, created a lightweight foamed concrete [117, 126, 127]. However, using such a high dosage of hydrogen peroxide can have serious problems for medical applications including DNA breakage in mammalian cells [128]. Therefore, hydrogen peroxide may not be a suitable candidate for self-setting cements compared with scaffolds which are normally constructed prior to implantation.

In 2002, Del Real *et al.* reported that mixing of 10 wt% sodium bicarbonate with the liquid phase containing citric acid induced 55-70 % porosity with the average pore size of 100 μm in CPCs by introducing CO_2 bubbles [115, 116]. This formulation significantly reduced the injectability and the early compressive strength of cement to 2 MPa [115, 116].

Kai *et al.* in 2009, reported that the addition of 5 wt% sodium bicarbonate to brushite cements induced up to 65 % porosity. A lot of pores were between 100 and 300 μm, which were favourable for cell migration and proliferation. Additionally, the 3-day compressive strength of the porous cement was 11 MPa which was significantly higher than identified values within the Del Real study, possibly due to difference in the starting materials and the concentration of sodium bicarbonate [124]. These compounds have shown promising results for CPCs, however the risk of embolism due to introduction of bubbles after the cement is implanted cannot be neglected [15].

1.10.3 Foaming agents

Fabrication of CPCs foams using foaming agents (so-called surfactants) has become an attractive method to induce pores throughout the setting of the cement [15, 119, 16]. This can be achieved by reducing the interfacial surface energy between liquid-gas interfaces via their amphiphilic nature to stabilise the formation of bubbles in the liquid phase [15, 119, 16]. For the development of a successful self-setting foamed cement, there are number of important criteria which should be considered for choosing the correct foaming agents [15]:

1. Water soluble

2. Non-toxic

3. No adverse effect on the setting of the bone cement

Foams are based upon colloidal system which consists of an internal phase (bubbles) and a continuous phase (liquid) [15, 119]. Fabrication of foams can be obtained by two main routes: i) mechanical stirring of the solution and ii) air pressuring of the foaming agent [15]. From the thermodynamic point of view, foams are not stable thus, during their lifetime the following steps take place which can be identified as follows [15]:

1. Formation of the foam by creation of a turbulent flow.

2. Maturation of the foam prior to the setting of the cement by continuous disruption of the foam. This could happen by gravitational separation of liquid, which causes a thinning of the bubble's wall and merging of small and large bubbles due to the pressure difference.

3. Hindering the foam to collapse during the setting of cement which generates a solid foamed cement.

Foaming agents are divided into two main categories according to molecular weight (MW) of either low or high [129]. Synthetic surfactants have low MWs and are mostly toxic by interfering with homoeostasis and damaging the cell membrane [15].

Polyoxyethylene-sorbitan-20-monooleate (polysorbate 80) is a non-ionic surfactants, which has been used in medical applications such as solubilising agent for creams, lotions, or as anti-cancer agents [16, 130]. Polysorbate 80 is derived from polyethoxylated sorbitan (hydrophilic), and oleic acid (hydrophobic tail). Synthetic surfactants have been shown to be more efficient in foaming capacity with a good foam stability and eliminate

the risk of immunogenic response which may occur for natural surfactants [15, 131].

Proteins are natural high MW surfactants with the foaming property relies on to the creation of a flexible interfacial film via its adsorption and unfolding at the surface which entraps air to create pores [15, 119]. Gelatine is an amphiphilic protein with an excellent foaming property and it is derived from a thermally-denatured collagen from skins or bones of animals [15]. The structural unit of gelatine is composed of multiple glycine (every 3 residues), 4-hydroxyproline and proline residues [132]. Gelatine is usually used in manufacturing of tablets, wound dressing and a gelling agent due to its temperature-dependent behaviour. A transparent thermoreversible gel forms when gelatine is cooled below its gelling point of 35 ^{o}C [15, 119].

A recent study showed that the addition of 5-20 wt% gelatine to CPCs at PLRs of 1.25-2.50 g/ml successfully increased the porosity of the cement to more than 60 % with no significant effect on the initial setting time of the cement [119]. In addition, the compressive strengths after 7 days of the setting for control, 10 wt% and 15 wt% foamed gelatine were 29.0, 15.5 and 11.3 MPa respectively [119]. Montufar *et al.* indicated that the addition of polysorbate 80 instead of gelatine induced larger and more interconnected pores to accommodate cell attachment [16, 131]. On the other hand, gelatine has an important advantage over synthetic surfactants and that is improving the injectability of the cement [16]. Additionally, the osteoblast attachment and spreading *in vitro* were higher compared with polysorbate 80 due to presence of the adhesive peptide motif in gelatine's composition [16, 131].

1.11 Aims of the present study

To date, PMMA remains the main bone cement being used for the PVP procedure. However, due to multiple disadvantages associated with PMMA, alternative materials are being actively researched. To establish a PC-based cement as a viable candidate for PVP, further modification of this novel cement by inducing large interconnected pores is necessary.

Radiopacifying agent is a very important component of the bone cement for PVP to allow live monitoring of the bone cement with radiography. Previous studies by Wynn-Jones *et al.* did not include bismuth oxide in the novel PC model system. To address this shortcoming the main aim of the first chapter of the present study will be establishing a new PC model system containing 20 wt% bismuth and a range of established additives at different PLRs. The key properties of the material including setting time, injectability, compressive strength and porosity will be measured to select the most appropriate formulation for the following experiments. During the initial stage of this study, the influence of cement ageing will be assessed on the effectiveness of additives using complementary techniques such as Fourier transform infrared spectroscopy (FTIR), SEM and X-ray diffraction (XRD) to characterise the setting of the PC.

Prior to the commencement of this research, there was no preliminary study on the methods to induce macroporosity in PCs for the biomedical applications. Therefore, a range of porogens will be selected and studied in the next two chapters to evaluate the influence of each porogen on the setting times and injectability of the PC. Other important

properties of the modified cement including compressive strength, total porosity and strut density will also be assessed. The modified cement will be then characterised in terms of macro and microstructural differences using SEM

Following the development of the potential porous injectable PC, further characterisation of the porous cement will be carried out by immersion of the material in various physiological fluids to mimic *in vivo* conditions. The crystalline phase of porous cement will be examined using XRD, while mercury intrusion porosimetry (MIP) will be used to measure the interconnectivity of open pores to select the best formulation which, fulfils both mechanical and biological requirements.

Chapter 2

Materials and Methods

2.1 Materials

All the chemicals used in this study were from Sigma Aldrich except where stated.

2.1.1 PC model system

The PC model system in this study consisted of type II grey Portland cement (Blue circle, Mastercrete, Lafarge, UK) due to its high early strength as previously established by Biomateruals unit at University of Birmingham [6, 102, 5]. Bismuth (III) oxide was added at concentration of 20 wt% to the powder phase as a radiopacifying agent [5, 102]. Different liquefying agents were used throughout this study:

- **Chapter 3**: 5-10 wt% calcium chloride and 2-5 wt % sodium citrate
- **Chapter 4 and 5**: 5 wt% calcium chloride

Cement powders and additives were ground together using a pestle and mortar for 10 min to achieve a homogeneous cement mixture. Distilled water (DW) used as the liquid phase and was added to the powder phase at different PLRs of 3.0 to 5.0 g/ml for chapter 3

and 4.0 to 5.0 g/ml for chapters 4 and 5 respectively. Throughout this thesis, the number in parentheses specifies the PLR used. Cement slurries were produced by hand mixing powder and liquid phases thoroughly using a spatula for 2 min [5].

2.1.2 Sample preparation of macroporous cement

For chapters 4 and 5, different methods of inducing macroporosity including soluble porogens, introducing bubbles and foaming agents were investigated as described in the following sections.

2.1.2.1 Soluble porogens

Mannitol and sucrose powders were used to modify the cement. The porogens were added to the powder phase at different wt% of 1, 5, 10 and 20 according to the Equation 2.1 [122].

$$weight\,\% = (\frac{Porogen}{Porogen + PC\,powder})\,x\,100 \tag{2.1}$$

2.1.2.2 Sodium bicarbonate

Sodium bicarbonate powder was added to the powder phase according to Equation 2.1 in order to compare the effect of compounds which introduce bubbles on the PC-based materials.

2.1.2.3 Foaming agents

Type B gelatine powder and polysorbate 80 were used as foaming agents. Firstly, these foaming agents were dissolved in DW at concentrations of 5, 10 and 15 wt% according to Montufar *et al.* [16]. The foaming process was modified from previous studies, by agitating the foaming agent solutions via magnetic shaker (Fisher Scientific, UK) at 1200 rpm for 4 min. The foaming process for gelatine was performed at 50 °C to prevent gelation. Afterwards, the foamed liquid was added to the cement paste (Figure 2.1) according to Equation 2.1, in order to minimise the shear stress and breaking down of bubbles.

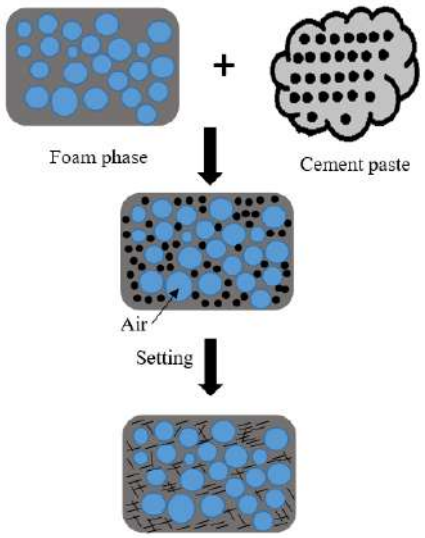

Figure 2.1: The addition of the foam phase to the paste to reproduce foamed cement.

2.2 Methods

2.2.1 Setting time measurements

Four grams of freshly made cement slurry (n = 3) were prepared and placed in a 12-well plate (Thermo Scientific, UK) with a surface area 4.0 cm^2 [5]. Once the cement paste was placed in the well plate, the surface of the cement was flattened by spatula and the initial setting time measurement was performed using a light Gilmore needle with 113.98 g weight and 2.11 mm diameter (ASTM C266-99) [6, 5]. The indentation was performed under laboratory conditions (22 $\pm$ 2 ^{o}C) by applying the needle at 90 ^{o} to the surface of the cement as shown in Figure 2.2 and it was repeated every 10 min until no indentation was observed [6, 5].

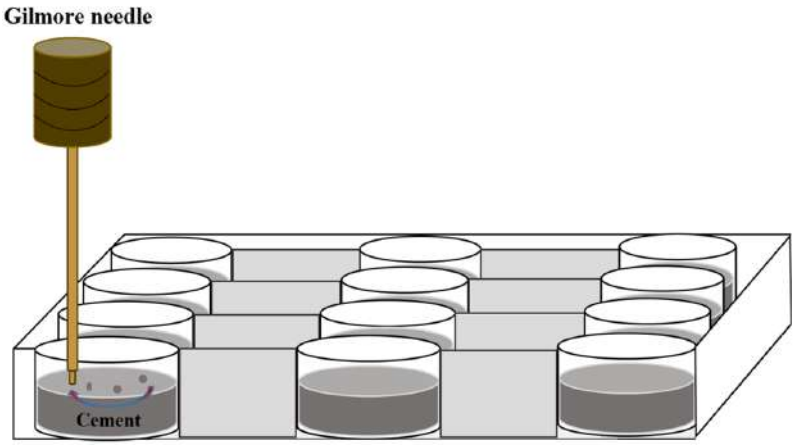

Figure 2.2: Schematic representation of Gilmore needle indentation on the surface of the cement. Needle was repeatedly applied until no indentation was observed which was determined to be the setting time.

2.2.2 Injectability measurement

Four grams of cement slurry were prepared (n = 4) and immediately transferred into a 5-ml disposable syringe (BD Plastipak, USA) before measuring the weight of syringe containing cement using an analytical balance (Pioneer Plus, USA) with accuracy of 0.001 g. A universal testing machine (Instron 5544, UK) with a 2 kN load cell was used to extrude the cement slurry through the syringe (outlet diameter = 2 mm) exactly 2.5 min after mixing the cement (Figure 2.3). The cement was extruded into the bijou within the wooden jig at a cross-head speed of 30 mm/min either until the cement was fully extruded or a maximum applied force of 100 N was achieved according to Wynn-Jones *et al.* [6]. The weight of remaining cement was measured after the test was finished to calculate the percentage of injectability according to Equation 2.2.

$$Injectability\,(\%) = \frac{M_i}{M_O}\,x\,100 \tag{2.2}$$

M_i = Mass of injected cement (g)

M_O = Mass of original cement (g)

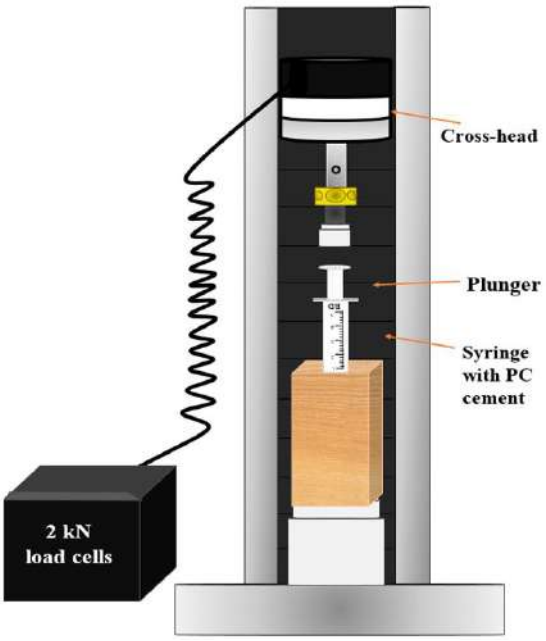

Figure 2.3: Schematic set up for the injectability measurements and how the cross-head pushes the plunger down to extrude the cement into the bijou within the wooden jig.

2.2.3 Foamability and foam stability of foaming agents

By measuring the increase in volume of solution containing foaming agent, the foamability of the foaming agents was characterised according to the Equation 2.3 [118, 16]. For each concentration, the test was repeated three times to measure the average values.

$$Foamability\,(\%) \;=\; (\frac{V_{\mathrm{f}} - V_{\mathrm{l}}}{V_{\mathrm{l}}})\,x\,100 \tag{2.3}$$

V_f = Volume increased after foaming (ml)

V_l = Initial volume of foaming agent solution (ml)

Afterwards, the foam stability was measured according to the method explained by

Montufar *et al*. Briefly, 10 ml of foam liquid (n = 3) was transferred into a Falcon tube and the time it took to form 1.4 ml of liquid at the bottom of tube was recorded [118, 16]. A reference liquid was used for comparison as shown in 2.4.

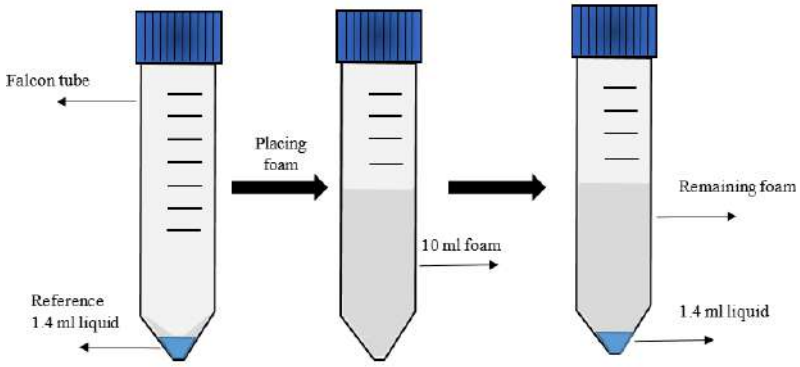

Figure 2.4: Foam stability procedure involved placing 10 ml foam in a Falcon test tube and measuring the time it took to form 1.4 ml of liquid at the bottom according to the reference tube.

2.2.4 Storage media

Phosphate buffered saline- Dulbecco A (PBS) tablets without calcium and magnesium (OXOID, UK) were dissolved in DW according to manufacturer instruction. Afterwards, 20 ml of different media at a pH of 7.4 $\pm$ 0.1 including DW, PBS and PBS supplemented with 10 % foetal calf serum (FCS) and 1 % antibacterial agent; penicillin/streptomycin (denoted as PBS/FCS) were used to investigate the effect of different media on the hydration of cement. Simulated body fluid (SBF) was prepared according to dual-solution formulation (Solution A and Solution B) previously described by Bohner *et al.* (Table

2.1) [133]. All solutions were sterilised either by filtering through a 0.22 μm membrane (Millex, Merck, Germany) or autoclaving at 121 ^{o}C for 2 h. The media were either changed on the daily basis (dynamic) or kept unchanged (static) throughout the experiment to investigate the effect of static and dynamic regimes on setting of the cement [134].

Table 2.1: Dual-solution preparation of SBF according to Bohner *et al.*

Starting materials	**Solution A**	**Solution B**
	Weight (g/l)	**Weight (g/l)**
NaCl	6.129	6.129
$NaHCO_3$	5.890	
$Na_2HPO_4.2H_2O$	0.498	
$CaCl_2$		0.540
	Volume of HCl solution (ml/l)	
HCl 1.00 M	0.934	0.934

2.2.5 Compressive strength measurement

To identify any changes in the bulk material property following the addition of porogens, compressive strength of the cement was measured. Cement slurries were cast either by spatula or 5-ml disposable syringe into a poly tetrafluoroethylene (PTFE) mould (6 mm diameter and 12 mm height). Cements were left to set for 6 h in the incubator (Hybaid, Thermo Hybaid, UK) at 37 $\pm$ 1 ^{o}C [5]. The set cements (n $>$ 7) were removed and

incubated further in different media at a liquid-to-cement volume ratio of 60:1 [134] for different time periods to assess both short and long-term strengths according to following regimes:

- **Chapter 3**: Samples stored in DW for 1 day.
- **Chapter 4**: Samples stored in DW for 7 days to allow complete dissolution of porogen .
- **Chapter 5**: Samples stored in different media for 7 and 30 days in DW, PBS/FCS, PBS and SBF.

At each time interval, the cements were removed from the incubator, weighed and the diameter and height of individual cylinder were measured at top, middle and bottom using a digital vernier calliper (Duratool, UK) with accuracy of $\pm$ 0.01 mm. Wet compressive strength was measured using a universal testing machine (MTS criterion 42, USA) at a cross-head speed of 1 mm/min using a 5 kN load cell (Figure 2.5). The mean wet CS (MPa) was then calculated according to the Equation 2.4 [5].

$$Compressive\,strength = \frac{L}{A} = \frac{L}{\pi \,.\, (\frac{d}{2})^2} \tag{2.4}$$

L = Load (N)

A = Cross section area (mm^2)

d = Diameter (mm)

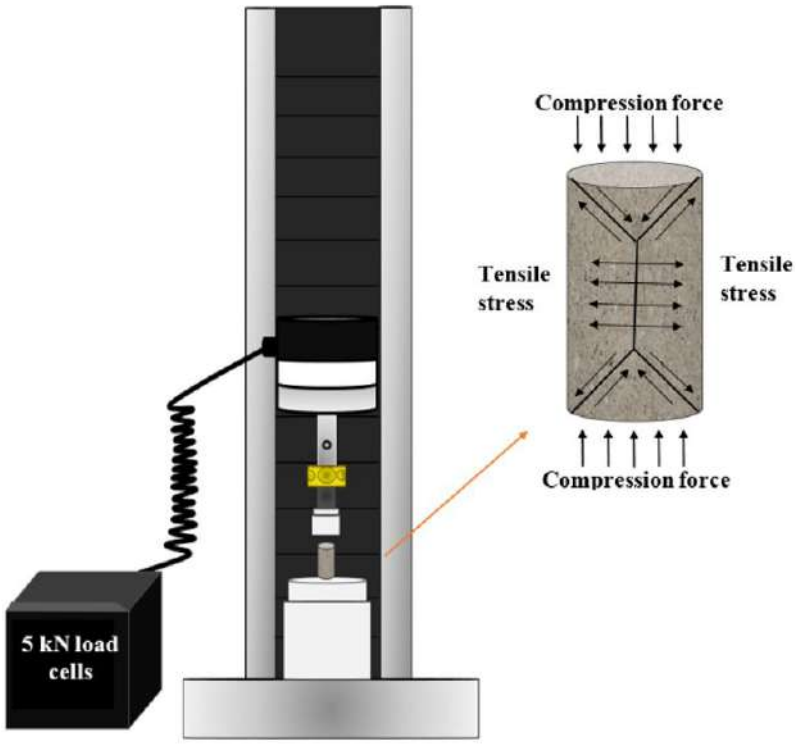

Figure 2.5: Schematic diagram indicating compressive strength testing and how the compression force translate into shear and tensile stresses.

2.2.6 Weight loss experiments

After mechanical testing, large fragments for each group were weighed and dried in the desiccator until a constant weight was achieved. The wet density (g/cm^3) was calculated using the wet mass and the volume of the cylindrical sample using Equation 2.5 [5].

$$Wet\,density = \frac{m}{\pi . r^2 . h . 1000} \tag{2.5}$$

m = Mass of fragments (g), r = Average radius (mm), h = Average height (mm)

From the obtained values from Equation 2.5, the apparent dry density of cement- that is the density of cement including pores and void spaces- was calculated using Equation 2.6.

$$\rho_{dry} = \frac{W_D}{W_W} x\, \rho_{wet} \tag{2.6}$$

ρ_{dry} = Apparent dry density (g/cm^3)

ρ_{wet} = Apparent wet density (g/cm^3)

W_D = Dry weight of fragments (g)

W_W = Wet weight of fragments (g)

2.2.7 Calculation of total porosity

The strut density of sample that is the specific density of the cement excluding pores and void spaces was measured using a helium pycnometry instrument (Ultrapyc 1200e, Quantachrome, USA). Following on from the strut density results, the mean percentage of total porosity was calculated (Equation 2.7) for each group to help interpret strength data [5, 66].

$$Total\, porosity\,(\%) = [1 - (\frac{\rho_{dry}}{\rho_{strut}})]\, x\, 100 \tag{2.7}$$

ρ_{dry} = Apparent dry density (g/cm^3)

ρ_{strut} = Strut density (g/cm^3)

To estimate the amount of extra porosity, it was assumed that all the extra porosity was introduced by the foaming agent, and the control specimen contained only intrinsic

porosity [16, 131]. Hence, the extra porosity was calculated from the apparent densities of foamed PC and control according to Equation 2.8 [16, 131].

$$Extra\,porosity\,(\%) = [1 - (\frac{\rho_{FC}}{\rho_{UFC}})]\,x\,100 \tag{2.8}$$

ρ_{FC}= Apparent dry density of foamed cement (g/cm^3)

ρ_{UFC}= Apparent dry density of unfoamed cement (g/cm^3)

2.2.8 Investigation of the effect of porogens on the materials constant

To investigate whether the porogens would change materials constant of PC, the strengths and porosity data for different groups were used to plot the natural logarithm of the compressive strength against relative porosity according to Griffith's theory (Equation 1.10) [101, 102].

2.2.9 Solubility test

The solubility of the foamed cement was assessed for up to 30 days different media using cylindrical samples (n = 3). The set cements after 6 h were extracted from the mould and the initial mass (m_0) of cement for each condition was measured. Afterwards, the samples were stored in 20 ml of PBS and PBS/FCS at 37 $\pm$ 1 ^{o}C which were refreshed on a daily basis. At each time interval, the samples were removed from the media and stored in a desiccator until their weights were stable and the dry mass (m_1) was measured.

The percentage of solubility of different PC formulations were then calculated according to Equation 2.9 [135, 136]

$$Solubility\,(\%) = (\frac{m_0 - m_1}{m_1})\,x\,100 \tag{2.9}$$

m_0 = Initial mass (g), m_1 = Dry mass (g)

2.2.10 Cohesion test

The porous PC should demonstrate sufficient consistency to prevent any disintegration after injecting within the body. To mimic *in vivo* conditions, a polyester sponge was immersed in the DW at 37 $\pm$ 1 ^{o}C for 1 h, and the cement paste was injected into the sponge using a disposable syringe (Figure 2.6). The cohesion of cement paste was assessed visually for disintegration of paste immediately after the injection for 2 h.

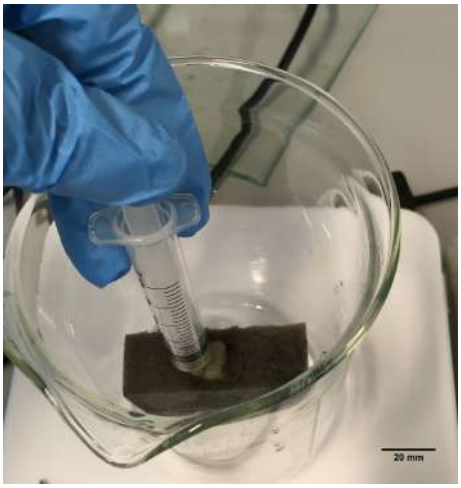

Figure 2.6: Image was taken during injection of cement paste into the polyester sponge to assess the cohesion of the paste.

2.2.11 Fourier transform infrared (FTIR) spectroscopy

To monitor the initial setting reaction of the PC with or without foaming agent, 1 g of freshly mixed cement paste was prepared. The attenuated total reflectance (ATR) technique of FTIR (Nicolet 6700, Thermo-Scientific, UK) was used to monitor the setting reaction at 37 ± 1 °C [5]. The glass slide was used to cover the cement to prevent drying during the experiment as shown in Figure 2.7. The FTIR absorbance spectra were recorded using mid-IR 4000-400 cm^{-1} after 60 and 120 min of hydration at a resolution of 6 cm^{-1} and scanning times of 32 [5]. To analyse the outer-surface of cements stored in different media after 7 and 30 days, disc-shaped cements (10 mm diameter and 2 mm height) were prepared. To ensure continuous contact between disc sample and the ATR diamond, a pressure unit was used when collecting the data.

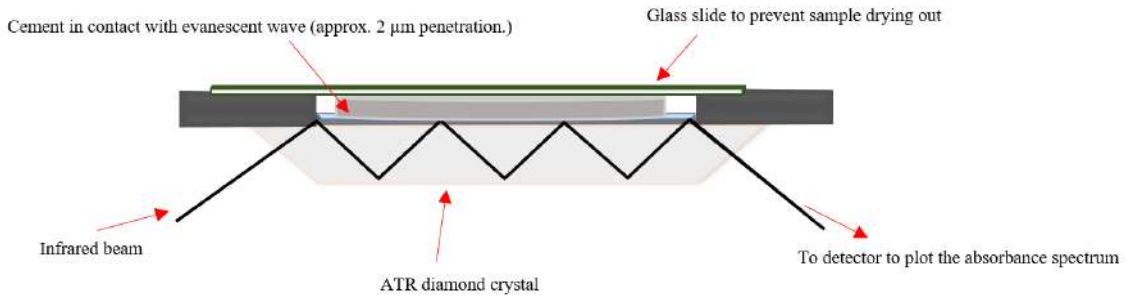

Figure 2.7: Schematic diagram illustrating multiple reflections of infrared beam which create evanescent waves to protrudes beyond the ATR crystal into the cement.

2.2.12 Scanning electron microscopy (SEM) analysis

For imaging the the outer and inner surface of dried fragments, a Zeiss EVO MA-10 SEM was used to distinguish any topographical difference between controls and porogens containing groups. Carbon tab (Agar Scientific, UK) was used to attach the fragments on aluminium stubs. The immobilised cements were then gold sputter coated (K550x, Emitech, UK) twice, to reduce the charging effect. The gold-sputtered cements were analysed by SEM at accelerating voltages of 5-20 kV at different magnifications from x40-6500.

2.2.13 Energy dispersive X-ray spectroscopy (EDS)

After SEM, the surface of cement was irradiated with electrons and the emitted X-rays by the elements were recorded using Inca detector (Oxford instrument, UK). Elemental analysis was carried out at three different locations to measure the average elemental wt% composition. The average wt% for each element was used to calculate the observed ratio for element pairs e.g. Ca/O, in order to compare it with the theoretical ratios. The percentage of difference in observed and theoretical ratios for each element pair was calculated using Equation 2.10 [5].

$$1 - (\frac{observed\,ratio}{theoretical\,ratio})\,x\,100 \tag{2.10}$$

2.2.14 Image analysis for pores size distribution

Pore size at any particular point is defined by "the diameter of the largest sphere which is completely within that pore" [41, 137]. Thereby, by connecting the pore diameters to each other the pore size distribution could be determined [137]. All image analysis was performed as described in the flowchart (Figure 2.8) using Fiji (distribution of ImageJ software, USA) according to an established method by Vyas *et al* [138, 139]. To normalise the obtained results, same area was selected as a region of interest randomly for 6 images per group.

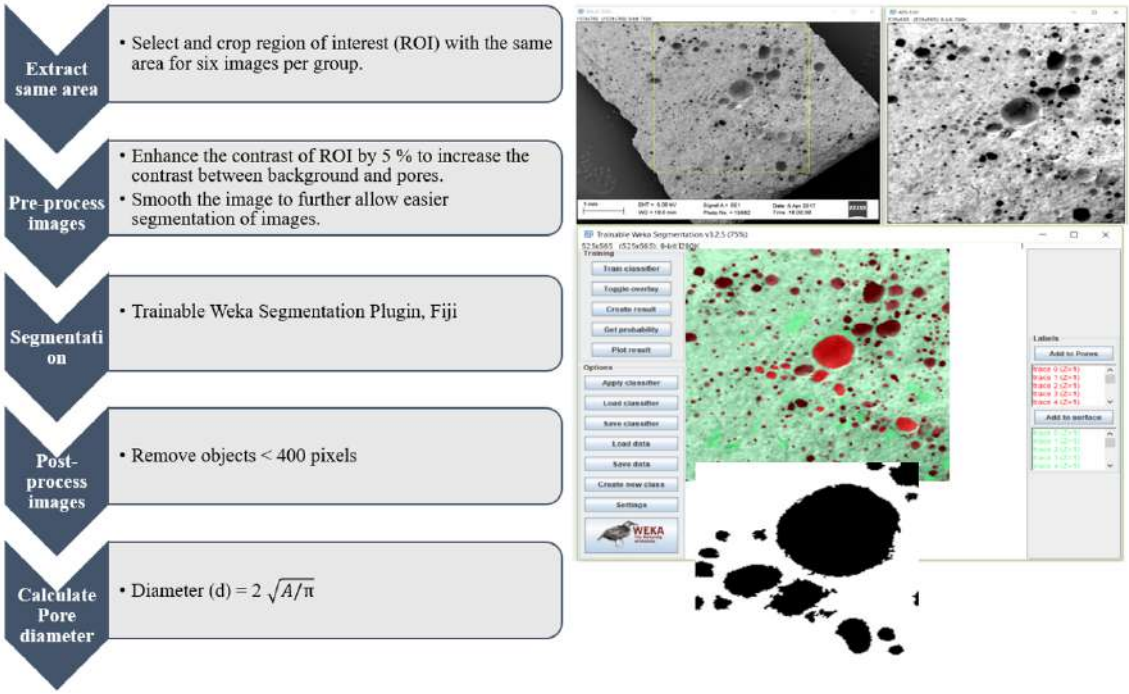

Figure 2.8: Flow chart highlighting the main steps in image analysis including selecting the area to pre-process the image, following by segmentation and post-processing stage to calculate pore diameter distribution.

- **Pre-processing of images**: The selected area for all images were processed by decreasing the brightness and increasing the contrast by 5 % using "enhanced contrast" plugin. The image was then smoothed using "smooth" plugin for a better recognition of pores from background.

- **Segmentation**: The porosity was segmented from cement surface using "Trainable Weka Segmentation" plugin which used a collection of algorithms to generate pixel-based segmentation of image. Each image will be binary pixel classified into pores (red colour) and surface (green colour) which the user can add traces to both classifications. If needed the segmented image can be further modified by the user to retrain the classifier for a better result.

- **Post-processing of images**: The segmented image was then converted to a binary image and any object of smaller than 400 pixels was considered as noise and was eliminated from analysis prior to using the "Analyse Particle" plugin. The obtained results were used to calculate the average frequency of pores diameter for different PC formulations.

2.2.15 Mercury intrusion porosimetery (MIP)

Mercury intrusion porosimetry (MIP) (AutoPore IV 9500, Micromeritics, UK) was used to measure the entrance pore size distribution of open pores for unmodified and foamed cements between 0.005-500 μm. The analysis was performed using a continuous

intrusion of a non-wetting liquid i.e. mercury into the tested sample under controlled pressure. The instrument then measured the volume of intruded mercury to achieve pore size distribution using Equation 2.11 [140].

$$D = \frac{-4\gamma \cos\theta}{P} \tag{2.11}$$

D = Diameter of entrance pore (μm)

γ = Surface tension of mercury (N/m)

θ = Contact angle between pore wall and mercury

P = Applied pressure (N/m^2)

2.2.16 Phase composition analysis using X-ray diffraction (XRD)

Dried fragments (n = 3) were flattened using P400 silicon paper prior to XRD analysis. Data sets were collected from 2θ = 5-40 ^{o} to detect the crystalline components using a Bruker Diffractometer (D8 Bruker, Germany). Data was baseline corrected in MATLAB. Peak identification was then carried out using ICSD data base using X'Pert HighScore for calcium hydroxide (PDF ref. 04-010-3117), bismuth oxide (PDF ref. 01-072-0398) and calcite (PDF ref. 00-05-586) [5, 6, 141].

2.2.17 Statistical analysis

All the raw data were tested for normality prior to further analysis using SigmaPlot software (Version 12.5, UK). The appropriate statistical test was then carried out such as t-test, one-way analysis of variance (ANOVA) and two-way ANOVA at a significant level of $p < 0.05$ followed using multiple comparison within groups using post-hoc Tukey tests.

Ceramic materials, including PCs, contain flaws of different size and orientation, which lead to a variability of strength data [6, 142]. Therefore, the measurement of a single average value may not be adequate to predict the performance of the ceramic material [6, 142]. A probabilistic approach can be used to describe the distribution of strength data using Weibull theory. According to this theory, the failure of a specimen occurs by the weakest link, and Weibull distribution can be used to quantify the reliability of material using Equation 2.12 [6, 142].

$$P_{\mathrm{f}} = 1 - exp\,[-V(\frac{\sigma - \sigma_{\mathrm{min}}}{\sigma_0})^{\mathrm{m}}] \tag{2.12}$$

P_{f} = Probability of failure

V = Volume of sample

σ = Failure stress (MPa)

σ_{min} = Threshold stress (MPa)

σ_0 = Scaling constant

m = Weibull modulus

As Weibull modulus describes the "brittleness" of a ceramic material, a close grouping of the compressive stress is an indication of a higher value of Weibull modulus. P_f is the failure probability which varies from 0-1 and can be calculated using Equation 2.13 [6, 142].

$$P_f = (\frac{n}{N+1}) \tag{2.13}$$

N = Total number of sample

n = The ranking number

The samples are classified in ascending order and the volume was ignored since it remained constant, hence the Equation 2.12 can be simplified further in the form of an equation of a straight line as shown in Equation 2.14 [6, 142].

$$lnln(\frac{1}{P_s}) = mln(\sigma) - mln(\sigma_0) \tag{2.14}$$

Where P_s is defined as the probability of survival (1-P_f) and the gradient of this equation is Weibull modulus (m). In the current study, Weibull analysis was carried out on the ranked data by plotting the lnln(1/P_s) against lnσ to calculate the gradient using a regression line [6]. To ascertain any statistical difference, the 95 % confidence intervals of the groups subjected to Weibull analysis were determined. There will be no significant difference between Weibull moduli of different groups when the 95 % confidence intervals overlap.

In addition, the survival probability graph was further assessed to determine whether the failure at low stress are caused by the same defects at higher stress level [6, 142].

Chapter 3

Batch stability: investigating the effect of cement ageing on its performance

3.1 Results

3.1.1 Setting time of old and new batches of PC containing additives

Comparison of a batch of PC from 2010 (old batch) with another batch from 2016 (new batch) indicated no significant difference ($p > 0.05$) in the setting time of cements containing 5-10 wt% calcium chloride, except when 5 wt% was added at 5.0 g/ml. Increasing the concentration from 5 to 10 wt% within each batch accelerated the setting time significantly ($p < 0.05$) at all PLRs except for the new batch at 5.0 g/ml (Figure 3.1).

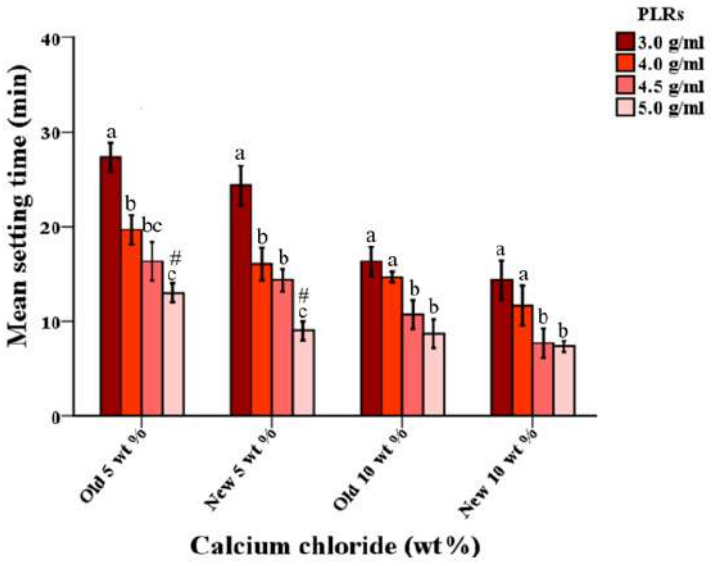

Figure 3.1: Mean setting time of the old and new batches of PC containing 5-10 wt% calcium chloride at different PLRs. There was no significant difference between batches at any concentration of calcium chloride except for 5 wt% at 5.0 g/ml (# $p < 0.05$). Values are expressed as mean $\pm$ SD. Dissimilar letters indicated significant differences ($p < 0.05$) between different PLRs at each concentration (n = 3).

Once the calcium chloride was replaced with sodium citrate, the setting time for the new batch was significantly reduced compared with the old batch for all PLRs ($p < 0.05$) as shown in Figure 3.2. The addition of 2-5 wt% sodium citrate to both batches at 3.0 g/ml acted as a retardant compared with other PLRs. At PLRs of 4.0 to 5.0 g/ml, increasing the concentration of sodium citrate within the old batch significantly reduced ($p < 0.05$) the setting time at each PLR. In contrast, the setting times of the new batch containing 2-5 wt% sodium citrate at PLRs of 4.5-5.0 g/ml were comparable with each other ($p > 0.05$).

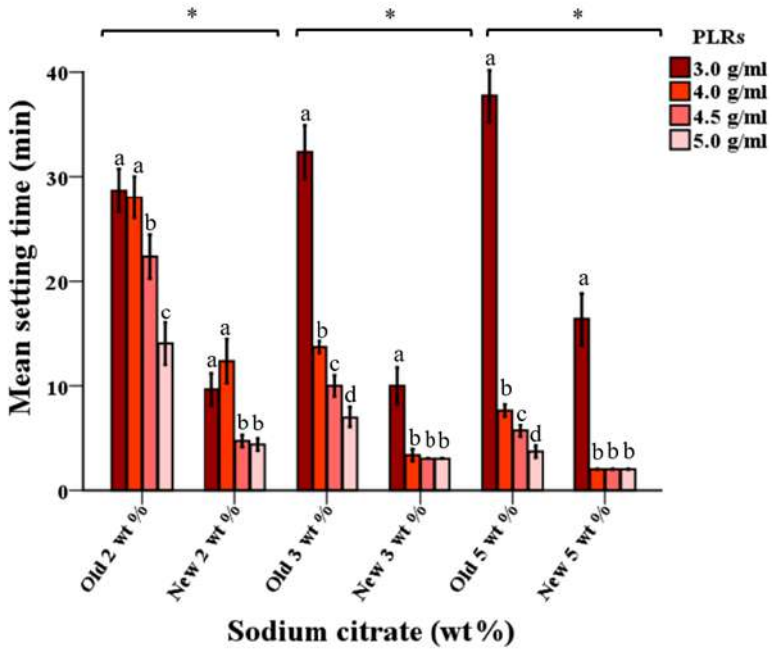

Figure 3.2: Mean setting time of old and new batches of cement containing 2-5 wt% sodium citrate at different PLRs. Addition of sodium citrate to the new batch reduced the setting time significantly compared with the old batch (* $p < 0.05$). Values are expressed as mean $\pm$ SD. Dissimilar letters indicated significant differences between different PLRs at each concentration (n = 3).

3.1.2 Injectability studies

Studies on the injectability of PC standard showed a general decrease in the injectability of the cement without additives with increasing the PLR. In addition, there was a significant difference ($p < 0.05$) between old and new batches when higher PLRs of 3.0-5.0 g/ml were used as shown in Figure 3.3.

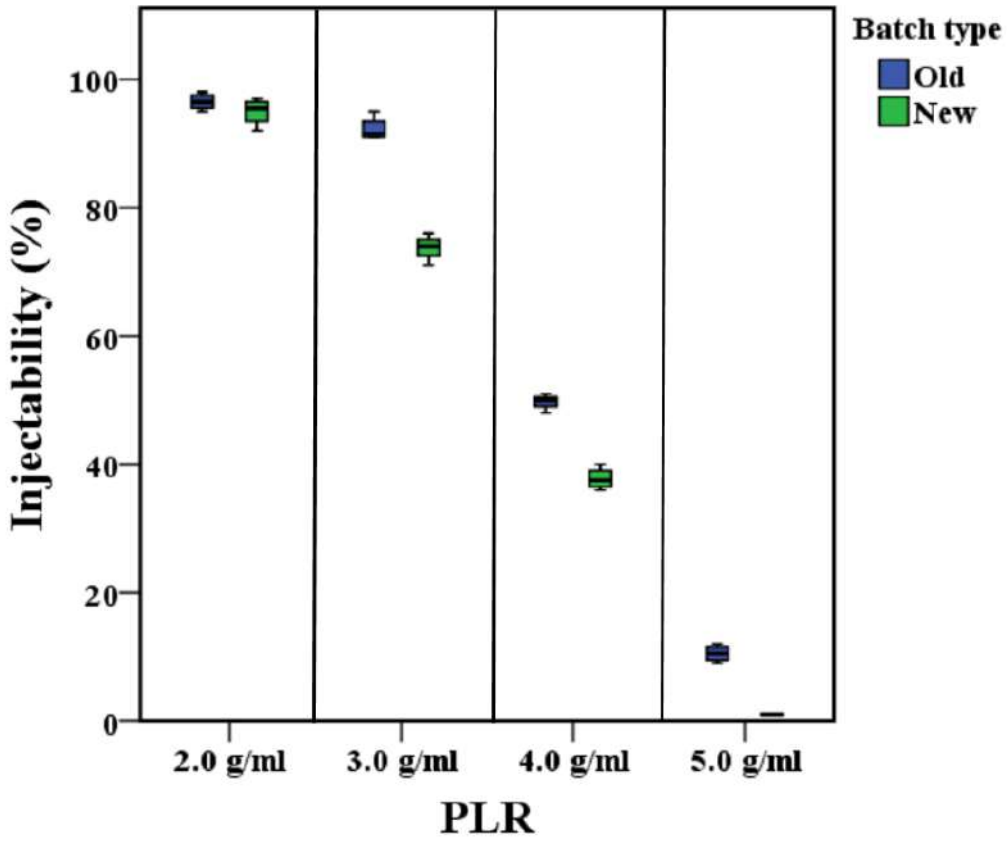

Figure 3.3: Mean injectability of old and new batches of PC standards containing no additives at different PLRs. A decreasing trend in injectability was observed as the PLR increased from 2.0 to 5.0 g/ml. The injectability of cement at PLRs 3.0 to 5.0 g/ml was significantly ($p < 0.05$) altered by changing the batch.

After injectability testing, the extruded paste for all PLRs was assessed for any noticeable differences. When the cement was extruded at a low PLR of 2.0 g/ml, phase-separation occurred by formation of two distinct layers of low and high density powder (Figure 3.4). This was not seen for other PLRs.

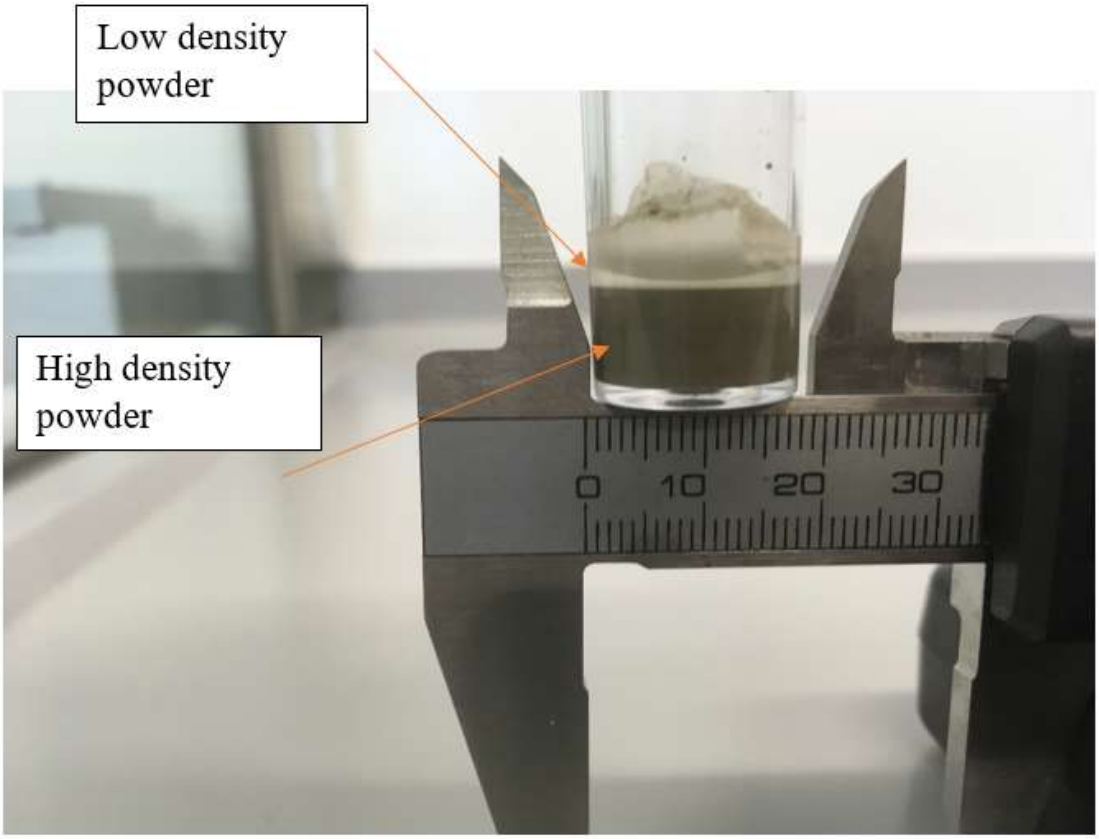

Figure 3.4: Image captured after injectability testing of a PC standard with no additives. Phase-separation of cement paste occurred at a PLR of 2.0 g/ml by formation of low and high density powder layers as indicated by the arrows.

3.1.2.1 Injectability of old and new batches of PC containing additives

When 10 wt% calcium chloride was added to both old and new batches, a high injectability of >90 % were achieved. These values were significantly higher ($p < 0.05$) than cements containing 5 wt% (Figure 3.5). Increasing PLR had a profound effect ($p < 0.05$) on the injectability of cement containing 5 wt% calcium chloride. It was also noted that the cement paste for the old batch containing 10 wt% calcium chloride at 3.0 g/ml had a very low viscosity to perform the test.

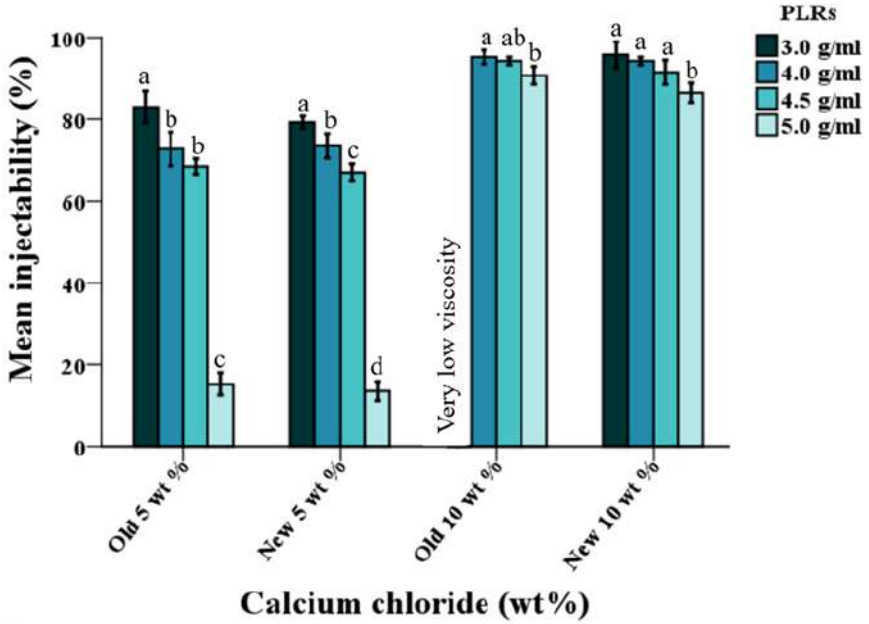

Figure 3.5: Mean injectability of old and new batches of PC containing 5-10 wt% calcium chloride at different PLRs. For both batches, increasing the concentration significantly ($p < 0.05$) improved the injectability within each PLR. The old batch containing 10 wt% calcium chloride at 3.0 g/ml seeped out of the syringe. Values are expressed as mean $\pm$ SD and dissimilar letters indicated significant differences ($p < 0.05$) between different PLRs at each concentration (n = 4).

Only the old batch containing 2 wt% sodium citrate at PLRs of 4.0 to 5.0 g/ml were injectable through the outlet diameter of 2 mm, while at a lower PLR the paste behaved as a liquid (Figure 3.6). Conversely, the addition of 2 wt% sodium citrate to the new batch caused flash setting of the cement which made it non-injectable. The flash setting of both batches also occurred when the concentration of sodium citrate was increased to 5 wt%.

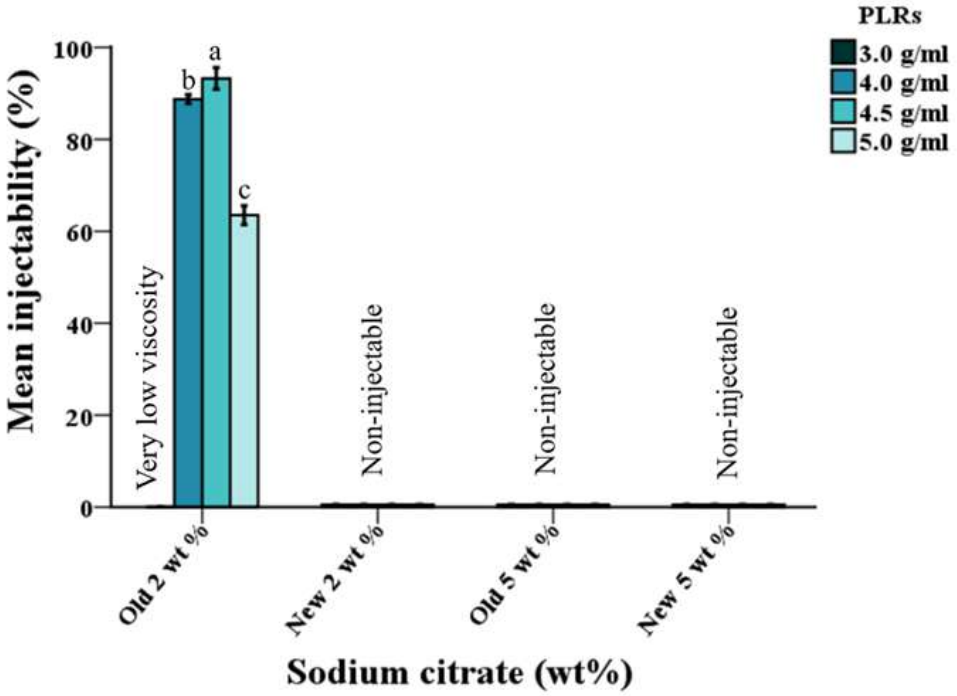

Figure 3.6: Mean injectability of old and new batches of PC cement containing 2-5 wt% sodium citrate at different PLRs. For 2 wt% sodium citrate addition, only the old batch at PLRs of 4.0 to 5.0 g/ml were injectable. Addition of 5 wt% sodium citrate caused flash setting of cements which were non-injectable. Values are expressed as mean $\pm$ SD and dissimilar letter indicated significant differences ($p < 0.05$) between different PLRs at each concentration (n = 4).

3.1.3 Compressive strength of old and new batches of PC containing additives

Following one day immersion of cements containing 5-10 wt% calcium chloride in DW at a PLR of 4.0 g/ml, the compressive strengths of both batches decreased significantly ($p < 0.05$) when the calcium chloride concentration was increased (Figure 3.7). Meanwhile, there was no significant difference ($p > 0.05$) between the batches containing 5-10 wt% calcium chloride.

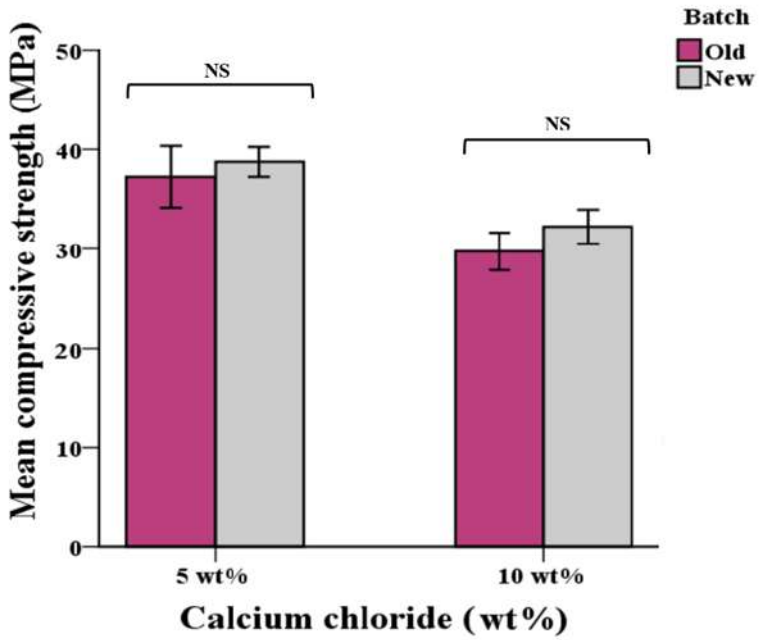

Figure 3.7: Mean compressive strength of old and new batches of PC containing 5-10 wt% calcium chloride at a PLR of 4.0 g/ml after one day of immersion. Increasing the concentration of calcium chloride reduced the strength significantly ($p < 0.05$), whilst there was no significant difference ($p > 0.05$) between batches at any concentration. Values are expressed as mean $\pm$ SD ($n > 7$, NS = non significant).

Similar to calcium chloride addition, increasing the concentration of sodium citrate for both batches significantly ($p < 0.05$) reduced the compressive strength of PC after one day of immersion at a PLR of 4.5 g/ml. In particular, the addition of 2 wt% sodium citrate to the new batch reduced the strength by 33 % compared with the old batch (Figure 3.8). There was no significant difference ($p > 0.05$) between two batches containing 5 wt% sodium citrate.

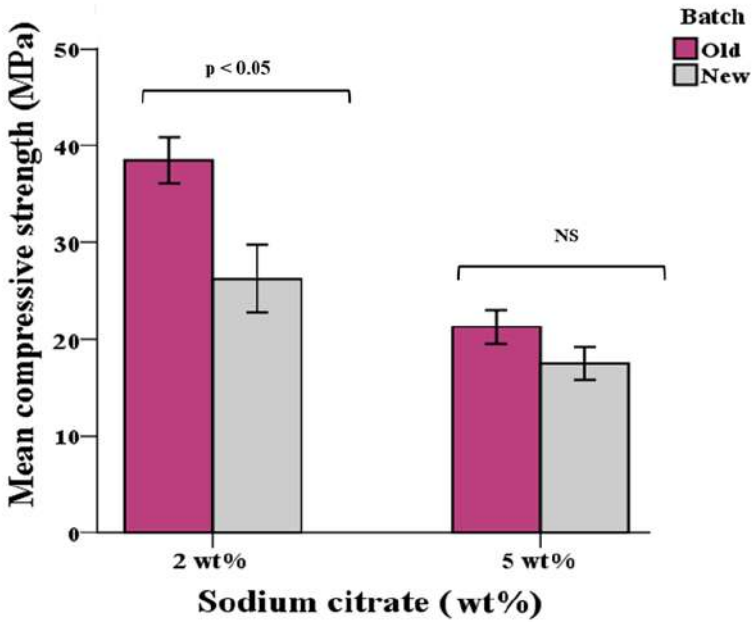

Figure 3.8: Mean compressive strength of old and new batches of PC containing 2-5 wt% sodium citrate at a PLR of 4.5 g/ml after one day of immersion in DW. Increasing the concentration of sodium citrate significantly reduced the strength for both batches. There was a significant ($p < 0.05$) difference between batches containing 2 wt% sodium citrate. Values are expressed as mean $\pm$ SD ($n > 7$, NS = non significant).

3.1.4 Relative porosity of old and new batches of PC containing additives

Increasing the calcium chloride concentration to 10 wt% increased the relative porosity of the both batches significantly ($p < 0.05$) for both batches after one day of storage in DW. On the other hand, there was no statistically significant difference ($p > 0.05$) in the total porosity of old and new batches of PC containing 5-10 wt% calcium chloride as shown in Figure 3.9.

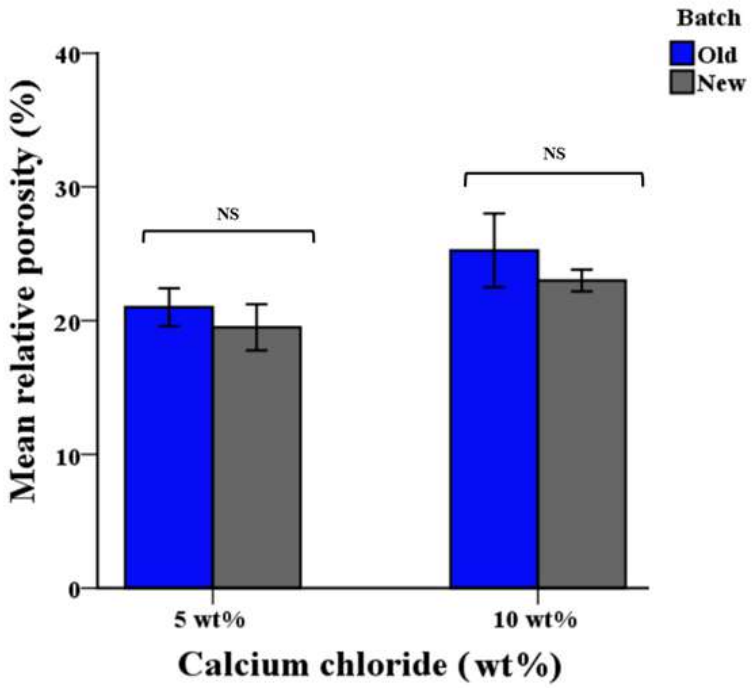

Figure 3.9: Mean total relative porosity of old and new batches of PC containing 5-10 wt% calcium chloride after one day of storage. There was no significant difference ($p > 0.05$) between old and new batches at any concentration. Values are expressed as means $\pm$ SD ($n > 7$, NS = non significant).

Moreover, the addition of a higher concentration of sodium citrate significantly increased the relative porosity ($p < 0.05$) of both batches after one day of storage. The new batch containing 2 wt% of sodium citrate had a significantly ($p < 0.05$) higher relative porosity compared with the old batch as shown in Figure 3.10. On the other hand, there was no significant ($p > 0.05$) difference between old and new batches of PC containing 5 wt% sodium citrate.

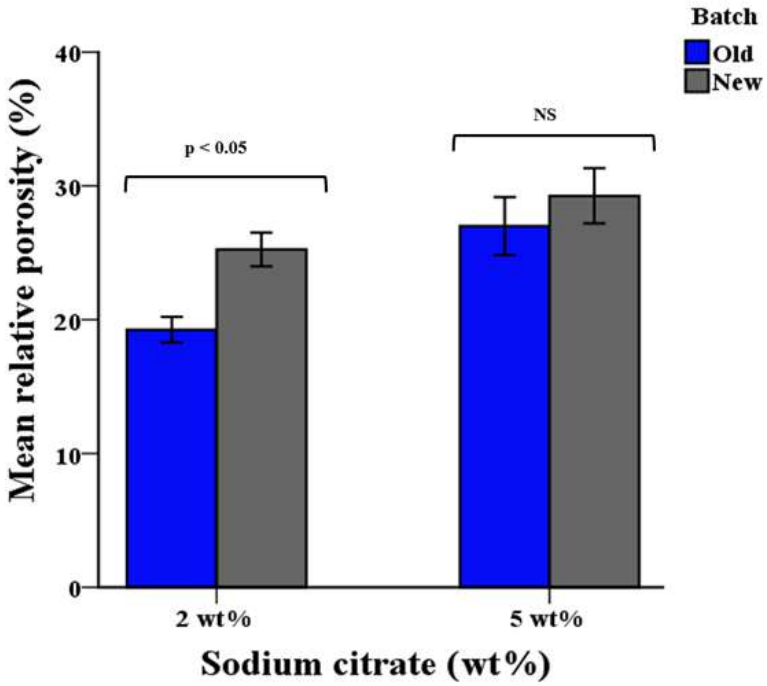

Figure 3.10: Mean total relative porosity of old and new batch of PC containing 2-5 wt% sodium citrate after one day of storage. The total porosity increased significantly ($p < 0.05$) by increasing the concentration of sodium citrate. There was a significant difference ($p < 0.05$) between old and new batches of PC when 2 wt% sodium citrate was added. Values are expressed as means $\pm$ SD ($n > 7$, NS = non significant).

3.1.5 Monitoring the hydration of PC using FTIR

Hydration analysis of old and new batches of PC using FTIR indicated that for cements containing 2 wt% sodium citrate, there was a decrease in the absorbance of OH stretching of water molecules at 3400-3500 cm^{-1} over 2 h. However, the υ_3 absorbance of SO_4^{2-} corresponded with unbound gypsum at 1100-1200 cm^{-1} was increased for the new batch (Figure 3.11 b) compared with the old batch (Figure 3.11 a) after 2 h.

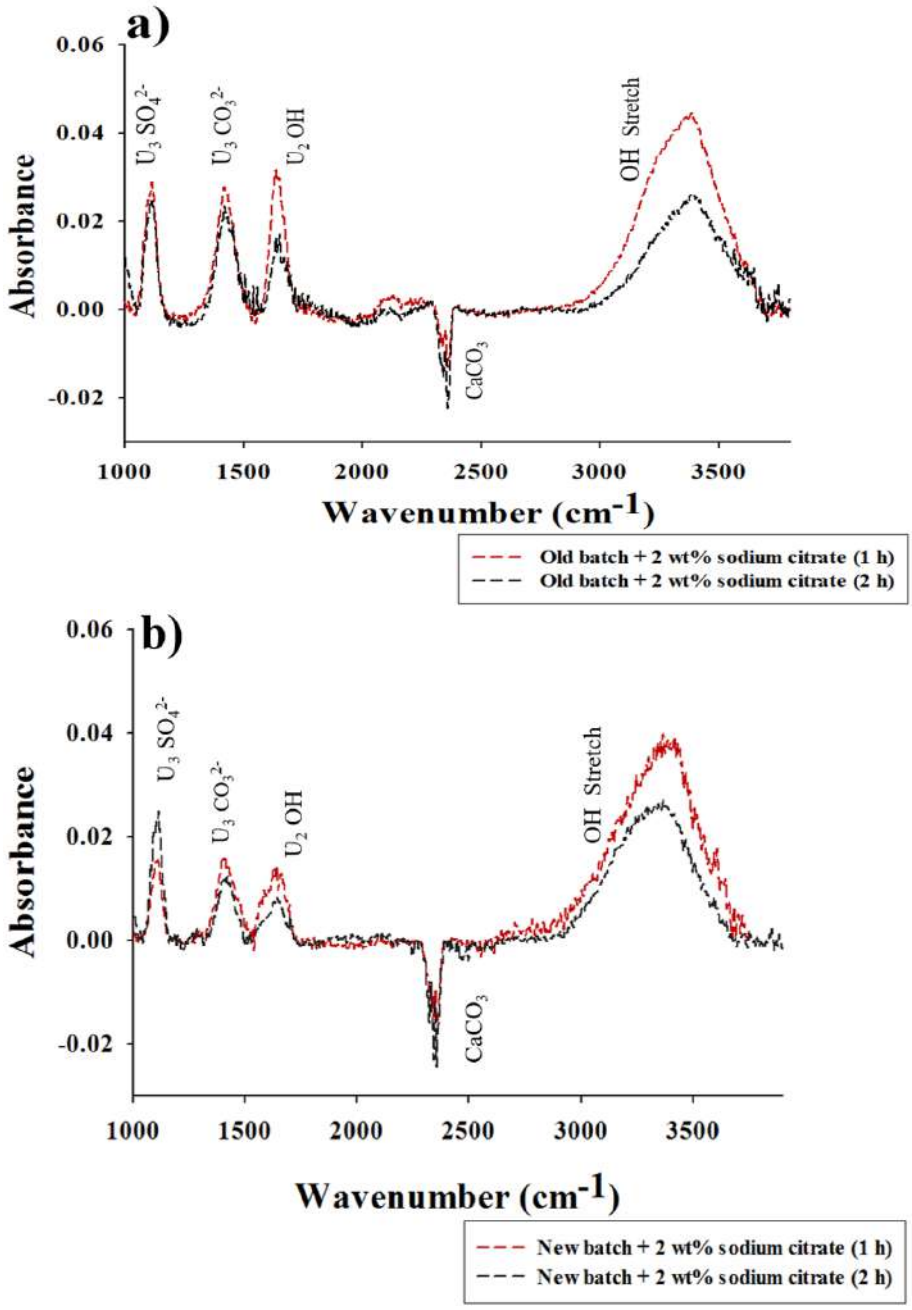

Figure 3.11: a) FTIR spectra of the old batch and **b)** new batch of PC containing 2 wt% sodium citrate during the first 2 h of hydration. For the new batch of PC there was a noticeable increased in the absorbance of υ_3 stretching of SO_4^{2-} that corresponded with unbound gypsum at 1100-1200 cm^{-1} after 2 h.

3.1.6 Elemental composition of PC batches

Comparison of the elemental composition of cement powder using EDS revealed that in the new batch, the average wt% of elements for the main clinker phases including calcium and silicon were noticeably higher compared with the old batch (Table 3.1). On the other hand, the old batch had a significantly ($p < 0.05$) higher amount of oxygen (51.22 %) compared with the new batch (47.01 %). There was a 13 % difference between observed and theoretical ratios of Ca/O for tetracalcium aluminoferrite in the new batch. This value was significantly higher for the old batch (approximately 30 %). Refer to appendix chapter, section 8.1 for full calculations.

Table 3.1: Average elemental analysis of old and new batches of PC using EDS. There were higher amounts of calcium and silicon in the new batch compared with the old batch. In contrast, the old batch had a higher oxygen content compared with the new batch. Dissimilar letter in rows indicated significant differences ($p < 0.05$).

Element	New batch		Old batch	
	Average wt%	SD	Average wt%	SD
O	47.01 (a)	2.12	51.22 (b)	0.85
Na	0.13 (a)	0.01	0.27 (a)	0.10
Mg	0.63 (a)	0.23	0.69 (a)	0.08
Al	1.99 (a)	0.41	1.90 (a)	0.53
Si	7.04 (a)	0.56	6.03 (a)	0.62
S	0.55 (a)	0.40	1.50 (a)	0.77
K	0.48 (a)	0.11	0.93 (a)	0.49
Ca	40.27 (a)	1.53	35.83 (b)	0.26
Fe	1.89 (a)	0.49	1.63 (a)	0.56

3.1.7 Phase analysis of new and old batches of PC using XRD

Studies of the phase analysis has shown that peak intensities for the old batch were relatively lower than the new batch (Figure 3.12). The full-width half peak maximum (FWHM) measurements using the Gaussian function, indicated that there was a general degradation of cement over time. The measured values corresponded with calcium silicates and aluminate phases (see table below) were relatively higher in the new batch than the old batch. In contrast, FWHM value for the calcite was higher in the old batch instead.

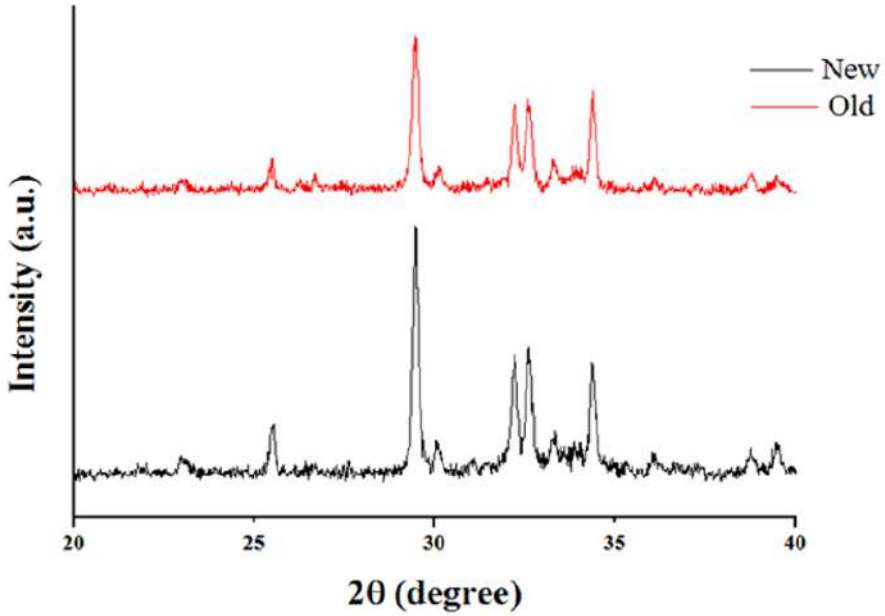

Peaks	2θ (°)	Full-Width at half maximum (FWHM)	
		New batch	Old batch
Calcite	29.4	0.194	0.211
Calcium silicate and aluminate phases	32.5	0.218	0.192
	32.8	0.212	0.197
	34.1	0.192	0.184

Figure 3.12: XRD spectra of new (black line) and old batches (red line) of PC with the table indicating the FWHM values for the clinker phases. Peaks intensities for the new batch were greater than for the old batch. Except for calcite peak, the FWHM values for calcium silicates and aluminate phases were higher in the new batch compared with the old batch.

3.2 Discussion

3.2.1 The effect of ageing on the setting times and injectability

3.2.1.1 PC setting times

The effectiveness of calcium chloride for reducing the setting time of PC was unaffected by the ageing process, whilst the new batch of PC created a narrower working window (in terms of wt%) when sodium citrate was used as the additive. In the literature, hydroxycarboxylic acids including sodium citrate have been reported to have a dual effect by acting as a retardant at low concentrations and as an accelerant when used at 5 wt% and higher [143, 144, 145]. However, in the present study examination using FTIR of the cement with addition of 2 wt% sodium citrate (Figure 3.11) revealed that, the peak increased at 1100 cm^{-1} corresponded with unbound gypsum [14]. As PC contains approximately 5 wt% of gypsum to control the reactivity of C_3A [59, 60], citrate addition to the new batch might have removed the protective layer of gypsum as the amount of unbound gypsum increased over time. As a result, the aluminate phases could have reacted with the water to form the undesirable C-A-H, which caused flash setting (Figure 3.2) [6, 14, 60].

In 2014, this behaviour was observed by Wynn-Jones *et al.* when 5 wt% sodium citrate was added to PC, while 2 wt% did not cause a flash set [6, 14, 146]. Although in this study usage of new or old batch has not been stated, but the present study concluded that ageing of the cement had a significant effect on the effectiveness of sodium citrate. During storage of the cement, the clinker phases could have been in contact with water

vapour and this may have led to the agglomeration of the old PC batch which reduced the reactivity of the main clinker phases including C_3S. However, the mechanism by which sodium citrate either acts as a retardant or an accelerant is not understood completely.

3.2.1.2 PC injectability

The first aim of injectability testing was to examine whether an injectability of higher than 90 % could be achieved by lowering the PLR of the cement to 2.0 g/ml. It was shown that an injectability of 90 % was achieved for both old and new batches of PC (Figure 3.3) without any liquefying agents. Unfortunately, at this PLR the cement sedimented at the bottom of the syringe causing phase-separation (Figure 3.4). This phenomenon has been reported to cause many problems for PVP including poor injectability, increasing porosity and decrease in compressive strength [6, 10, 52, 147, 148].

Increasing the concentration of calcium chloride improved the injectability of PC (Figure 3.5) presumably via charge neutralisation of cement particles as suggested by Wynn-Jones *et al* [6, 13]. Conversely, increasing the concentration of sodium citrate made the paste non-injectable (Figure 3.6). This behaviour showed that removal of gypsum from the surface of C_3A not only caused flash setting of the cement, it also limited its injectability. Unfortunately, when the new batch of PC with 2 wt% sodium citrate was used, flash setting still occurred which limited the use of this additive for further experiments in this study.

3.2.2 Influence of batch variation and additives on the strength and porosity

Both calcium chloride and sodium citrate have been reported to act as setting accelerant for PC-based cement according to previous studies [6, 13, 149]. Therefore, it was expected to observe an increase in the compressive strength of the cement as the concentration of additives increased, however the opposite was observed (Figure 3.7 and 8). Results obtained for calcium chloride addition also indicated that, the reduction in the strength of the cement that occurred when additives were increased, may have happened due to an increase in the relative porosity of the cements. This could have reflected a higher proportion of additives being washed out during setting of the cement which was also reported by Wynn-Jones *et al* [13].

The lower porosity of the old batch containing 2 wt% sodium citrate (Figure 3.10) indicated that more water was consumed during hydration of PC [102]. However, the significant decrease in the strength of the new batch of PC may have occurred mainly due to the flash setting of the cement (Figure 3.8). The rapid onset of the cement which was accelerated by the increase in the concentration of sodium citrate, did not allow the consumption of the water by reactants. Therefore, these interactions increased the relative porosity of the cement.

To summaries, the PC model system containing 75 wt% PC, 20 w% bismuth oxide and 5 wt% calcium chloride demonstrated the most appropriate properties to fulfil the

requirements of suitable bone cement for PVP. Thus, this model system was chosen for further experiments

3.2.3 Effect of ageing on elemental and phase composition of PC

3.2.3.1 Elemental analysis of PC powder

Following the FTIR analysis (Figure 3.11) which indicated a clear difference in the amount of unbound gypsum during the early hydration of old and new batches of PC, further characterisation of the PC was undertaken using EDS to identify the consistency of the starting material. The EDS analysis (Table 3.1) indicated that the amount of calcium and oxygen were significantly lower and higher respectively in the old batch compared with the new batch. This may have occurred due to the partial carbonation of cement powder which has been reported previously [150, 151]. In addition, the difference between the optimum and theoretical ratios of the clinker phases was higher in the old batch compared with the new batch which could suggest the partial reaction of PC with water vapour and carbon dioxide [62].

3.2.3.2 Phase composition of PC

Due to the partial hydration of the old batch, it was expected to identify peaks corresponded with hydration phases for the old batch (Figure 3.12), however no trace of hydration phases was detected. This could have occurred due to forming very small amounts of hydration phases in the amorphous phase (e.g. C-S-H) which could not be identified by

XRD [152]. Additionally, the reactant may have partially degraded into compounds with similar structure to the clinker phases which were unable to interact with water forming the main hydration phases [6]. However, previous studies reported formation of Portlandite and C-S-H but in their study the cement was heated at an elevated temperature. This could have transformed the amourphous C-S-H to crystalline phase [150, 151].

As a result, the clinker phases may have agglomerated and decreased the reactivity of cement which limited its interaction with additives such as sodium citrate. Therefore, the consistency of cement batches was shown to be an important factor for future commercial products.

3.3 Summary

Calcium chloride acted as both an accelerant and liquefying agent for the both batches of PC, whilst the new batch of PC reduced the working window for sodium citrate. Addition of 2-5 wt% sodium citrate appeared to remove the gypsum at the surface of the C_3A phase and caused flash setting of the cement. This resulted in poor injectability and a loss in compressive strength. Thus, for the next two chapters only the new batch of PC with 5 wt% calcium chloride addition was used and investigated.

Chapter 4

Investigation of soluble porogens for inducing macroporosity

4.1 Results

4.1.1 Setting time measurements

The highest setting time values were achieved when 20 wt% mannitol was added to PC at all PLRs (Figure 4.1). In comparison, 1 to 10 wt% mannitol additions all decreased setting times to levels lower or comparable ($p > 0.05$) with the control except for 10 wt% mannitol at 4.0 g/ml.

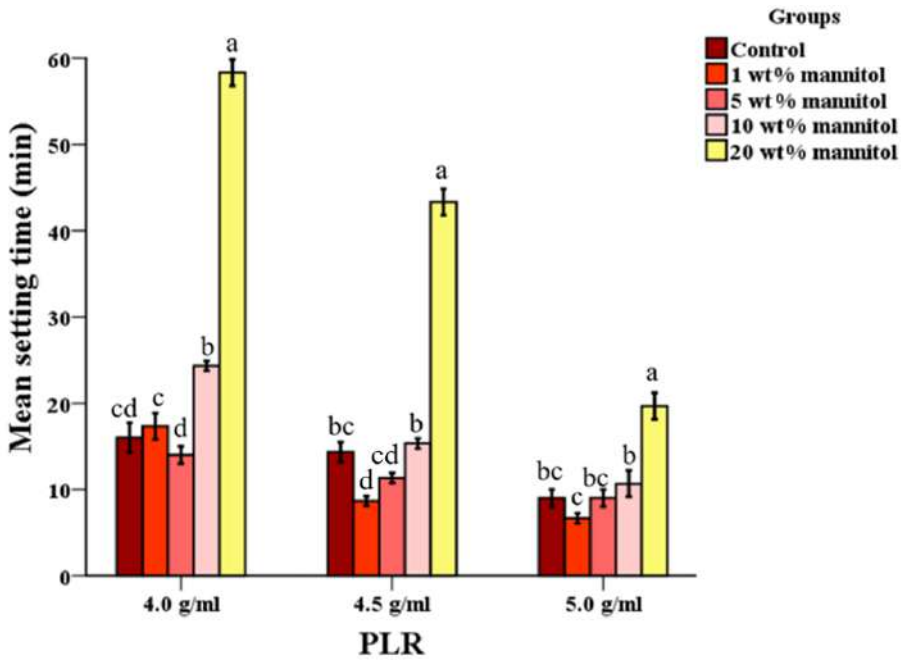

Figure 4.1: Mean setting time of control and cements with 1-20 wt% mannitol additions at different PLRs. Addition of 20 wt% mannitol significantly ($p < 0.05$) retarded the setting time compared with lower concentrations. Values are expressed as mean $\pm$ SD. Dissimilar letters indicated significant differences ($p < 0.05$) between different groups at each PLR (n = 3).

Similar to mannitol, the addition of 20 wt% sucrose retarded the setting time significantly ($p < 0.05$) compared with the control at all PLRs (Figure 4.2). At PLRs of 4.0 and 4.5 g/ml, the addition of 1 wt% sucrose also acted as a retardant ($p < 0.05$). In case of samples with 5 and 10 wt% sucrose, the setting time significantly increased ($p < 0.05$) at a PLR of 5.0 g/ml compared with the control.

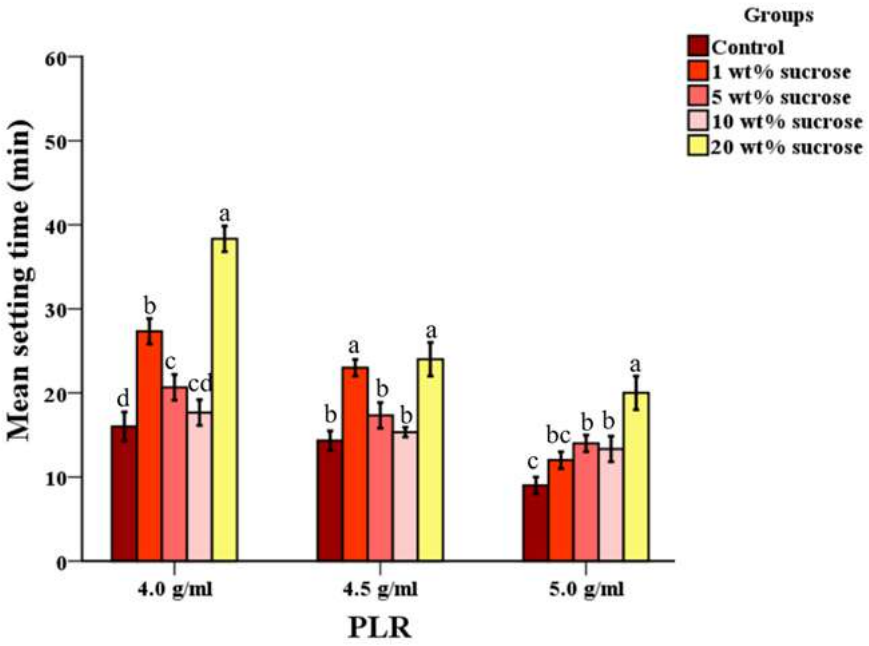

Figure 4.2: Mean setting time of control and cements with 1-20 wt% sucrose additions at different PLRs. Addition of 1 or 20 wt % sucrose significantly lengthened ($p < 0.05$) the setting time compared with the control. Values are expressed as mean $\pm$ SD. Dissimilar letters indicated significant differences ($p < 0.05$) between different groups at each PLR (n = 3).

Addition of sodium bicarbonate reduced the workability of PC, which resulted in the paste becoming too dry to handle. Results obtained have shown that for PLRs of 4.0 and 4.5 g/ml, addition of 1 or 5 wt% significantly ($p < 0.05$) reduced the setting time to less than 10 min in comparison to the control. Regardless of the concentration of sodium bicarbonate used, at a PLR of 5.0 g/ml cements were too dry to form a homogeneous paste to allow setting time measurements to be carried out (Figure 4.3).

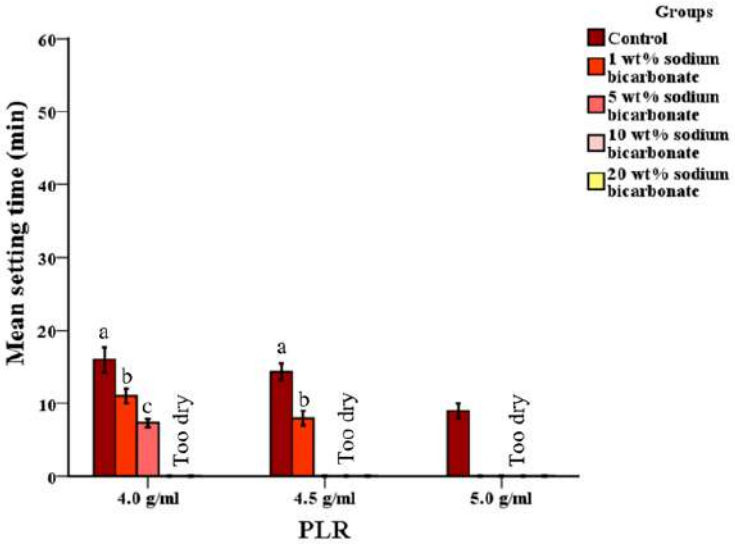

Figure 4.3: Mean setting time of control and cements with 1-20 wt% sodium bicarbonate additions at different PLRs. Addition of 1 or 5 wt% sodium bicarbonate significantly ($p < 0.05$) reduced the setting time at PLRs of 4.0 and 4.5 g/ml. While, at higher concentrations, cements were too dry to allow setting time measurements to be measured. Values are expressed as mean $\pm$ SD. Dissimilar letters indicated significant differences ($p < 0.05$) between different groups at each PLR (n = 3).

4.1.2 Injectability measurements

Addition of only 1 wt% mannitol was enough to significantly ($p < 0.05$) improve the injectability of cements at PLRs of 4.0 and 4.5 g/ml compared with the controls. Unfortunately, with all the concentrations above 1 wt%, the paste started to act as a liquid and could not withstand its own weight which prevented the injectability testing from being carried out (Figure 4.4).

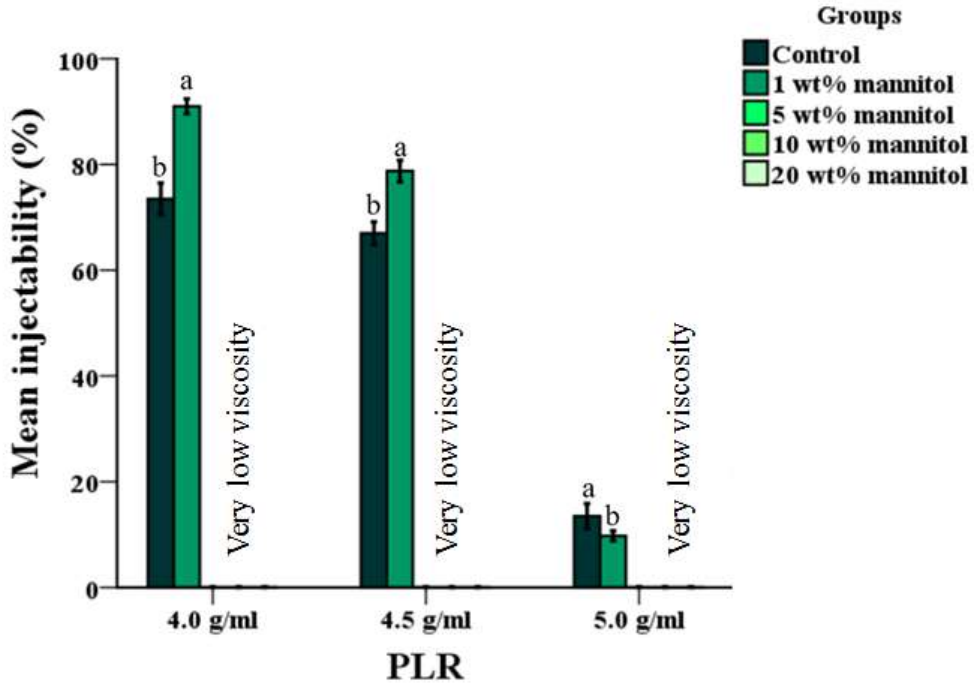

Figure 4.4: Mean injectability of control and cements with 1-20 wt% mannitol additions at different PLRs. Exceeding the concentration of 1 wt% made the paste to act a liquid. Values are expressed as mean ± SD. Dissimilar letters indicated significant differences ($p < 0.05$) between different groups at each PLR (n = 4).

For samples containing 1 and 5 wt% sucrose at PLRs of 4.5 and 5.0 g/ml, the injectability improved significantly ($p < 0.05$) compared with the controls. The highest injectability values were obtained for 5 wt% sucrose addition. Meanwhile, at 4.0 g/ml only 1 wt% sucrose was injectable through the needle. At higher concentrations, cements seeped out of the syringe prior to injectability testing (Figure 4.5).

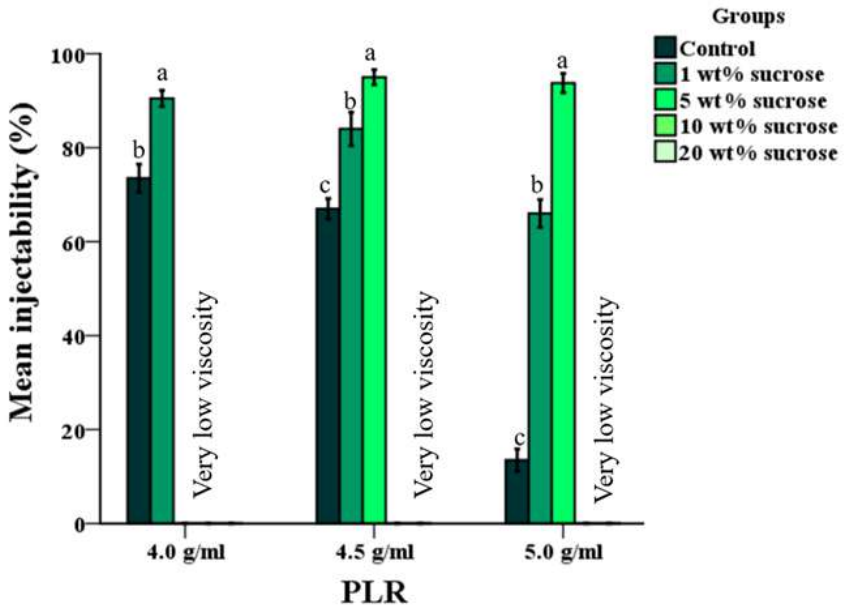

Figure 4.5: Mean injectability of control and cements with 1-20 wt% sucrose additions at different PLRs. Only addition of 1 or 5 wt% sucrose improved the injectablility significantly. Whilst at higher concentration, the paste behaved as a liquid. Values are expressed as mean $\pm$ SD. Dissimilar letters indicated significant differences ($p < 0.05$) between different groups at each PLR (n = 4).

Addition of 1 wt% sodium bicarbonate significantly reduced ($p < 0.05$) the injectability of cement by 58 % and 75 % compared with the control at PLRs of 4.0 and 4.5 g/ml respectively. Whereas, the addition of 5 to 20 wt% of sodium bicarbonate made the paste too dry to form a homogeneous paste to perform the injectability testing. In comparison, none of the sodium bicarbonate groups were injectable when PLR of 5.0 g/ml was used as the paste became too dry (Figure 4.6).

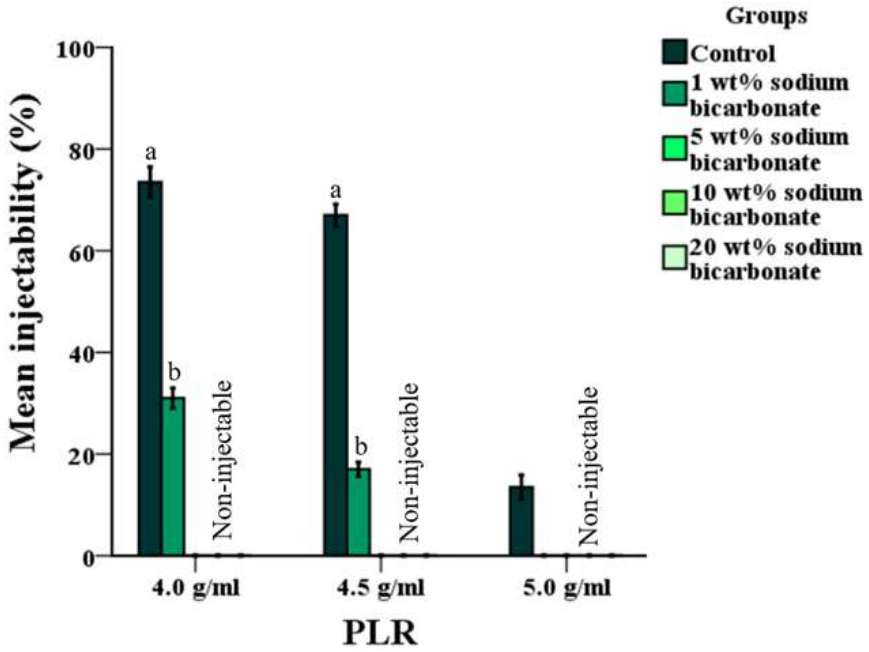

Figure 4.6: Mean injectability of control and cements with 1-20 wt% sodium bicarbonate additions at different PLRs. Exceeding the concentration of 1 wt% made the paste too dry for injectability testing at PLRs of 4.0 and 4.5 g/ml. At 5.0 g/ml, all the sodium bicarbonate groups were non-injectable. Values are expressed as mean ± SD. Dissimilar letters indicated significant differences ($p < 0.05$) between different groups at each PLR ($n = 4$).

4.1.3 Compressive strength and relative porosity studies

The groups of cements that possessed the injectability of more than 80 % and suitable setting times upon addition of mannitol were selected for compressive strength and porosity studies. The addition of 1 wt% mannitol at 4.0 and 4.5 g/ml significantly ($p < 0.05$) reduced the compressive strength after 7 days by 90 and 87 % respectively compared with the control (Figure 4.7 a). At the same time, the relative porosity of mannitol containing groups were doubled compared with the control (Figure 4.7 b).

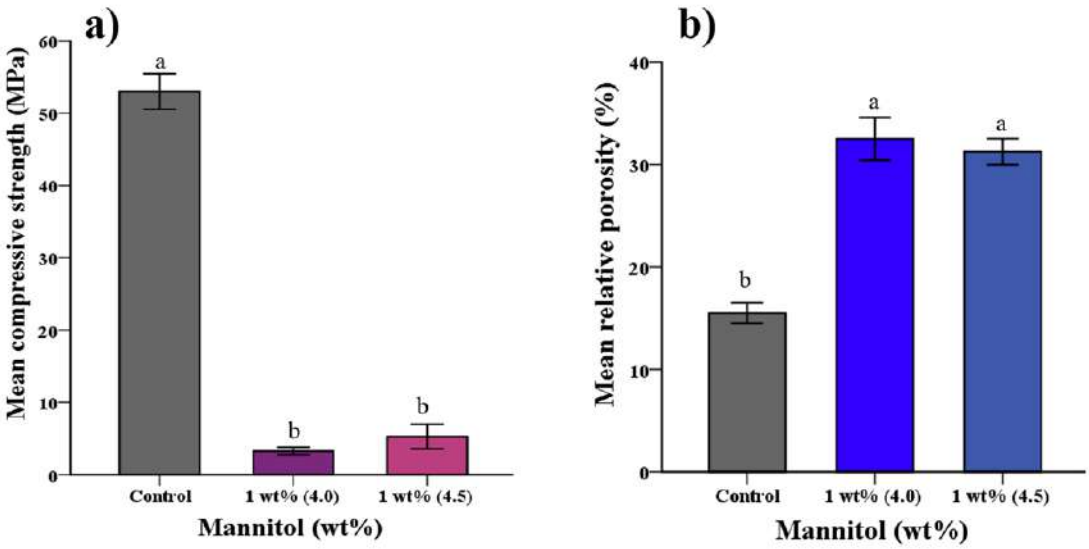

Figure 4.7: a) Compressive strength and **b)** relative porosity of control and cements containing 1 wt% mannitol at different PLRs after 7 days in DW. Addition of mannitol significantly ($p < 0.05$) reduced the strength and increased the total porosity compared with the control. Values are expressed as mean $\pm$ SD. Dissimilar letters indicated significant differences ($p < 0.05$) between different groups ($n > 7$).

Furthermore, groups containing 1 and 5 wt% sucrose at PLRs of 4.0 to 5.0 g/ml were selected for compressive strength and porosity studies. Addition of sucrose at both concentrations significantly ($p < 0.05$) reduced the compressive strength of the cement compared with the control after 7 days in DW. Increasing both PLR and concentration of sucrose improved the strength ($p > 0.05$) as shown in Figure 4.8 a. Meanwhile, addition of sucrose at any concentration significantly increased ($p < 0.05$) the total porosity compared with the control (Figure 4.8 b).

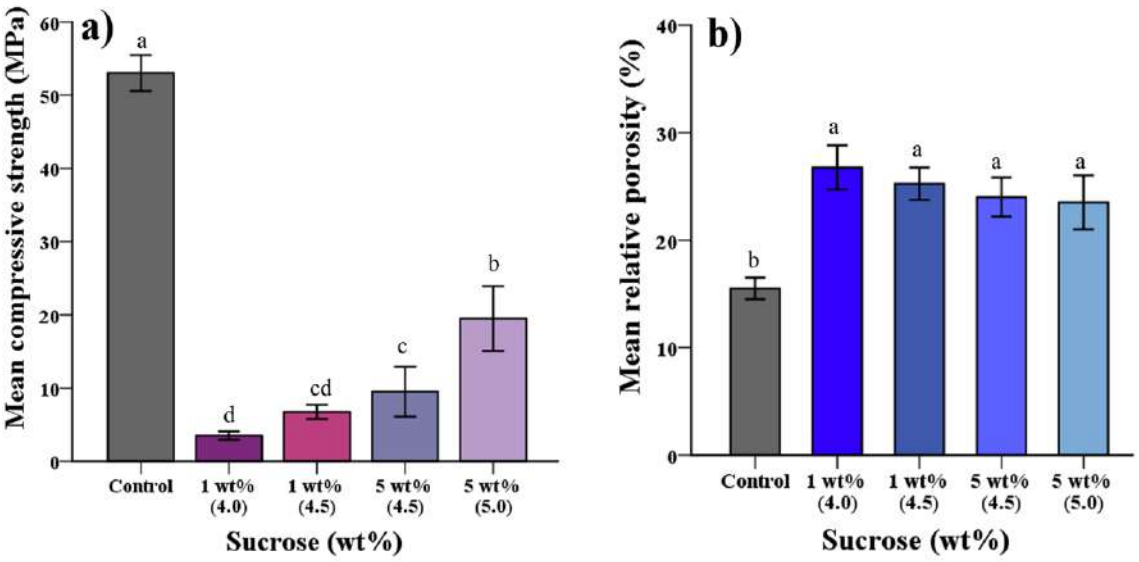

Figure 4.8: **a)** Compressive strength and **b)** relative porosity of control and cements containing 1 or 5 wt% sucrose at different PLRs after 7 days in DW. Addition of sucrose at any concentration and PLR significantly ($p < 0.05$) reduced the strength and increased the porosity compared with the control. Values are expressed as mean $\pm$ SD. Dissimilar letters indicated significant differences ($p < 0.05$) between different groups ($n > 7$).

4.1.4 Compressive strength as a function of porosity

Plotting natural logarithms of 7-day compressive strengths against relative porosity for the control and porogen containing cements is shown in Figure 4.9. A strong linear relationship ($R^2 = 0.95$) was fulfilled once sucrose was added to the PC-based cement. However, the control PC departed from this linear relationship, thus sucrose addition altered materials constant of PC-based system.

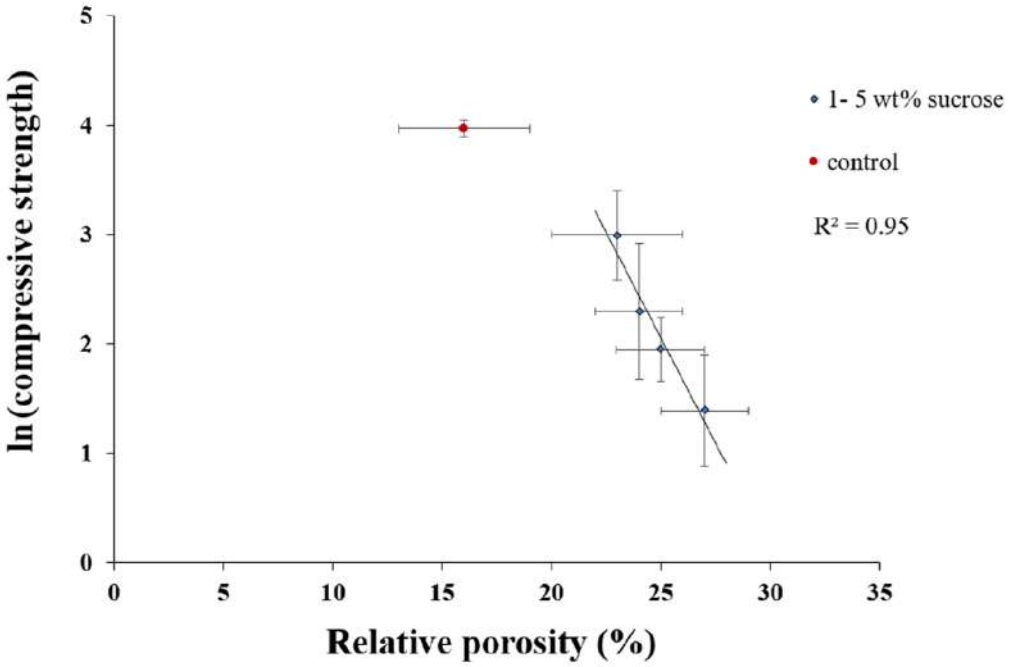

Figure 4.9: The strong linear relationship between ln(compressive strength) and relative porosity of cement with 1-5 wt% sucrose additions. Departure of control cement from this relationship was an indication of the strength-deteriorating effect of sucrose.

4.1.5 Strut density studies

Addition of soluble porogens significantly increased ($p < 0.05$) the strut densities of PC after 7 days of storage compared with control (Figure 4.10). In addition, those group containing 1 wt% mannitol had the highest strut density of 3.04 g/cm^3 compared with 2.56 g/cm^3 for the control.

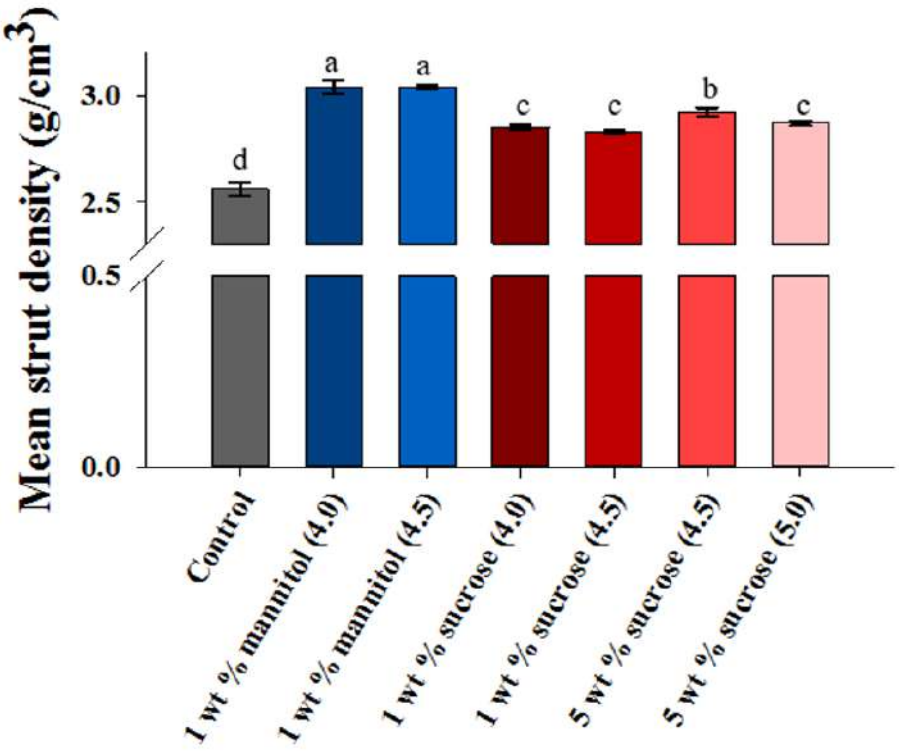

Figure 4.10: Mean strut densities of control and groups containing different concentrations of porogens. The strut densities of all modified cements significantly ($p < 0.05$) increased compared with the control. Values are expressed as mean $\pm$ SD. Dissimilar letters indicated significant differences ($p < 0.05$) between different groups ($n > 7$).

4.1.6 Surface topography using SEM

SEM examination of fractured surface of cements at a low magnification indicated that addition of 1 wt% mannitol (4.0) did not increase the surface porosity compared with the control (Figure 4.11). However, there were multiple cracks in samples containing mannitol compared with the control. At a higher magnification, the surface of the control was predominantly covered by 5-10 μm needle-like ettringite crystals and large hexagonal crystals of calcium hydroxide. On contrary, mannitol containing group possessed mainly ettringite crystals with traces of unhydrated powder reactant. The SEM micrograph for 1 wt% mannitol at 4.5 g/ml indicated that there were less pores and cracks compared with 1 wt% mannitol at 4.0 g/ml (Figure 4.11).

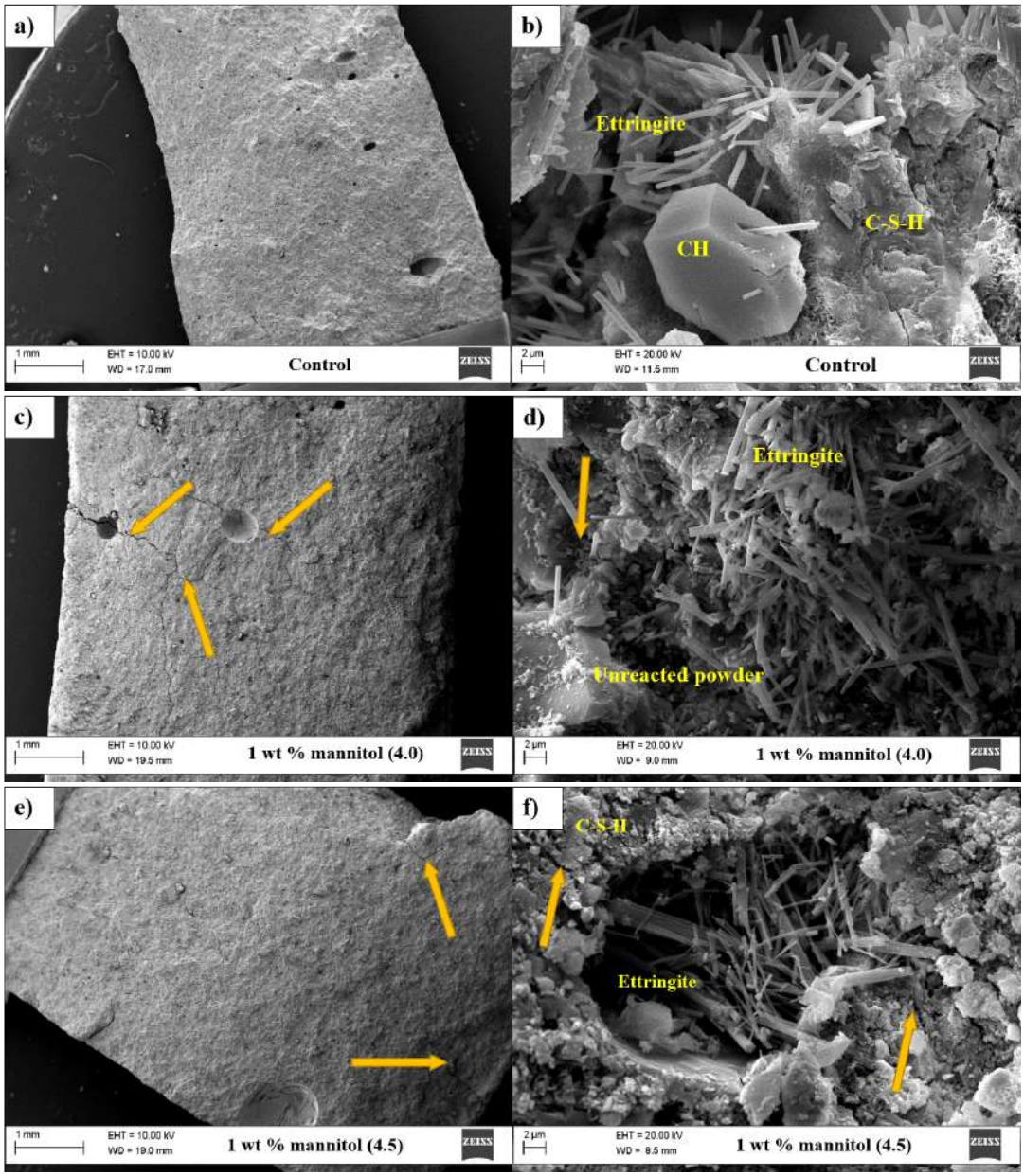

Figure 4.11: SEM micrographs of control (a and b), 1 wt% of mannitol at 4.0 g/ml (c and d) and at 4.5 g/ml (e and f) at x40 and x6500 respectively. There was no increase in surface porosity upon addition of mannitol, except there were more cracks (indicated by arrows) compared with the control. Control PC revealed large crystals of calcium hydroxide (CH) which were not identifiable in the mannitol group.

SEM micrographs for 1 wt% sucrose at PLRs of 4.0 and 4.5 g/ml also indicated that there was no increase in the surface porosity of the cement compared with the control (Figure 4.12). However, the microstructural examination illustrated that sucrose groups possessed aggregate-like crystals and shorter needle-like ettringite crystals surrounded by multiple microcracks.

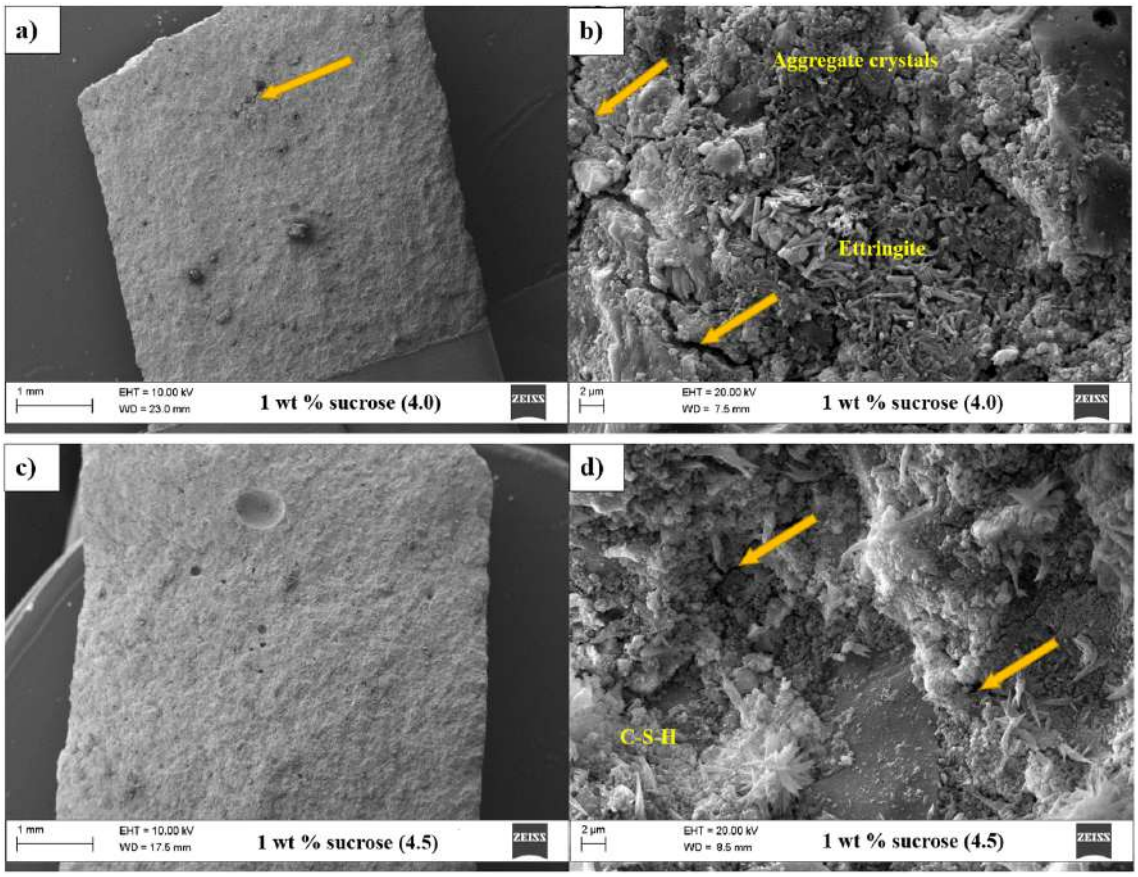

Figure 4.12: SEM micrographs of 1 wt% sucrose at 4.0 g/ml (a and b) and 4.5 g/ml (c and d) at two magnifications of x40 and x6500 respectively. The surface of cement for both groups were smooth with few pores. At high magnification, both group possessed C-S-H gel and shorter ettringite crystals with microcracks (indicated by arrows).

Increasing the concentration of sucrose to 5 wt% at PLRs of 4.5 and 5.0 g/ml had no influence on the surface porosity of the set cement as shown in Figure 4.13. In addition, ettringite crystals and multiple microcracks were still observed.

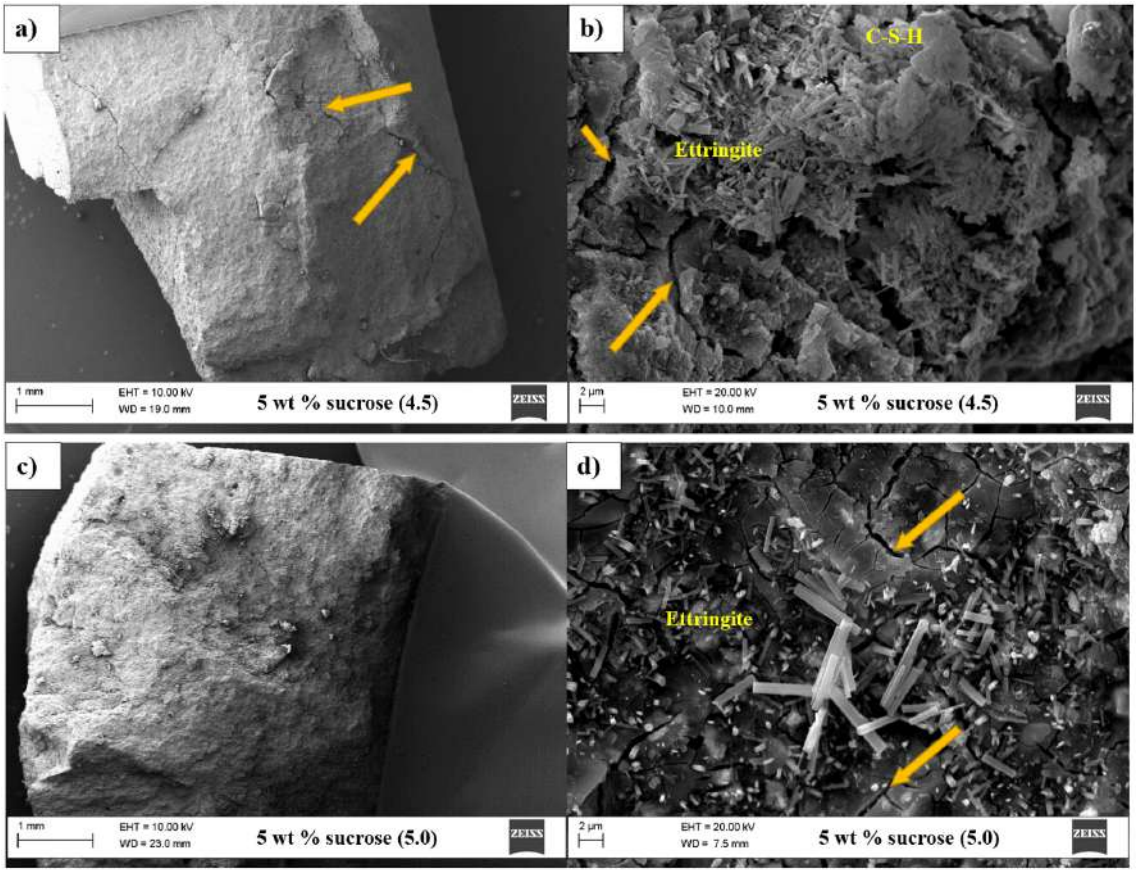

Figure 4.13: SEM micrographs of 5 wt% sucrose at PLRs of 4.5 g/ml (a and b) and 5.0 g/ml (c and d) at two magnifications of x40 and x6500 respectively. There were multiple cracks at the surface of cement (indicated by arrows). Whilst, both group possessed clusters of needle-like ettringite crystals.

4.2 Discussion

4.2.1 Influence of sugars and bicarbonate on setting time and injectability of PC

4.2.1.1 Addition of mannitol

Addition of sugars such as sucrose and mannitol have been shown to induce macroporosity for the CPC system [104, 106, 122, 153], however, these sugars are also known to act as a retardant [154, 155, 156]. The results determined (Figure 4.1-5) in the present study confirmed the negative effect of these two sugars on the setting time and injectability of the PC. In fact, even in the presence of a strong accelerant (calcium chloride), the adverse effect of aforementioned sugars was noticeable.

Addition of the sugar as low as 1 wt% caused a liquefying effect on the cement's injectability compared with the control (Figure 4.4). This behaviour may have occurred due to the solubilising effect of organic admixtures on the PC-based cement according to multiple studies [154, 155, 156]. Sugars are categorised according to their stability in alkaline conditions into two groups: a not stable reducing sugar (mannitol) and a stable non-reducing sugar (sucrose) [156]. Hydration of reactive clinkers including C_3A and C_3S increased the local pH and the reducing sugars have shown to be unstable in this condition [156]. Subsequently, mannitol underwent a ring-opening and degradation process to form saccharinic acid. This acid contains (OH-C-C=O) group which may have acted as a ligand to form complexes with metal ions present within the cement phases. As a result,

dissolution of the ions from calcium-silicate phases is promoted which increased the concentration of ions in the solution [154, 156]. Moreover, the sugar-metal ions complexes could also precipitate on the surface of reactants during the hydration of the cement which prevented the precipitation of hydration phases such as C-S-H and Portlandite, thus only increased the dissolution of ions [157, 158].

4.2.1.2 Addition of sucrose

Sucrose has been shown to be stable at a high pH, thus it interacted with the surrounding $Ca^{+}OH$ to form a half-salt RO^{-}—-$Ca^{+}OH$ which could interact with the surrounding sucrose to form bulky saccharides [156, 159]. This set of reactions would favour the Ca, Al and Fe ions chelation which may have precipitated on the lattice site of C-S-H and Portlandite. Resultant interactions could lead to the accumulation of calcium and hydroxide ions in the solution, which poisoned the hydrate surfaces in a similar manner to mannitol [154, 156, 160].

To summarise, the interactions of sugars could have two major influences on the setting of PC-based cement; firstly, accelerating the dissolution of the cement reactants without precipitation of hydration products (poisoning effect), thus retarded the setting time. Secondly, coating the clinker surface with sugars has been shown to increase the negative surface charge of cement particles. The net charge formed might have caused an electrostatic repulsion between particles and hence a liquefying effect [154, 156]. Couple of studies have shown that reducing sugars have a 10-fold greater affinity for the calcium

than non-reducing sugars, thus mannitol could have had a stronger solubility effect on the cement, which correlated with the injectability results (Figure 4.4-5) [154, 156].

4.2.1.3 Addition of sodium bicarbonate

Addition of sodium bicarbonate between 1 and 10 g/l has been previously shown to act as strong retardants for PC without any additives due to formation of tetracalcium aluminate carbonate 12-hydrate [161]. However, in the present study, addition of 1-20 wt% of sodium bicarbonate made the paste too dry (Figure 4.6). This contradictory result could have arisen due to using a higher PLR in the present study. Additionally, the bicarbonate in solution could have created an intermediate form of carbonic acid and possibly introduced hydrogen ions into the liquid phase [162]. Consequently, the hydrogen ions might have disrupted the setting reaction of PC in a similar manner to citric acid as described by Wynn-Jones *et al* [14, 162].

4.2.2 Effect of sugars on setting of PC

4.2.2.1 The compressive strength and relative porosity of PC

The incorporation of both mannitol and sucrose, significantly reduced the compressive strength of cements (Figures 4.7 and 8). The retardation and solubilisation effects of the sugars could have increased the amount of unconsumed water, which increased the relative porosity of cements containing porogens compared with controls (Figures 4.7 and 8) [154, 158]. Increasing relative porosity inversely alters the compressive strength

thus, in the present study with increasing sugar concentrations it was expected to observe an increase in the relative porosity but the opposite was observed (Figures 4.7 and 8). This could be explained by the greater degree of solubilisation of the cement paste at higher concentrations, which improved the workability of the paste. The better workability is an indication of a superior flow properties of the cement paste, while no segregation takes place [163, 164]. This highlighted that having a sufficient working time to mix the paste could have a significant effect on the ultimate properties of the cement [163, 164].

4.2.2.2 The strut density of PC

The dense powder (3.1 g/cm^3) was hydrated into a less dense structure (2.5 g/cm^3) by reacting with water [6, 102]. Hence, a low strut density was an indication of a high degree of hydration [6, 5]. However, the modified cements indicated a lower degree of hydration compared with the control PC (Figure 4.10) which potentially arose due to the inhibitory effect of sugars on the precipitation of hydration phases.

The strut density result was supported by microstructural analysis which demonstrated higher numbers of unreacted particles compared with control (Figure 4.11). The strength-deteriorating effect of sugars (Figure 4.9) also confirmed the detrimental effect of these porogens on cement's setting possibly by altering the materials constant such as critical flaw size. Studies on CPCs have shown that the inhibitory effect of mannitol on the setting of the cement was temporary as the XRD data indicated no major difference [104, 153]. On the other hand, the strut densities obtained could suggest that the adverse effect of

sugars lasted longer in PC-based cements. Either of sugar used, mannitol containing cements had the highest strut density values compared with sucrose. This could be again explained by the greater affinity of mannitol for calcium which accelerated its inhibitory effects.

4.2.3 Effect of sugars on macro and microstructure of the set cement

4.2.3.1 Macrostructure of PC

Despite the increase in the relative porosity of the samples containing porogens, SEM analysis after 7 days indicated no induction of macropores nor major difference between the modified cements and control PC (Figure 4.11-13). In the literature, the induction of large interconnected pores in CPCs upon addition of mannitol and sucrose has been reported even after 5 days of setting [105, 106, 122, 153]. This contradictory observation might have occurred due to the greater degree of adsorption and interaction of sugars on the surface of PC reactants, which limited the dissolution of these sugars during the setting of the cement to induce macroporosity.

4.2.3.2 Microstructure of PC

The microstructure studies indicated that in the presence of organic admixtures, the typical large needle-like ettringite crystals did not develop compared with the control PC (Figure 4.11-13). It has been shown by multiple studies that the size and density of ettringite crystals can be altered by additives [14, 65, 144, 165]. The capability of

sugars to interact with calcium and aluminium phases is due to the presence of multiple hydroxyl groups (-OH) within the structure of sugars. These hydroxyl groups could have undergone deprotonation to create multidentate charged molecules and hydrogen ions (H^+) [166]. As a result, these hydrogen ions might have reduced the local pH below the range (10.5-13.0), which ettringite is generally stable thus limiting its formation [166]. Therefore, a less stable mineral; calcium aluminate monosulphate was formed which did not contribute toward the early strength of PC [166]. This was in accordance with previous studies which observed the similar influence upon addition of 2-5 wt% sucrose to the PC [144, 166].

In addition, SEM micrographs indicated the presence of multiple microcracks within the samples containing sugars. Studies revealed that in the presence of sugars, a secondary ettringite was more likely to be formed once the cement hardened [144, 167]. This secondary ettringite was shown to exert expansive forces upon the surrounding crystals which could have led to cracking and disintegration of the cement and therefore loss of compressive strength [144, 167].

4.3 Summary

Addition of soluble porogens including sugars and sodium bicarbonate to PC had an adverse effect on the setting reaction of this novel cement. Sugars retarded the setting reaction through a series of adsorption, precipitation and poisoning of the nucleation sites

for C-S-H and Portlandite, which adversely influenced the setting time, injectability and compressive strength [154, 156]. Conversely, sodium bicarbonate interrupted the alkaline setting reaction and generated an unworkable paste [161]. The surface topography analysis of the sugar containing paste did not show any macropores at the surface presumably due to the inhibitory effects of sugar which limited its pore-generating capability. At the same time, the microstructural analysis indicated these additives had a negative influence on the ettringite crystals. Therefore, the use of soluble porogens to induce macroporosity into PC-based cements for the purpose of vascularisation and bone ingrowth would be unlikely to be suitable and other methods should be investigated for this purpose.

Chapter 5

Development of novel foamed PC

5.1 Results

5.1.1 Assessment of foams

The foamability of gelatine and polysorbate 80 at different concentrations are shown in Figure 5.1. Polysorbate 80 possessed significantly ($p < 0.05$) higher foamability than gelatine. However, the 15 wt% gelatine solution was too thick to be foamed and was excluded from further experiments.

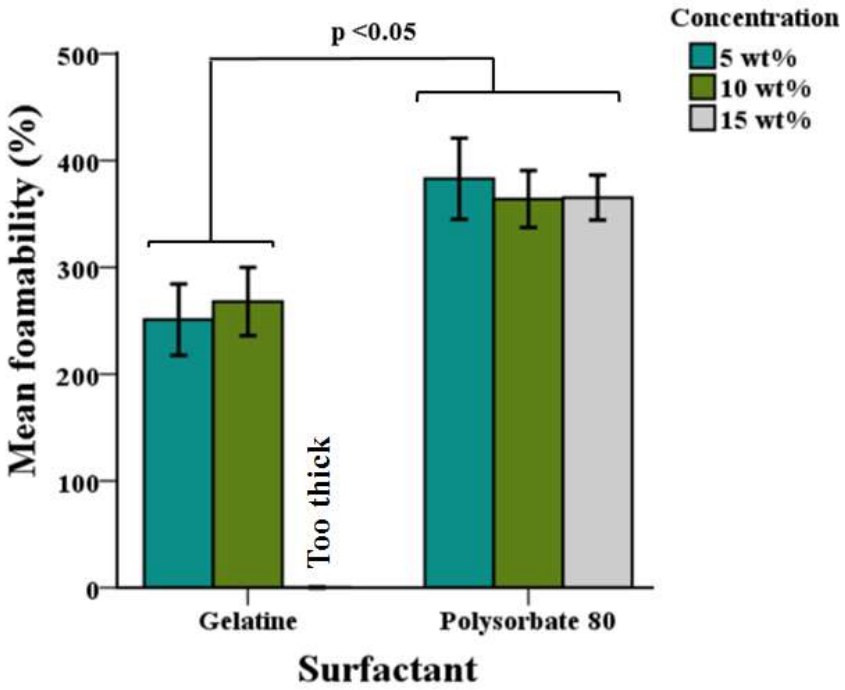

Figure 5.1: Mean foamability of 5-15 wt% of gelatine and polysorbate 80. At all concentrations, polysorbate 80 indicated significantly higher foamability compared with gelatine. Values are expressed as mean $\pm$ SD (n = 3).

Assessment of foam stability for the same concentrations of gelatine and polysorbate 80 indicated that, addition of 5-15 wt% of the either of foaming agents increased the foam stability in a concentration-dependent manner (Figure 5.2). The highest value was obtained for 10 wt% FG with 30 min stability.

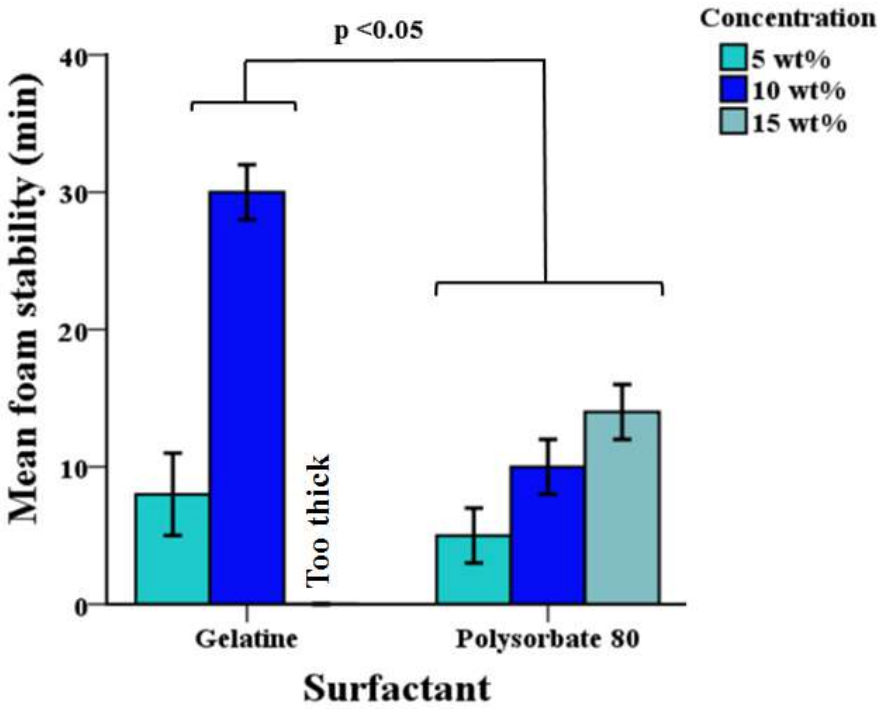

Figure 5.2: Mean foam stability of 5-15 wt% of gelatine and polysorbate 80. Gelatine at 10 wt% FG demonstrated the highest foam stability compared with others. Values are expressed as mean ± SD (n = 3).

5.1.2 Effect of foaming agents on the setting time

Foamed gelatine (FG) was prepared at either 5 or 10 wt% for setting time measurements (Figure 5.3). The setting time of the cement containing 1 % FG was comparable ($p > 0.05$) with the controls at all PLRs. On the other hand, regardless of the FG concentration, the setting time of cement with 10 and 20 % FG significantly ($p < 0.05$) increased compared with the controls at all PLRs. In addition, increasing the concentration of gelatine solution from 5 to 10 wt% significantly ($p < 0.05$) reduced the setting time of samples with 10 and 20 % of FG at PLRs of 4.0 and 4.5 g/ml.

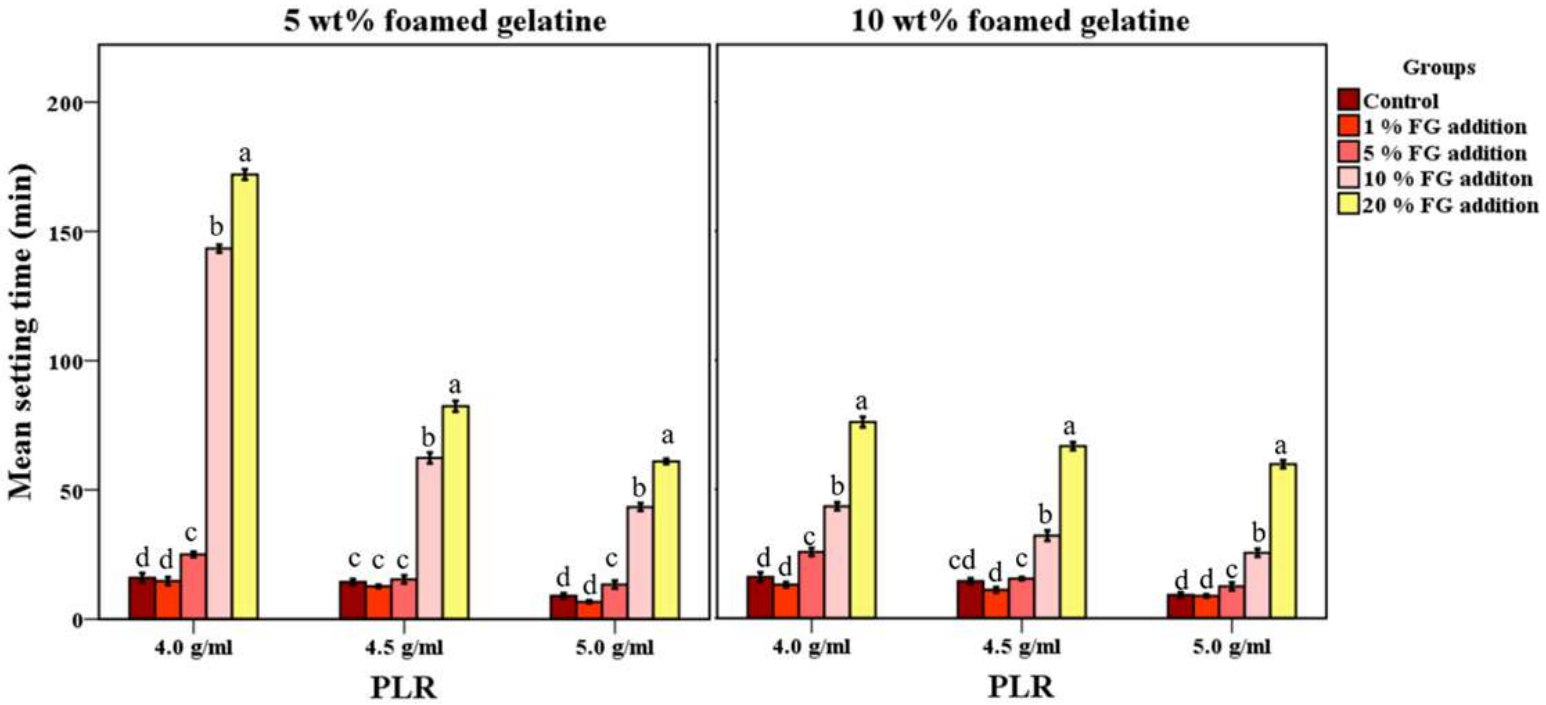

Figure 5.3: Mean setting time of PC at different PLRs with 1 to 20 % of added FG at gelatine concentrations of 5 and 10 wt%. Regardless of which FG concentration and PLR were used, the setting of the cement increased significantly ($p < 0.05$) upon addition of 10 and 20 % of FG compared with the control. Values are expressed as mean ± SD. Dissimilar letters indicated significant differences ($p < 0.05$) between different groups of cement at each PLR ($n = 3$).

Polysorbate 80 solution was prepared at three concentrations of 5, 10 and 15 wt% (Figure 5.4). The setting time of PC was reduced significantly ($p < 0.05$) or lowered to the level comparable with control when 1 and 5 % foamed polysorbate 80 (FP) were added to the cement. The setting time of cements with 10 and 20 % FP were significantly ($p < 0.05$) higher compared with controls regardless of which PLR was used. At each PLR the setting times of the cements with 10 and 20 % FP were reduced significantly ($p < 0.05$) upon increasing the polysorbate 80 concentration to 10 and 15 wt% compared with 5 wt%.

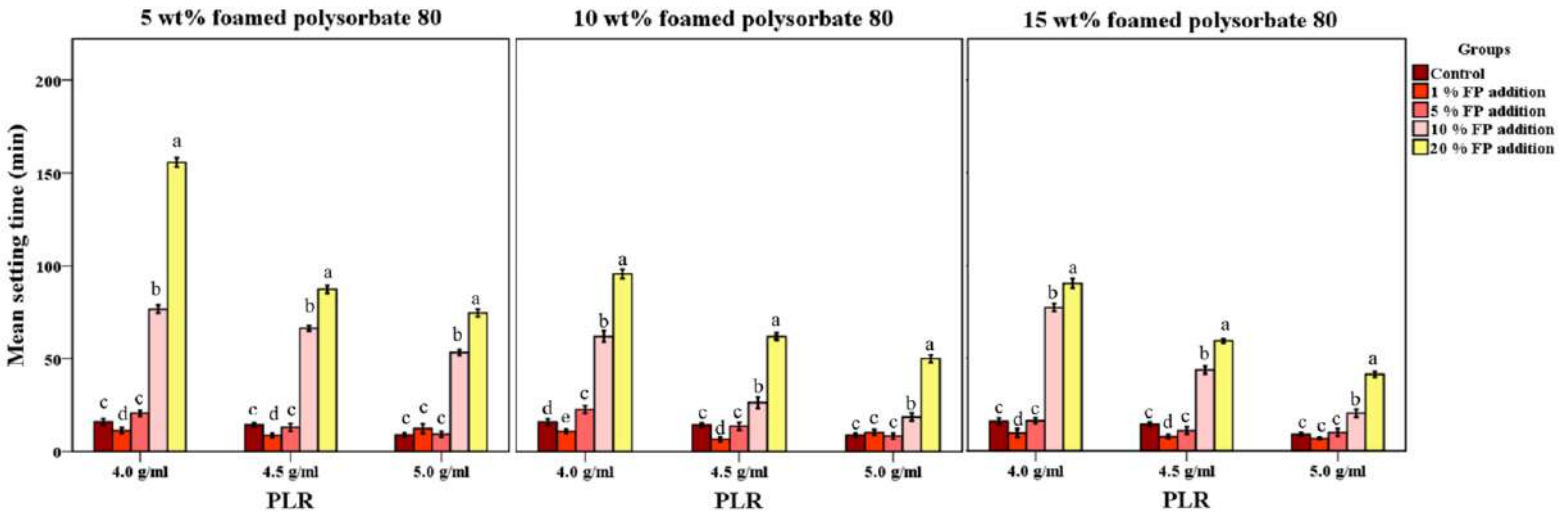

Figure 5.4: Mean setting time of PC at different PLRs with 1 to 20 % of added FP at polysorbate 80 concentrations of 5, 10 and 15 wt%. Regardless of which FP concentration and PLR were used, the setting of cements increased significantly ($p < 0.05$) upon addition of 10 and 20 % of FP compared with the controls. Values are expressed as mean $\pm$ SD. Dissimilar letters indicated significant differences ($p < 0.05$) between different groups of cement at each PLR (n = 3).

5.1.3 Effect of foaming agents on the injectability of PC

When 1 and 5 % FG at a gelatine concentration of 5 wt% were added to the cement, the injectability of cements were significantly ($p < 0.05$) reduced compared with the controls at PLRs of 4.0 and 4.5 g/ml (Figure 5.5). However, the addition of 10 and 20 % FG significantly enhanced ($p < 0.05$) the injectability to > 90 % even with a high PLR of 5.0 g/ml. In contrast, when gelatine concentration was increased to 10 wt% the injectability of cements with 5 to 20 % of FG were significantly improved ($p < 0.05$) compared with the controls at all PLRs.

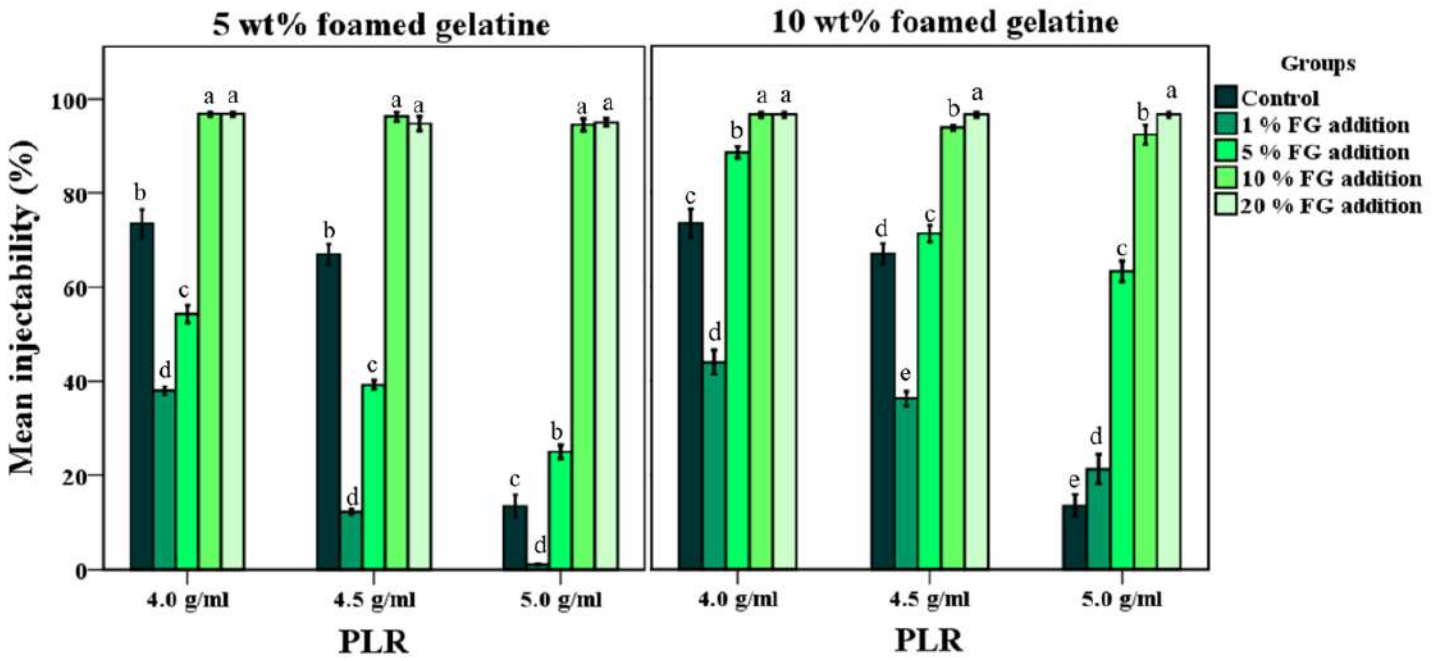

Figure 5.5: Mean injectability of PC at different PLRs with 1 to 20 % FG at two gelatine concentrations. At 5 wt% gelatine concentration, only the addition of 10 and 20 % FG significantly ($p < 0.05$) improved the injectability of PC at all PLRs. Whilst at 10 wt%, the injectability of cements were significantly increased when 5 to 20 % FG was added to the PC compared with controls. Values are expressed as mean $\pm$ SD. Dissimilar letters indicated significant differences ($p < 0.05$) between different groups of cement at each PLR (n = 4).

At all three polysorbate 80 concentrations, only cements with addition of 1 and 5 % FP were injectable through the needle at PLRs of 4.0 and 4.5 g/ml (Figure 5.6). At a PLR of 5.0 g/ml only the cement containing 5 % FP was injectable, whilst the addition of 10 and 20 % of FP caused the paste to seep out of the syringe due to a very low viscosity prior to the injectability testing at all PLRs.

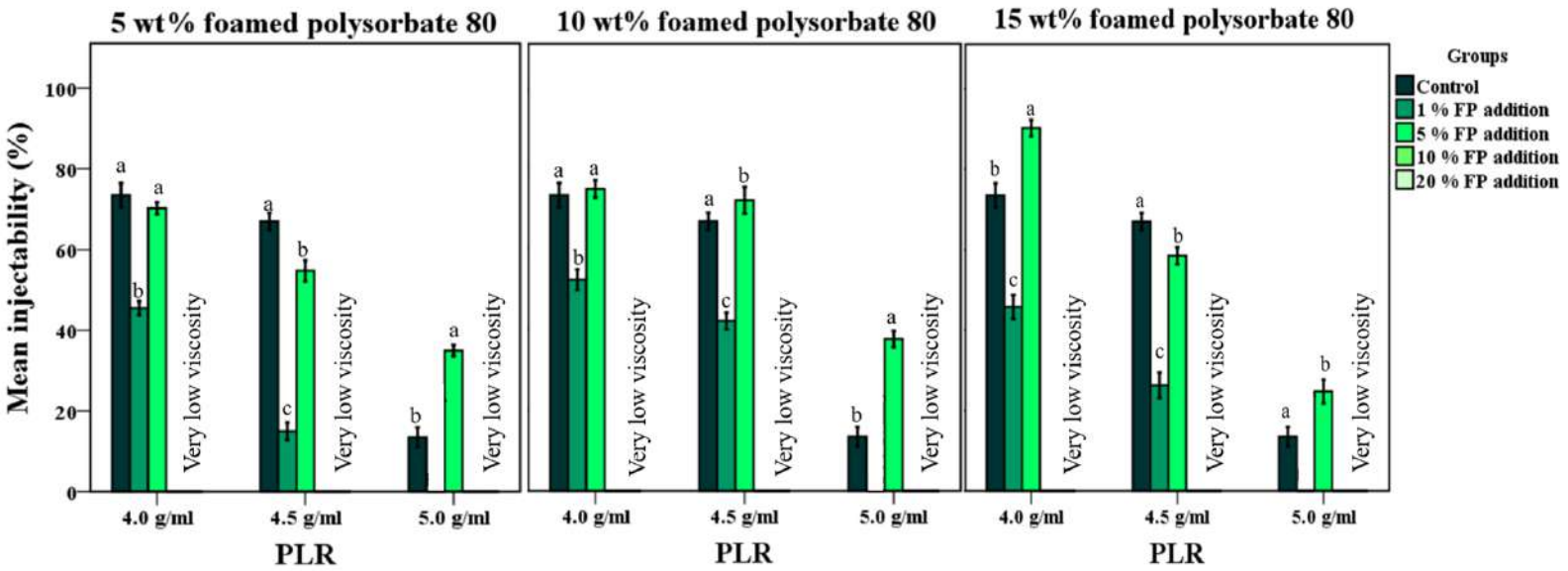

Figure 5.6: Mean injectability of PC at different PLRs with 1 to 20 % of FP at three polysorbate 80 concentrations. Addition of 10 and 20 % FP to the cement caused the cement to seep out of the syringe prior to injectability testing. Values are expressed as mean $\pm$ SD. Dissimilar letters indicated significant differences ($p < 0.05$) between different groups of cement at each PLR (n = 4).

5.1.4 Extension graphs for the injectability of cement containing FG

The addition of 5-10 % FG at the highest gelatine concentration was selected for further experiments. The control cement containing $CaCl_2$ was injectable as a constant force was needed (Figure 5.7). A sudden decrease in the applied force occurred when the air bubbles were pressed out of the syringe. All foamed cements demonstrated a homogeneous extrusion with a characteristic plateau. The plateau load, which is the force in which constant flow occurs, of foamed cement was lower than the control (<20 N). After 12-16 mm displacement, the force increased to 100 N since the syringe was almost empty. A sharp continuous increase in the required force was measured for displacement of the cement without any liquefying agent.

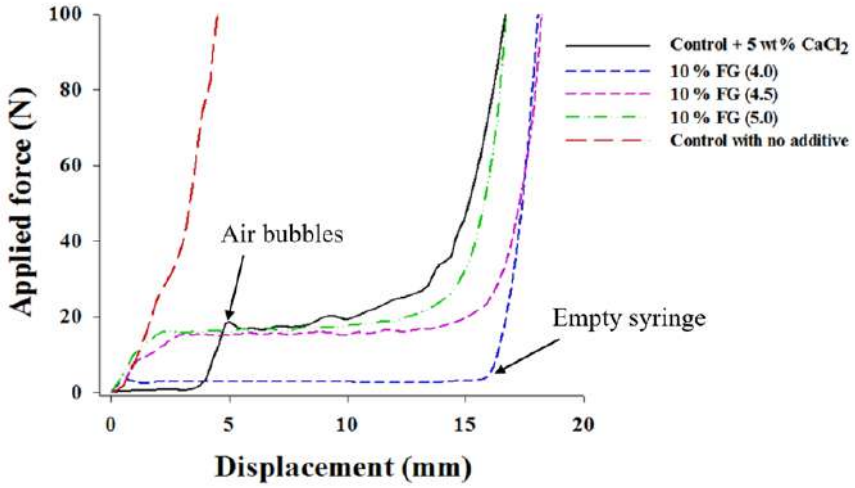

Figure 5.7: Force-displacement graph generated during injectability testing of different PC formulations. The cement with 10 % FG at all PLRs reduced the required force to extrude the paste through the syringe compared with the control with or without calcium chloride.

5.1.5 Compressive strength and porosity studies for static media

The highest compressive strengths for samples stored in DW were obtained for the controls after 7 and 30 days (Figure 5.8 a). The addition of 5-10 % FG reduced the strength values significantly ($p < 0.05$) in a concentration-dependent manner. Increasing the PLR of foamed cements improved the strength significantly ($p < 0.05$). The total relative porosity of controls were the lowest, whilst the addition of 5-10 % FG at any PLR, significantly increased the total porosity up to 37 % compared with the control (Figure 5.8 b).

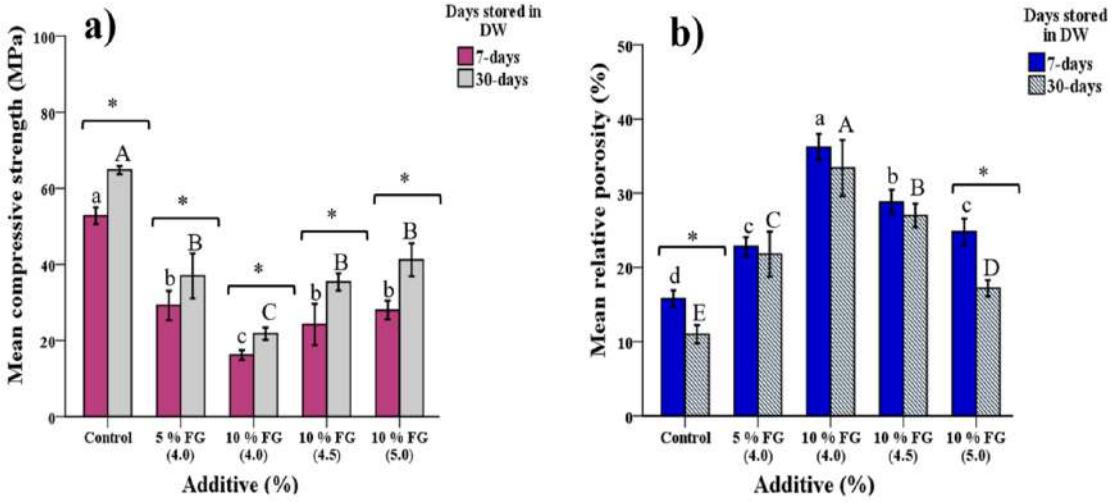

Figure 5.8: a) Mean compressive strength and **b)** relative porosity of controls and cement with 5-10 % FG after 7 and 30 days in DW. The compressive strength of the cement was significantly ($p < 0.05$) reduced upon increasing the FG by increasing the total porosity ($p < 0.05$) compared with controls. Values are expressed as mean $\pm$ SD. Dissimilar lower and upper case letters indicated significant differences ($p<0.05$) between groups after 7 and 30 days respectively ($n > 7$ per group, * $p < 0.05$).

Meanwhile, comparison of intrinsic and extra porosity values for foamed cement calculated from the total porosity indicated that the proportion of extra porosity after 30 days increased significantly ($p < 0.05$) or to a level comparable with 7-days (Figure 5.9 a). In contrast, the intrinsic porosity significantly ($p < 0.05$) reduced after 30 days (Figure 5.9 b). The foamed cement at a PLR of 4.0 g/ml had the highest extra porosity values of 26 % compared with other samples.

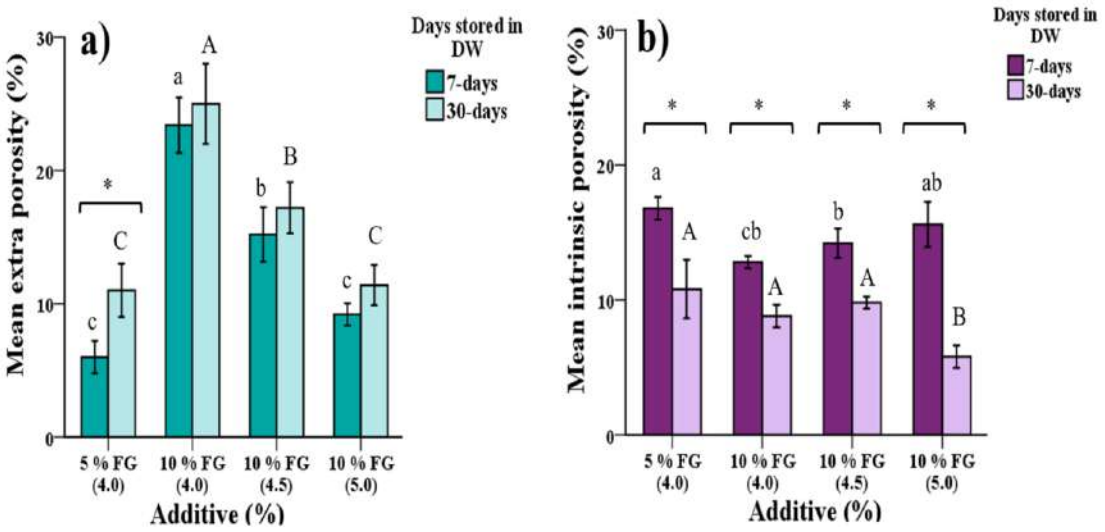

Figure 5.9: a) Mean extra porosity and **b)** intrinsic porosity of FG groups after 7 and 30 days storage in DW. Extra porosity values were comparable or significantly higher as the storage time increased. The intrinsic porosity values decreased significantly over 30 days. Values are expressed as mean $\pm$ SD. Dissimilar lower and upper case letters indicated significant differences ($p < 0.05$) between groups after 7 and 30 days respectively ($n > 7$ per group, * $p < 0.05$).

Similar to DW medium, the highest compressive strength values were obtained for the controls stored in PBS at both storage times (Figure 5.10 a). The addition of 5-10 % FG at 4.0 g/ml, significantly ($p < 0.05$) reduced the strength compared with the controls at both storage times, while increasing the PLRs and storage times both improved the strength of FG groups by 15 % and 47 % after 7 days and 23 % and 39 % after 30 days respectively. Addition of 5-10 % FG at all PLRs significantly increased ($p < 0.05$) the total porosity compared with the control (Figure 5.10 b).

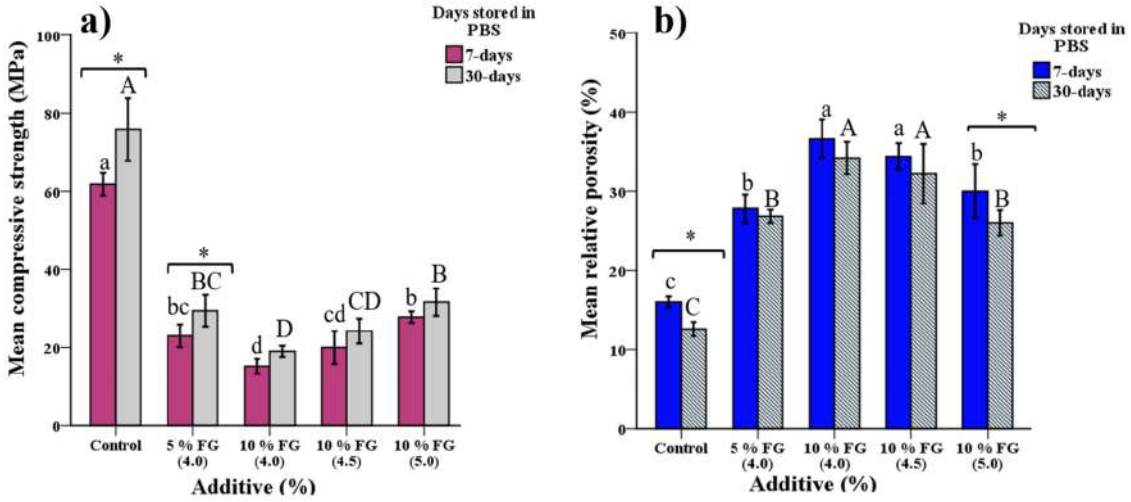

Figure 5.10: a) Mean compressive strength and **b)** relative porosity of control and cements with 5-10 % FG in PBS at two storage times. Increasing the amount of FG, significantly ($p < 0.05$) reduced the strength compared with controls by increasing the total porosity of the foamed cement ($p < 0.05$). Values are expressed as mean $\pm$ SD. Dissimilar lower and upper case letters indicated significant differences ($p < 0.05$) between groups after 7 and 30 days respectively ($n > 7$ per group, * $p < 0.05$).

After 30 days of storage in PBS, the extra porosity values of samples were significantly higher ($p < 0.05$) or to a level comparable with the 7-days values, with the highest values for the cements with 10 % FG at 4.0 and 4.5 g/ml (Figure 5.11 a). Conversely, the intrinsic porosity was reduced significantly ($p < 0.05$) by increasing the storage times as shown in Figure 5.11 b.

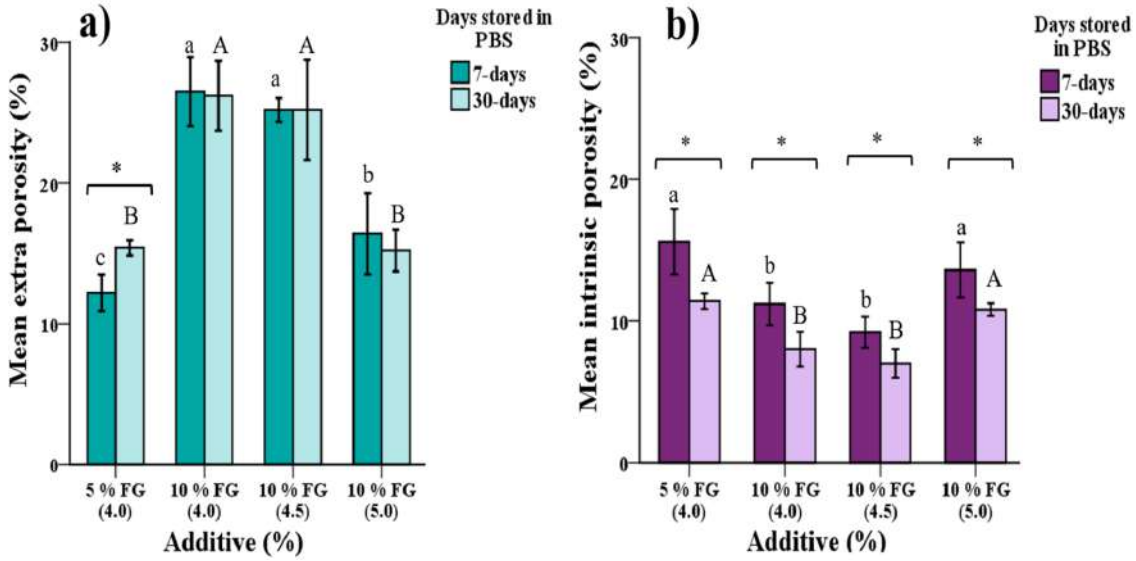

Figure 5.11: a) Mean extra porosity and **b)** intrinsic porosity of FG groups stored in PBS after 7 and 30 days. There was no significant difference ($p > 0.05$) between 7 and 30 days extra porosity except for the 5 % FG group. Meanwhile, the intrinsic porosity significantly ($p < 0.05$) reduced over 30 days. Values are expressed as mean $\pm$ SD. Dissimilar lower and upper case letters indicated significant difference ($p < 0.05$) between groups after 7 and 30 days respectively ($n > 7$ per group, * $p < 0.05$).

The strength values of the controls and foamed cements stored in PBS/FCS for 30 days were significantly higher ($p < 0.05$) or to a level comparable with 7-days values (Figure 5.12 a). Cement with 10 % FG at 4.0 g/ml had the lowest strength, while increasing the PLR of the foamed cement to 5.0 g/ml improved the strength significantly ($p < 0.05$). However, the foamed cements still maintained a high total porosity of 25-37 % compared with the control (Figure 5.12 b).

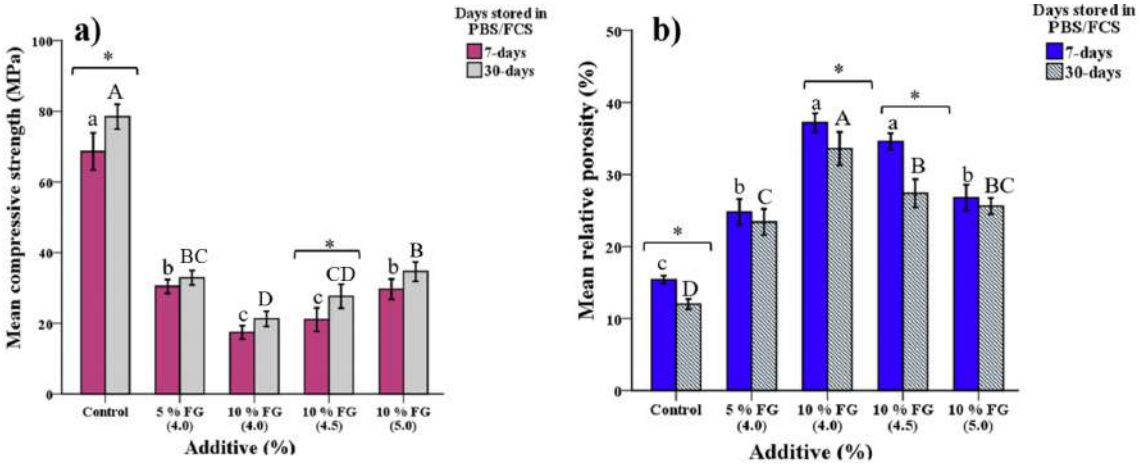

Figure 5.12: a) Mean compressive strength and **b)** total porosity of the control and cements with 5 to 10 % FG in PBS/FCS at two storage times. Increasing the amount of FG, significantly ($p < 0.05$) reduced the strength by increasing the total porosity ($p < 0.05$) compared with control. Values are expressed as mean $\pm$ SD. Dissimilar lower and upper case letters indicated significant differences ($p < 0.05$) between groups after 7 and 30 days respectively ($n > 7$ per group, * $p < 0.05$).

After 30 days of storage in PBS/FCS, the extra porosity of foamed cement after 30 days were significantly higher ($p < 0.05$) or to a level comparable with 7-days values. The highest value was measured for cements with 10 % FG at 4.0 g/ml (Figure 5.13 a). On the other hand, the intrinsic porosity values reduced significantly ($p < 0.05$) over the 30 days (Figure 5.13 b).

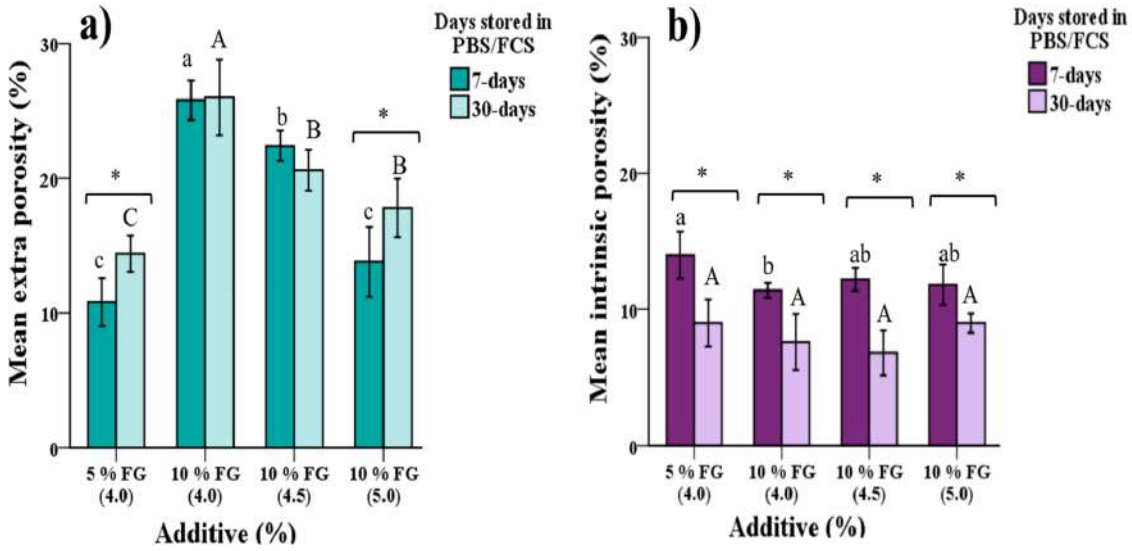

Figure 5.13: a) Mean extra porosity and **b)** intrinsic porosity of FG groups stored in PBS/FCS after 7 and 30 days. For all the groups, the extra porosity values after 30 days were significantly higher or comparable with the 7-days values. Meanwhile, the intrinsic porosity values were significantly reduced over 30 days. Values are expressed as mean $\pm$ SD. Dissimilar lower and upper case letters indicated significant differences ($p < 0.05$) between groups after 7 and 30 days respectively ($n > 7$ per group, * $p < 0.05$).

5.1.6 Compressive strength as a function of relative porosity

Plotting natural logarithms of 7-day compressive strengths in DW against relative porosity for the control and cements with 5-10 % FG at different PLRs is shown in Figure 5.14. There was a linear relationship for the foamed cements ($R^2 = 0.90$), whilst the control possessed significantly higher compressive strength values which was shown to depart from the linear relationship.

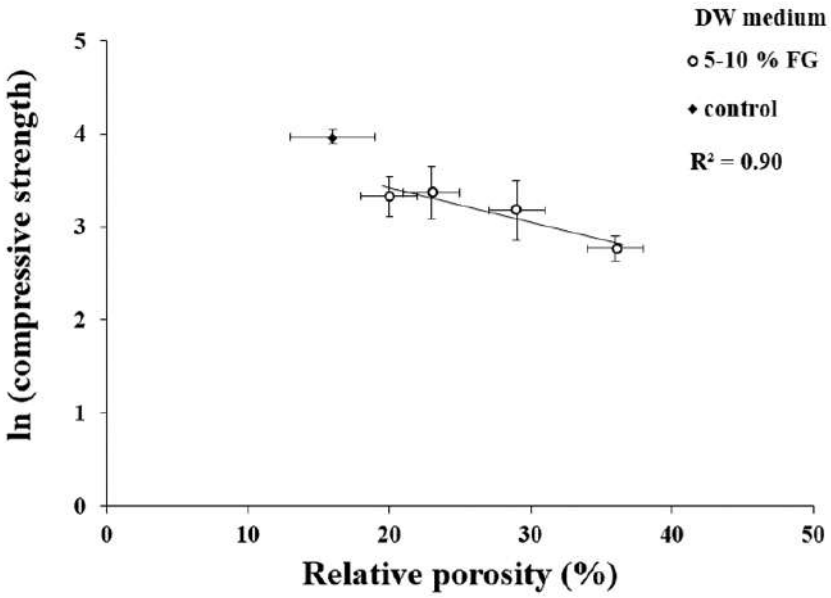

Figure 5.14: Graph of ln(compressive strength) against relative porosity for the control and cements with 5-10 % FG after 7 days in DW. The control departed from the linear relationship for the foamed cements which indicated the strength-deteriorating effect of FG when stored in DW.

When samples were stored in PBS or PBS/FCS, there was a strong linear relationship; $R^2 = 0.95$ and 0.97 respectively, which indicated that the storage of the foamed cements in the physiological media did not alter the materials constant of the cement compared with immersion in DW.

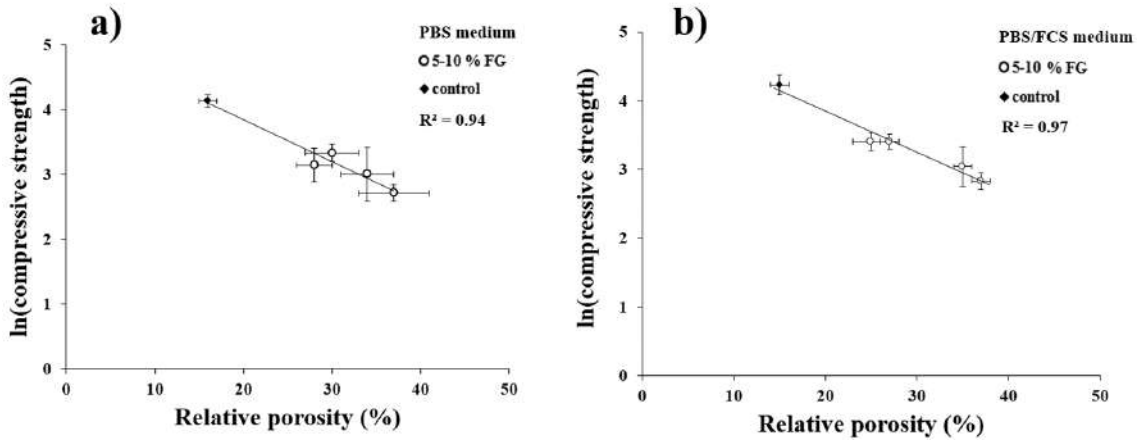

Figure 5.15: Graph of ln(compressive strength) against relative porosity for the control and cements containing 5-10 % FG after 7 days in **a)** PBS and **b)** PBS/FCS. The linear relationship between samples showed that the foaming agents did not alter the material constants of PC in both media.

5.1.7 Effect of dynamic regime on the compressive strength and total porosity

The compressive strengths of samples stored in dynamic PBS or PBS/FCS were generally lower compared with the static regime (Figure 5.10 and 5.12), for the full analysis refer to appendix chapter, section 8.2. The control PC possessed the highest compressive strength values compared with the others at both storage times (Figure 5.16). The cement with 10 % FG at 4.0 g/ml stored in PBS possessed the lowest strength values, however this value was still higher than the compressive strength of healthy cancellous bone.

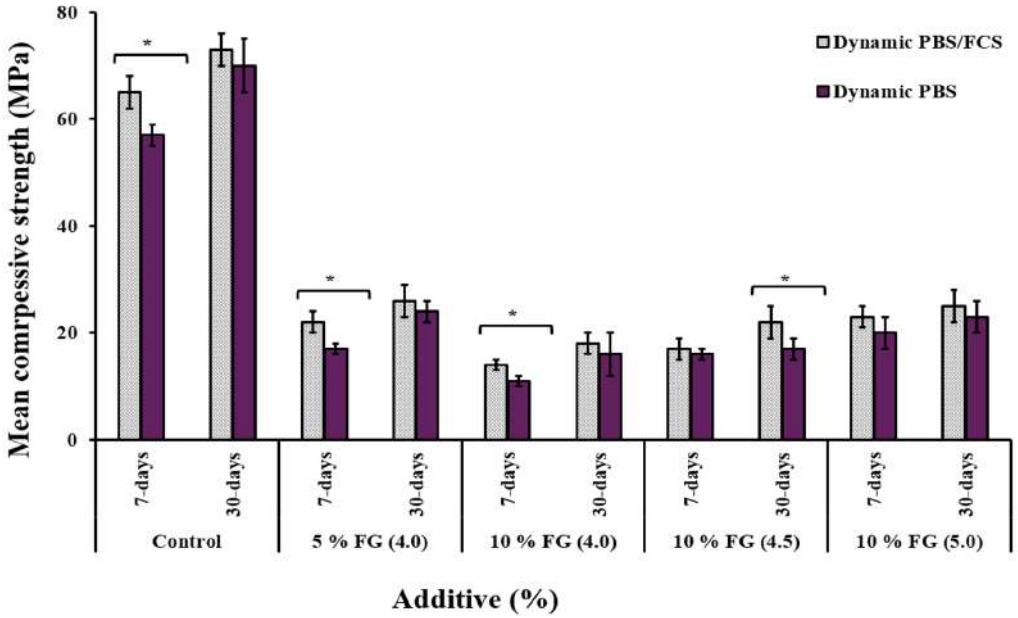

Figure 5.16: Mean compressive strength of samples in dynamic PBS and PBS/FCS for 7 and 30 days. The strength values of samples in PBS/FCS were significantly higher ($p < 0.05$) or comparable to a level with PBS medium. Values are expressed as mean $\pm$ SD ($n > 7$ per group, * $p < 0.05$).

The total porosity of cements in dynamic PBS and PBS/FCS were comparable with or significantly higher ($p < 0.05$) than the static regime (for full analysis refer to appendix chapter, section 8.2). Foamed cements with 5-10 % FG still possessed a high porosity of 30-40 % compared with the controls (14-20 %). All the samples immersed in PBS apart from the 7-day control and the cement with 5 % FG showed a relatively higher ($p > 0.05$) total porosity values compared with PBS/FCS as shown in Figure 5.17.

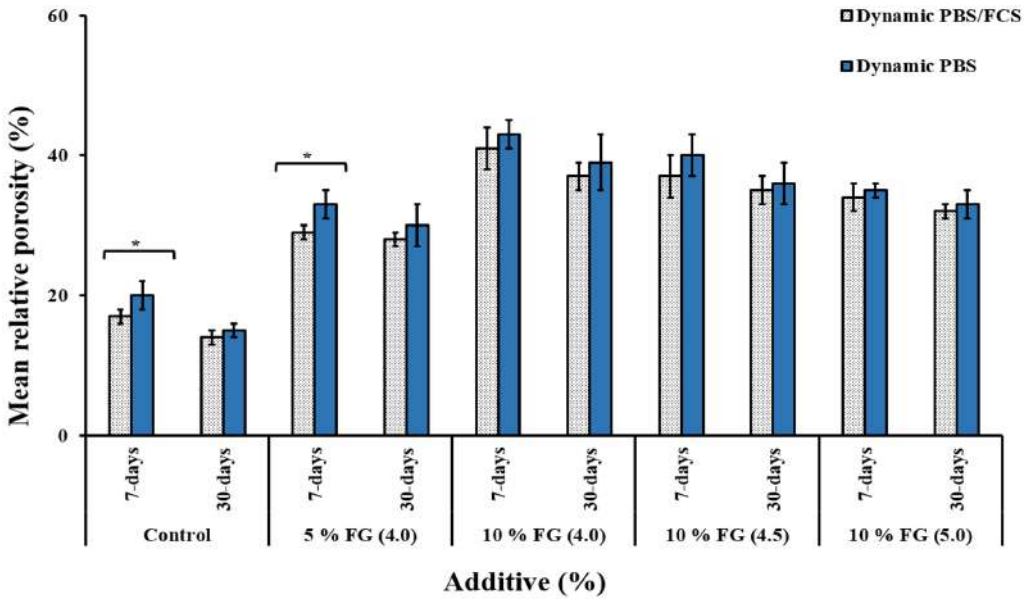

Figure 5.17: Mean total porosity of samples in dynamic PBS and PBS/FCS for 7 and 30 days. The porosity of the cements stored in PBS were generally higher compared with PBS/FCS. Values are expressed as mean $\pm$ SD ($n > 7$ per group, * $p < 0.05$).

5.1.8 Strut density studies

The strut density measurements for the samples stored in different media after 7 days is shown in Figure 5.18. There was no significant difference ($p > 0.05$) in the strut densities of the control and foamed cement in any media. Storage of cements in SBF was carried out for the control to compare the effect of different physiological fluids on the strut density of PC. Within each group, there was an increasing trend in the strut density of cement in order of DW = SBF $<$ PBS $<$ PBS/FCS.

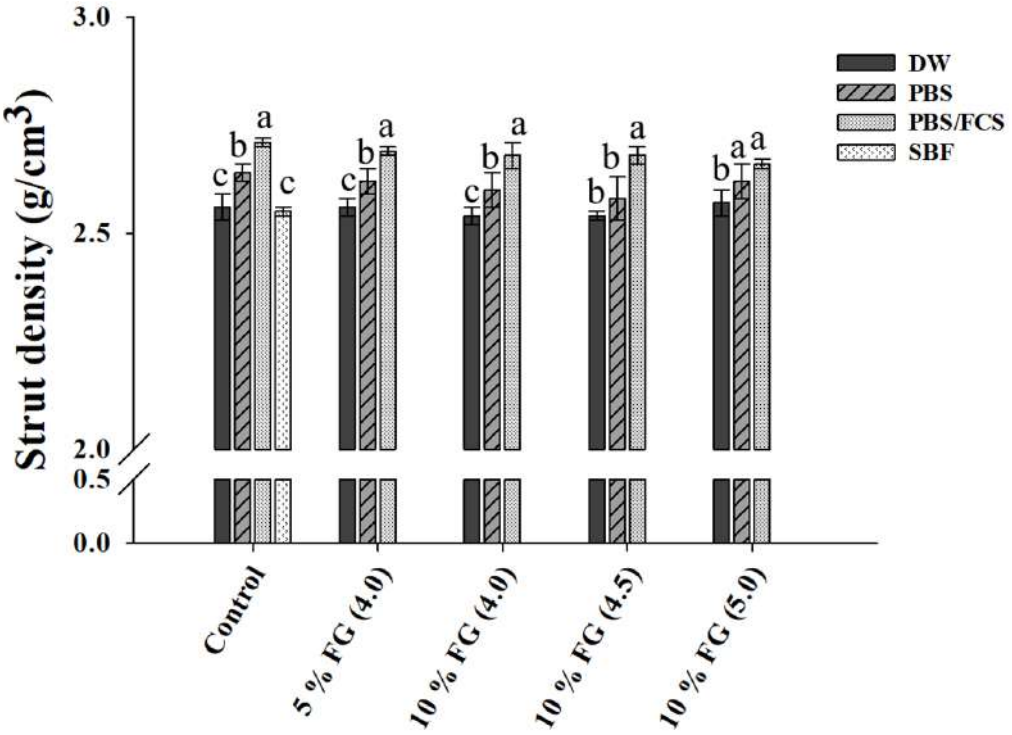

Figure 5.18: Mean strut density of samples stored in various media for 7 days. At any media, the strut density values of the control and foamed cements were similar ($p > 0.05$). Cements immersed in PBS/FCS possessed the highest strut density values compared with the others. Dissimilar letters indicated significant differences ($p < 0.05$) between media for each group. Values are expressed as mean $\pm$ SD (n $>$7 per group).

Continuing the hydration of cements for 30 days lowered the strut densities of all the samples compared with 7-day values (Figure 5.19). There was no significant difference ($p > 0.05$) between the control and foamed cements for PBS and PBS/FCS media. However, within DW, the foamed cement at 5.0 g/ml had a significantly lower ($p < 0.05$) strut density compared with the control.

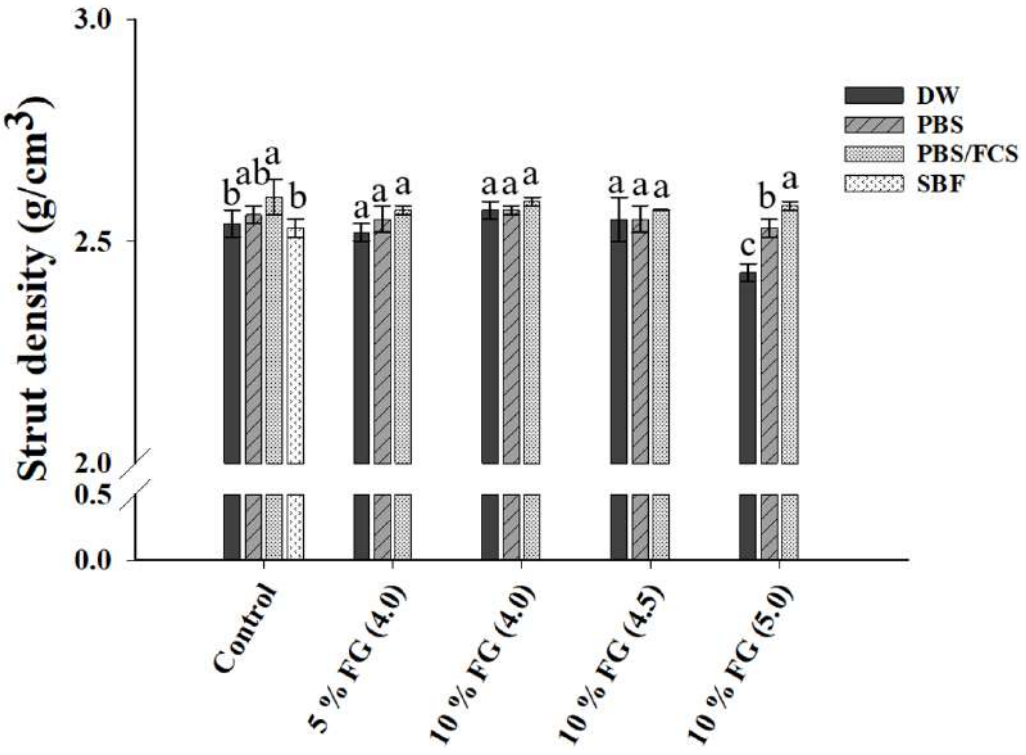

Figure 5.19: Mean strut density of samples stored in various media for 30 days. The strut density values for the foamed cements were comparable ($p > 0.05$) with each other except at a PLR of 5.0 g/ml. The control PC stored in SBF and DW had significantly lower densities compared with PBS/FCS medium. Dissimilar letters indicated significant differences ($p < 0.05$) between media for each group. Values are expressed as mean $\pm$ SD (n >7 per group).

5.1.9 Solubility of the PC in dynamic PBS and PBS/FCS

The solubility of the control and foamed cements decreased after 30 days of storage except for the foamed cement at a PLR of 4.0 g/ml (Figure 5.20). After 30 days of storage in PBS, the solubility of control PC was 3.5 % which was significantly ($p < 0.05$) lower than foamed cements at PLRs of 4.0-4.5 g/ml (5.7-13.1 %). Amongst the foamed cements, there was no significant ($p > 0.05$) difference in the solubility of cements between 3-14 days of storage in PBS. However, after 1 and 30 days, the solubility values of foamed cement at a PLR of 5.0 g/ml were considerably lower ($p < 0.05$) than the PLR of 4.0 g/ml (refer to appendix, section 8.3).

The solubility values of the control PC stored in dynamic PBS/FCS were significantly ($p < 0.05$) lower compared with the PBS medium at all storage times (refer to appendix, section 8.3). The solubility values of foamed cements in PBS/FCS were at a comparable level ($p > 0.05$) with values identified in PBS during the first 7 days. Whilst, during 14 to 30 days the solubility values of PBS/FCS medium were significantly ($p < 0.05$) lower than the PBS values. Nevertheless, the control group and 10 % FG (4.0) had the lowest and highest solubility respectively after 30 days.

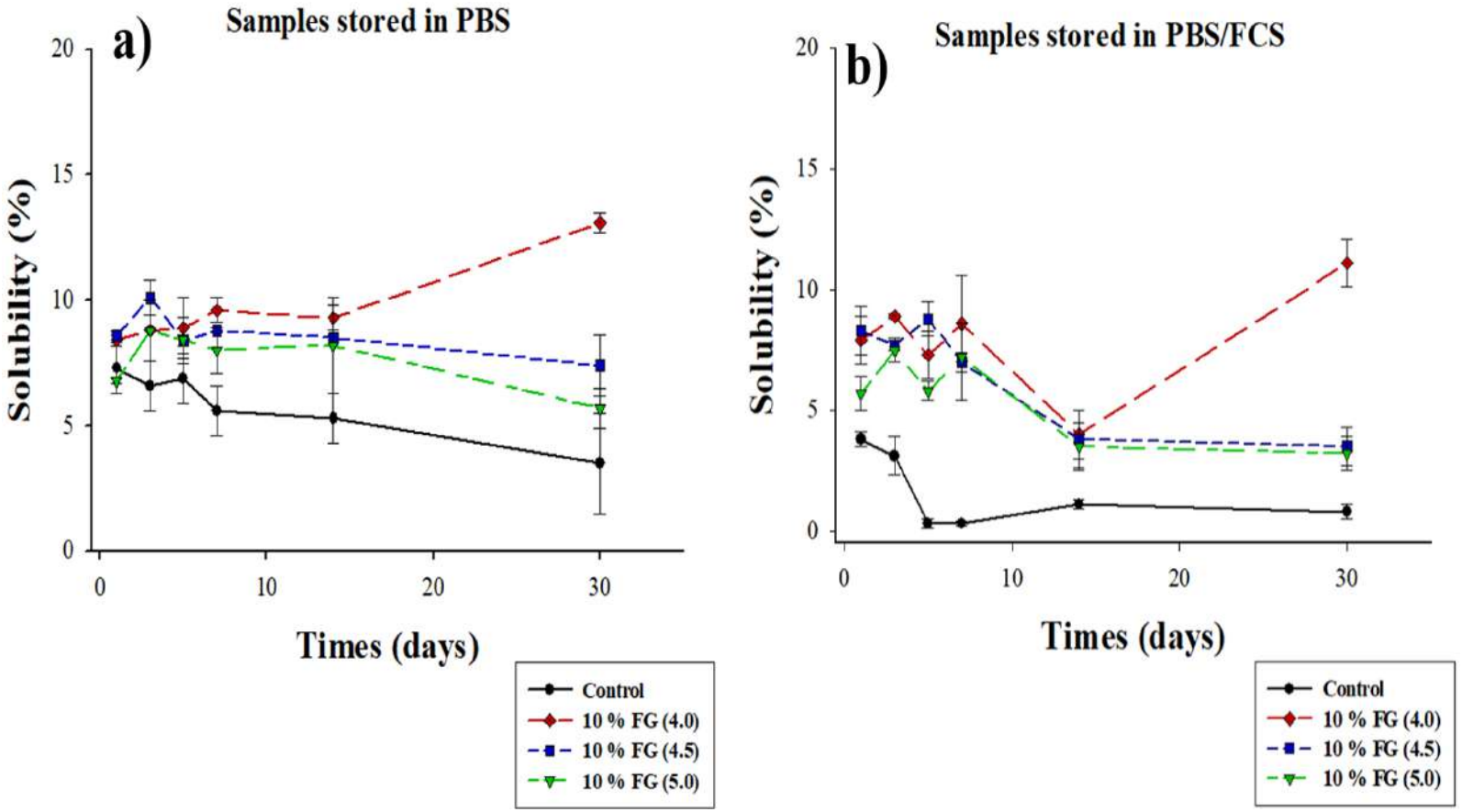

Figure 5.20: Mean solubility of control and the cements with 10 % FG at three PLRs over 30 days of dynamic storage in **a)** PBS and **b)** PBS/FCS. The solubility of all cements apart from the PLR of 4.0 g/ml reduced at the end of 30 days (n = 3).

5.1.10 Influence of FG on the Weibull modulus

The combined Weibull distributions was used to measure the Weibull modulus (m) and the corresponding R^2 values of the control and cements with 5 and 10 % FG after 7 days in DW and PBS/FCS (Figure 5.21). The highest Weibull modulus was obtained for the control, whilst there was a decreasing trend in the reliability of strength data as the amount of added FG was increased. Furthermore, immersion of the cements in PBS/FCS increased the reliability of data compared with DW.

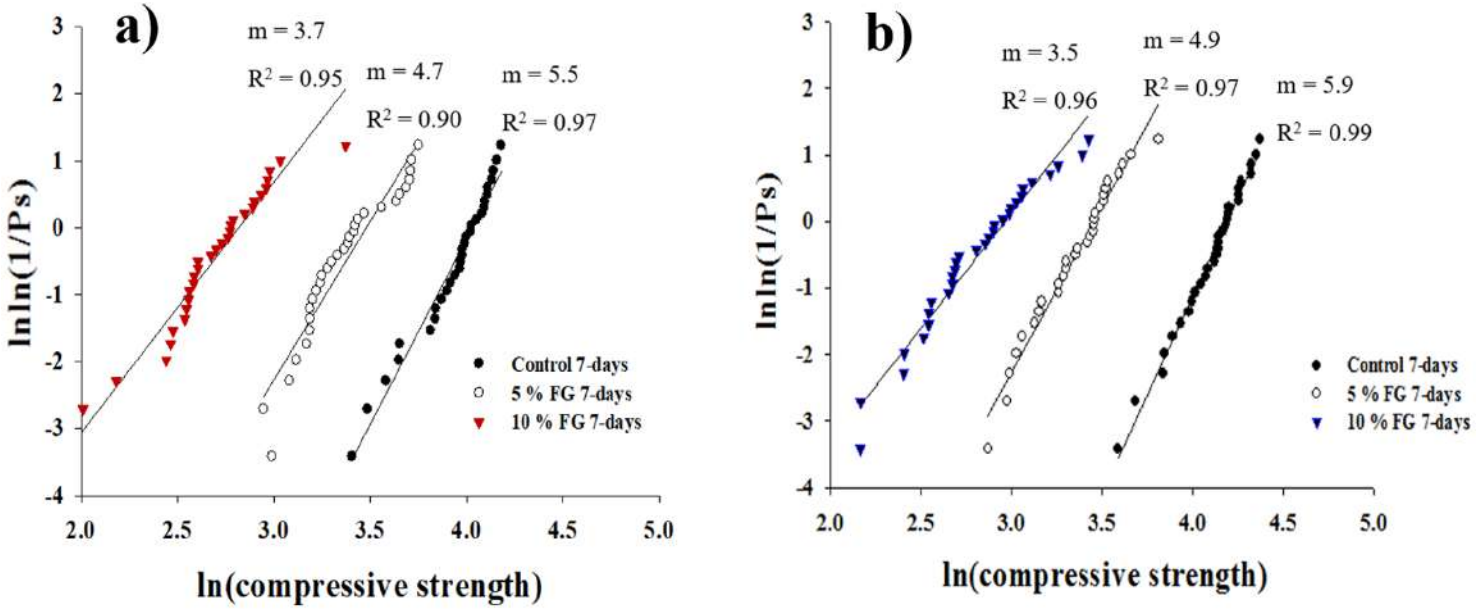

Figure 5.21: Weibull distributions indicating the Weibull modulus (m) and R^2 of the control and cements with 5-10 % FG after 7 days of storage in **a)** DW and **b)** PBS/FCS. Increasing the amount of added FG reduced the Weibull modulus and reliability of PC. Storage of the PC in PBS/FCS increased the Weibull modulus values compared with DW values (n = 30).

Increasing the storage time of the cement improved the reliability of the strength data for both media as shown in Figure 5.22. Nevertheless, the control PC still showed the highest Weibull modulus values compared with the foamed cements stored in either media. In contrast to 7-day Weibull distribution data, there was a noticeable increase in the Weibull moduli of samples in PBS/FCS for 30 days compared with DW and the R^2 values of all samples were still greater than 0.90.

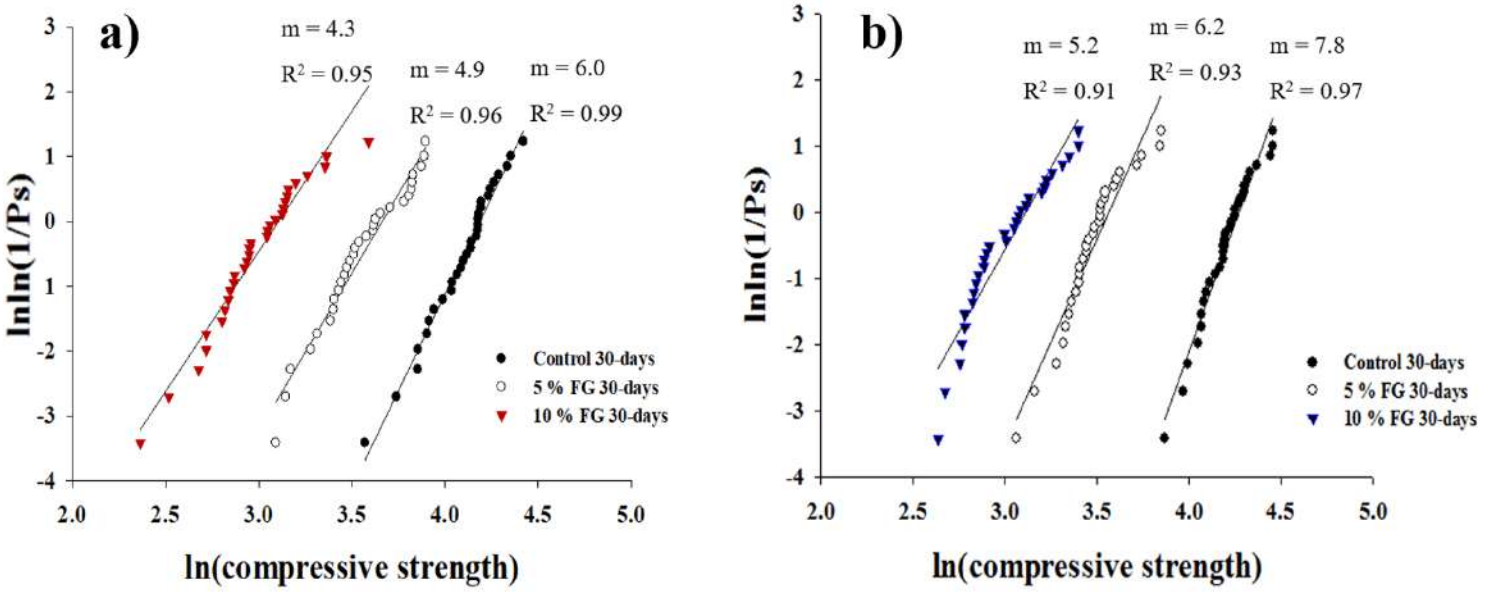

Figure 5.22: Weibull distributions indicating the Weibull modulus (m) and R^2 of the control and the cements with 5-10 % FG after 30 days of storage in **a)** DW and **b)** PBS/FCS. Cements stored in PBS/FCS medium were more reliable compared with samples immersed in DW (n = 30).

The probability of survival against the ranked 7-day compressive strength data for the control and the foamed cements in DW and PBS/FCS is shown in Figure 5.23. Storage of foamed cements in PBS/FCS exhibited a more symmetrical distribution of data at both low and high stress compared with DW medium. Meanwhile, the control PC exhibited an increased in asymmetry at a lower strength compared with foamed cements.

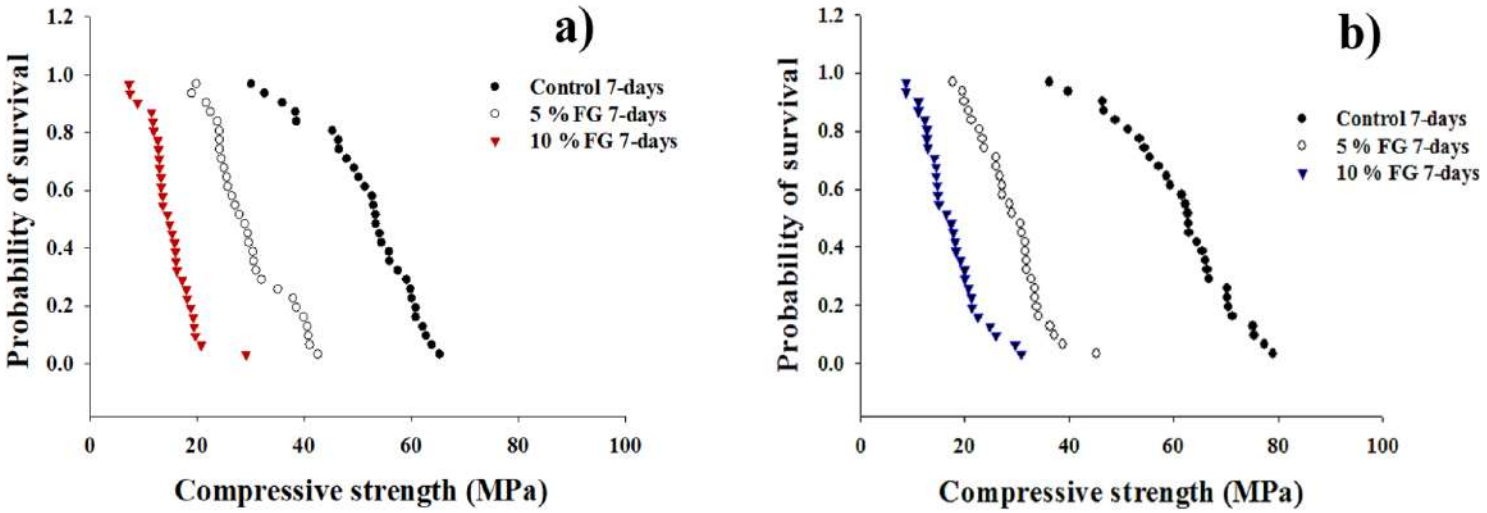

Figure 5.23: The probability of survival of the compressive strength of the samples stored in **a)** DW and **b)** PBS/FCS for 7 days. The foamed cements stored in PBS/FCS showed a symmetrical distribution of data at low and high stress compared with DW. Whilst, the control PC generated an asymmetrical distribution at a lower strength compared with the foamed cements.

Continuing the hydration of cements for 30 days indicated a similar pattern to 7-day data. The distribution of data for the foamed cements in PBS/FCS were more symmetrical at both extremes compared with DW (Figure 5.24). In addition, the control PC still showed an asymmetrical distribution at low stress in both media.

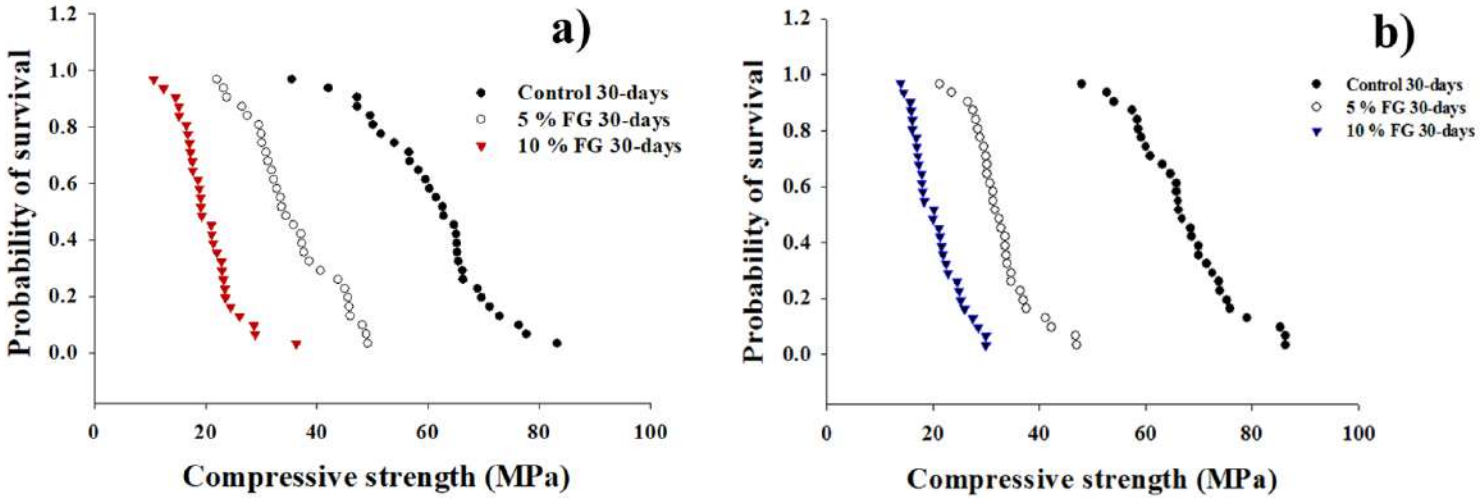

Figure 5.24: The probability of survival of the compressive strength of the samples stored in **a)** DW and **b)** PBS/FCS for 30 days. Hydration of the cements in PBS/FCS showed a symmetrical distribution of data at both low and high stress compared with DW medium. While, the control PC still exhibited an asymmetrical distribution at a low stress.

The 95 % confidence interval for Weibull moduli of the control and the cement with 5 % FG overlapped at both storage times in contrast with 10 % FG group, indicating that the addition of FG above 5 % did significantly ($p < 0.05$) affect the distribution of defects within PC-based cement as shown in Figure 5.25.

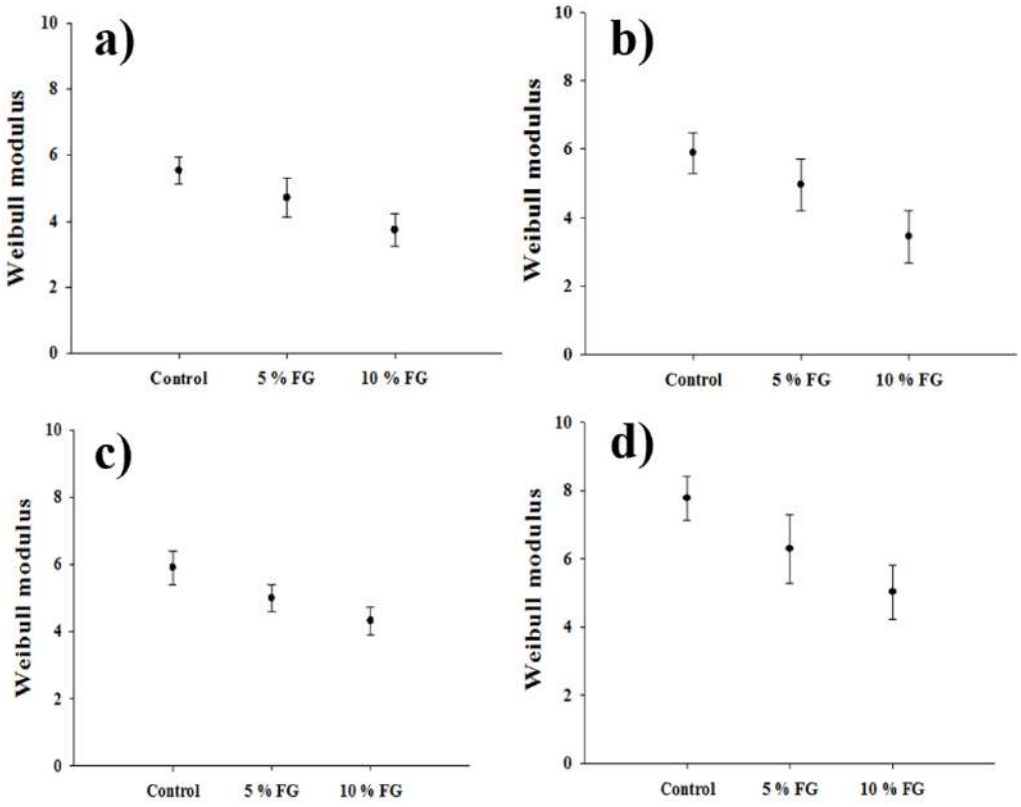

Figure 5.25: The Weibull moduli of different PC formulations including 95 % confidence interval after 7 and 30 days in days in DW (a and c) and PBS/FCS (b and d) respectively. For each plot, only the confidence intervals of the control and the cement containing 5 % FG overlapped.

5.1.11 Cohesion test

Integrity and cohesion of cements with 10 % FG at different PLRs were assessed using a pre-soaked hollow sponge in DW at 37 °C as shown in Figure 5.26. Addition of the FG had no adverse effect on the integrity of PC during the first 2 h of setting with no sign of disintegration.

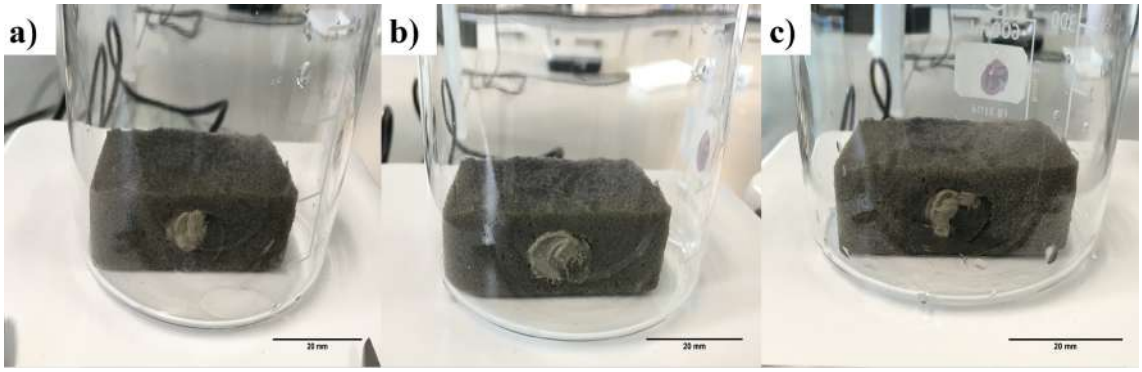

Figure 5.26: Image captured after 2 h of the setting of the cement paste containing 10 % FG at PLRs of a) 4.0 g/ml, b) 4.5 g/ml and c) 5.0 g/ml. All the foamed cements showed a good integrity with no disintegration of the cement.

5.1.12 Monitoring early hydration of cement using ATR-FTIR

The FTIR spectrum of the gelatine indicated absorbance peaks for amide I and II bands at 1657 and 1551 cm^{-1} respectively (Figure 5.27). The FTIR spectra for the control PC and cements with 10 % FG after 1 h of the setting showed the standard FTIR pattern for the typical PCs (Figure 5.28). However, foamed cements possessed relatively lower absorbance peaks for the PC bands compared with the control. The peak corresponded to unbound gypsum at 1100 cm^{-1} for all groups decreased over 2 h of the setting. The control PC developed an additional peak at 980 cm^{-1} which corresponded with the formation C-S-H. In contrast, the foamed cements indicated a small peak at the same wavenumber compared with the control.

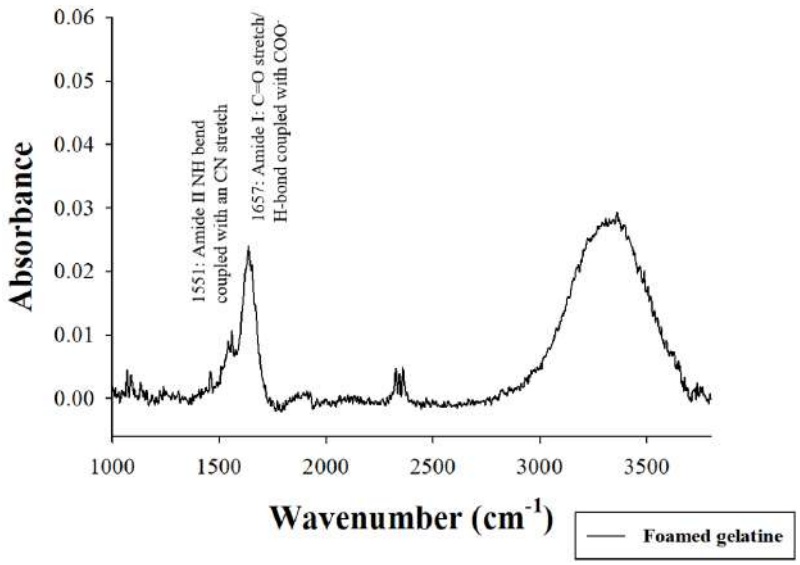

Figure 5.27: FTIR of the foamed gelatine indicating the amide I and II bands.

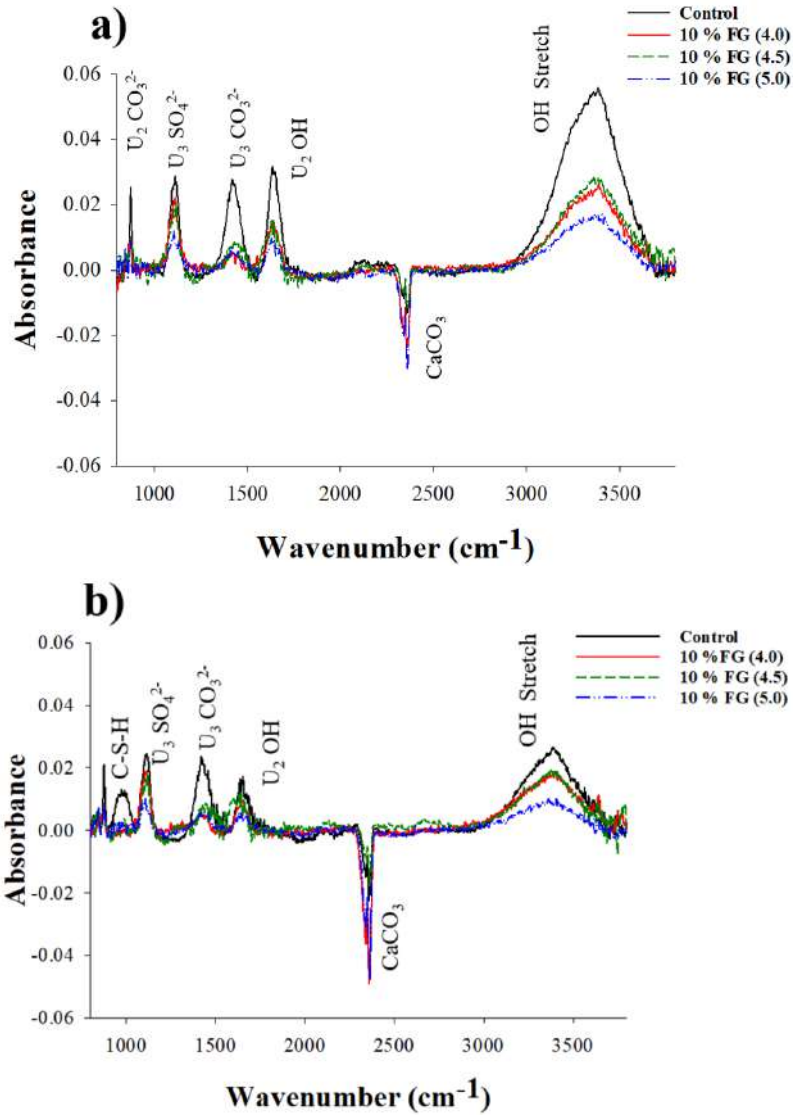

Figure 5.28: FTIR spectra for the control and cements with 10 % FG at different PLRs after **a)** 1 h and **b)** 2 h of setting. The peak at 1100 cm^{-1} for ν_3 stretching of SO_4^{2-} corresponded with unbound gypsum decreased over 2 h of the setting for all groups. A broad peak at 980 cm^{-1} corresponded to C-S-H was developed for the control after 2 h of setting.

5.1.13 Effect of the soaking media on the setting of PC

There was noticeable difference between the cements soaked in DW and PBS/FCS. The cements stored in DW were covered by multiple hexagonal crystals on the outer-surface (see appendix chapter for EDS analysis, section 8.4, subsection 8.4.1). Whilst, cements immersed in PBS/FCS were covered by a white deposit as shown in Figure 5.29.

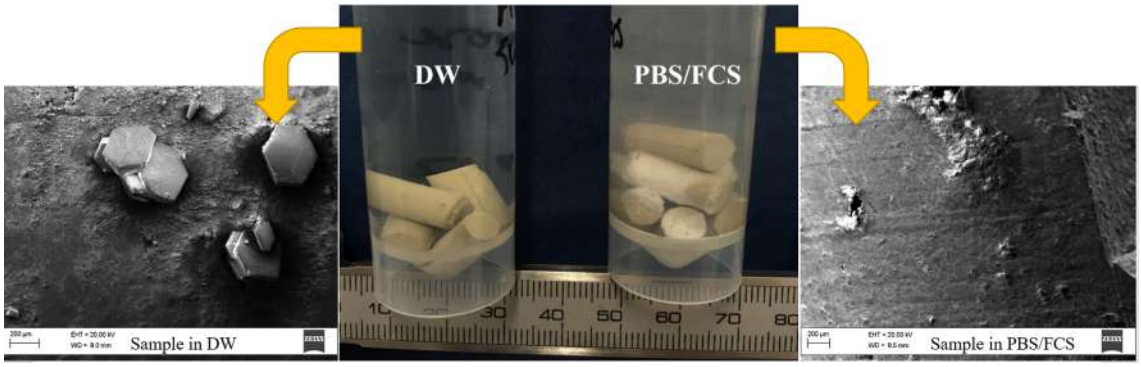

Figure 5.29: Image captured from the cements soaked in DW (left) and PBS/FCS (right) with corresponded SEM images. A white deposit covered the outer-surface of the cements stored in PBS/FCS. While, for samples in DW large hexagonal crystals were visible.

The cross-section of the cements stored in DW, SBF, PBS and PBS/FCS were analysed using SEM/EDS technique (for full analysis refer to appendix, section 8.4, subsection 8.4.2). SEM analysis was carried out using both secondary and backscattered electron imaging to detect differences in chemical composition. SEM images of the cement stored in DW revealed no additional deposit on the outer-surface of cement and only the bright bulk cement was apparent as shown in Figure 5.30. Conversely, immersion of cements in other media than DW indicated formation of a deposit according to EDS analysis.

Samples stored in PBS/FCS showed the thickest deposit compared with other media as shown in Figure 5.31.

The elemental analysis of the powder scraped from the surface of SBF, PBS and PBS/FCS groups revealed a considerable amount of phosphorous, carbon and calcium, which suggested the presence of carbonated apatite layer although the Ca/P atomic ratio varied between the different samples. The 7-day Ca/P ratios for SBF, PBS and PBS/FCS were 3.83, 1.60 and 3.95 respectively. The Ca/P ratio values were further reduced to 2.26, 1.37 and 2.89 respectively after 30 days (refer to appendix,section 8.4, subsection 8.4.2).

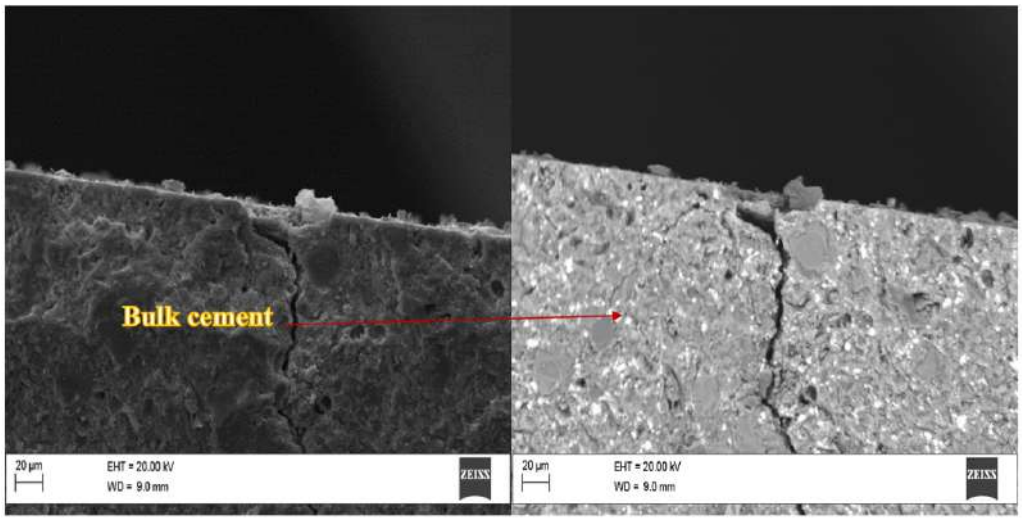

Figure 5.30: Secondary electron image (left) and backscattered electron image (right) of the cement (x6 k) after 30 days of hydration in DW. There was no deposit on the outer-surface of the cement.

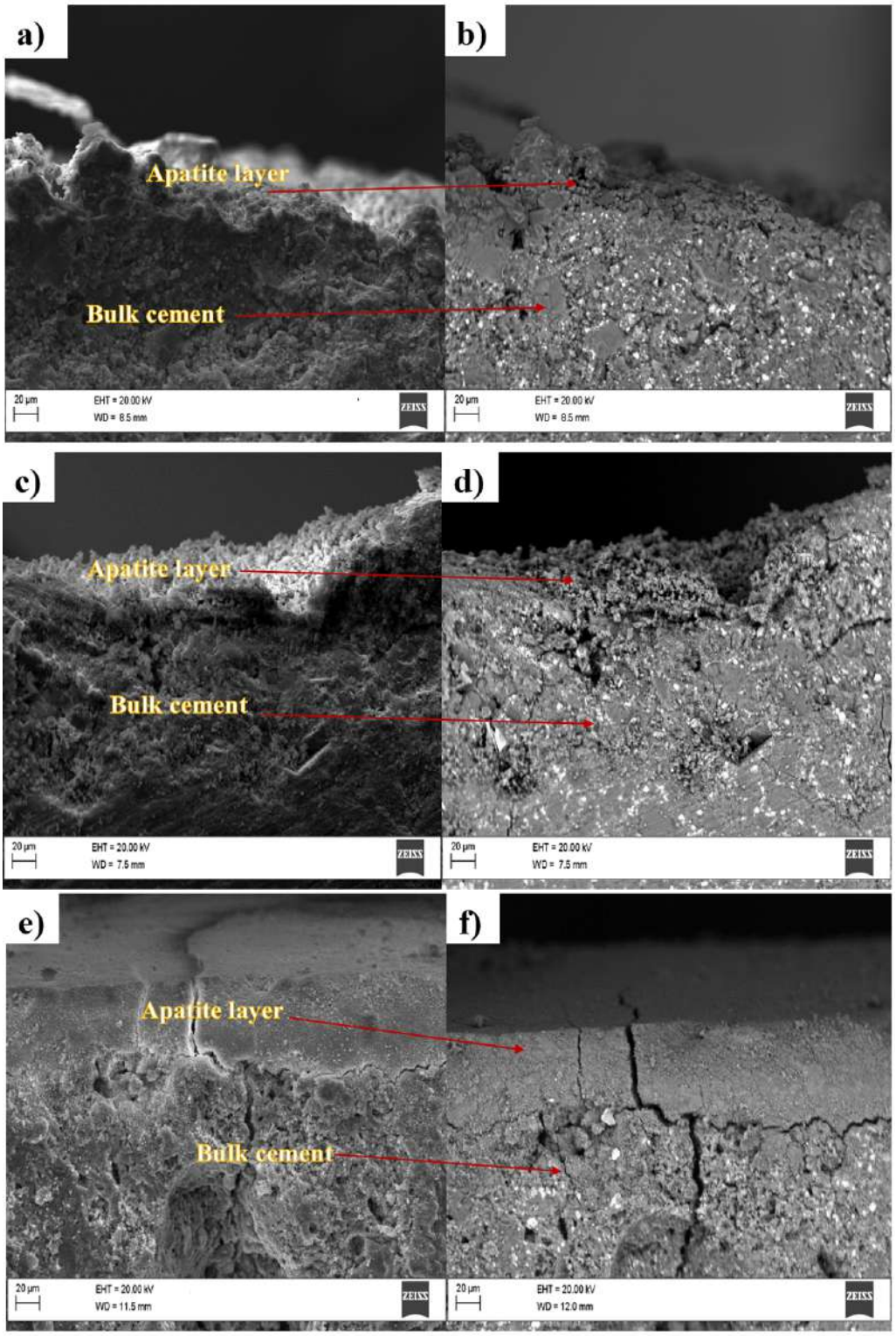

Figure 5.31: Secondary electron (left) and backscattered electron images (right) of the cements (x6 k) which were soaked in SBF (a and b), PBS (c and d) and PBS/FCS (e and f) for 30 days. The most uniform carbonated apatite layer was observed for PBS/FCS group.

FTIR analysis on the outer-surface of cements stored in different media is shown in Figure 5.32. The absorption of the typical PC bands increased over time for the cement stored in DW including a broad band for C-S-H at 980 cm^{-1} and intensive peaks at 700 and 870 cm^{-1} for calcium carbonate in the forms of calcite and aragonite. In contrast, cements stored in other media than DW, showed an extra peak at 1020-1030 cm^{-1} for ν_3 stretching of PO_4^{3-} which was the main chemical group for apatite and its absorption increased over time. There was a weak peak for CO_3^{2-} group of carbonated apatite at 870 cm^{-1} which was shown to increase with time.

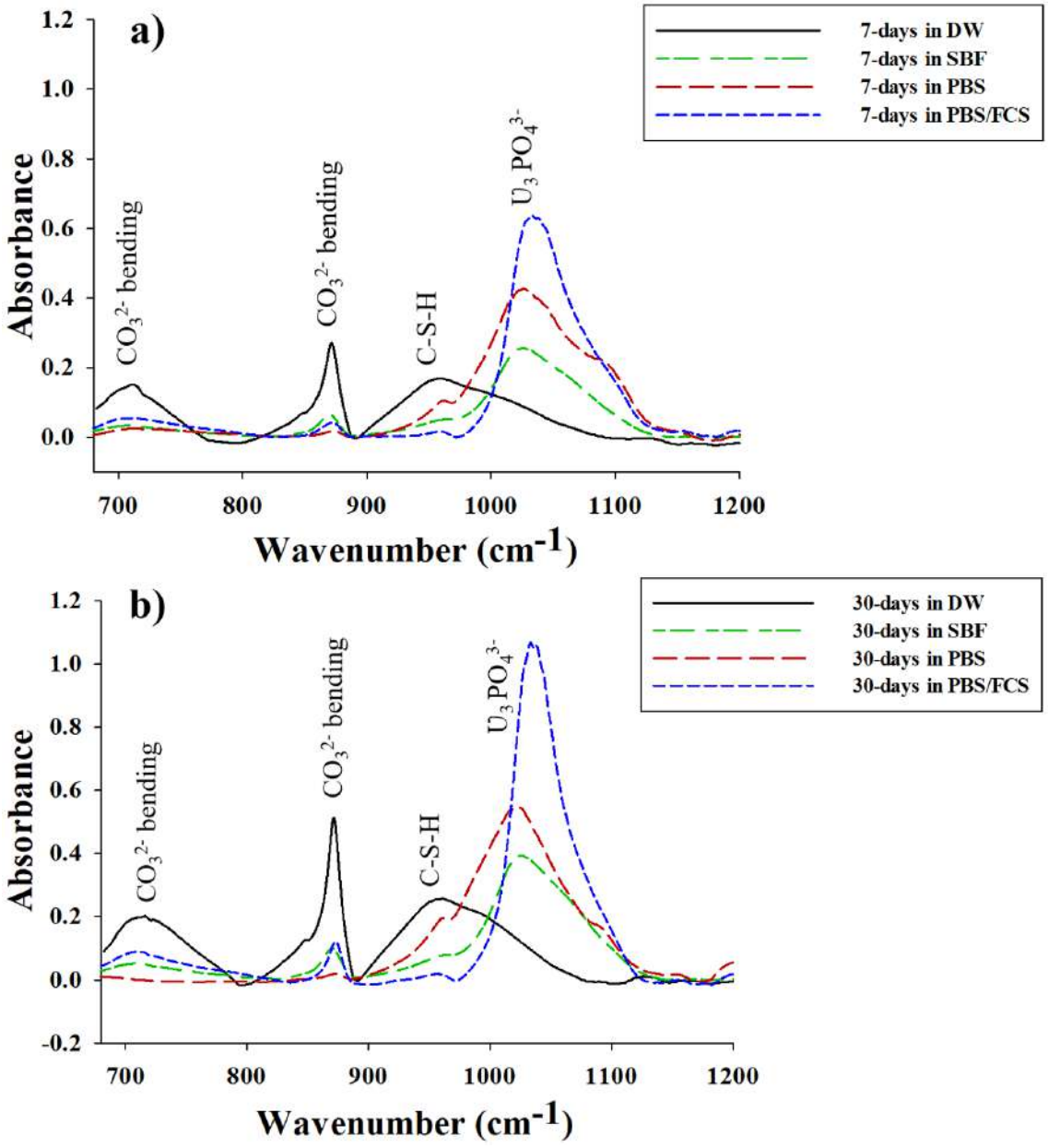

Figure 5.32: FTIR spectra of the outer-surface of the cement stored in different media after **a)** 7 days and **b)** 30 days. Only the cement immersed in DW developed a broad peak for C-S-H at 980 cm^{-1}. When cements were stored in other media than DW, there was an additional absorbance peak around 1020-1030 cm^{-1} for ν_3 stretching of PO_4^{3-} of apatite.

5.1.14 Microstructure analysis of the foamed cements

SEM examination of the inner-surface of the control and cements with 10 % FG at three PLRs is shown in Figure 5.33. All groups showed the main hydration phases including C-S-H gel, hexagonal calcium hydroxide and needle-like ettringite crystals. For the foamed cements increasing the PLR increased the size and number of calcium hydroxide crystals.

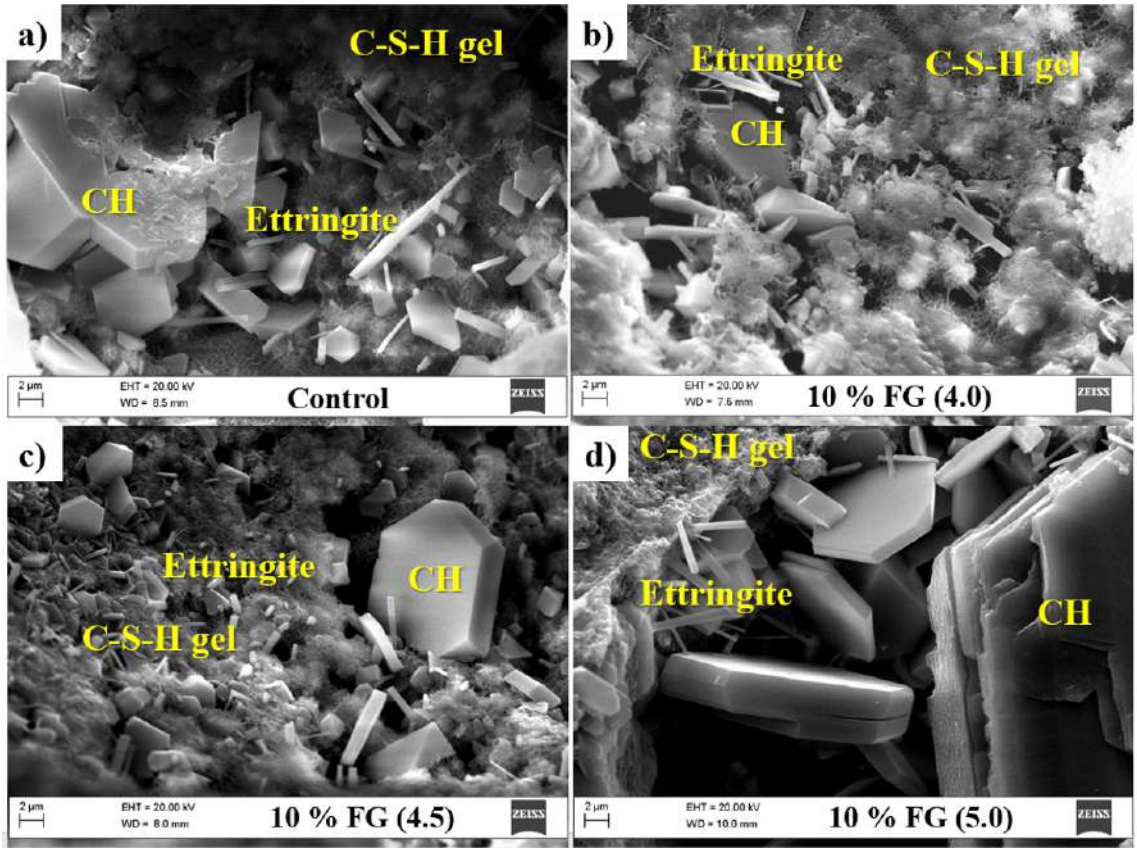

Figure 5.33: SEM micrographs of **a)** control and foamed cements at PLRs of **b)** 4.0 g/ml, **c)** 4.5 g/ml and **d)** 5.0 g/ml. All the samples indicated the presence of C-S-H gel, calcium hydroxide (CH) hexagonal crystals and needle-like ettringite crystals like the control.

5.1.15 Pore size distribution of the porous cement

SEM micrographs of the control and the foamed cements indicated a distinct difference upon addition of the FG. The inner-surface of the control cement was relatively smooth with few pores/voids at after 7 and 30 days (Figure 5.34). Meanwhile, the foaming process induced large spherical pores as shown in Figure 5.35. The pores appeared to be interconnected by many smaller pores which were clearly visible in SEM images. However, it was shown that increasing the PLR of the foamed cement to 5.0 g/ml reduced the number of large pores compared with the lower PLRs although they were still interconnected.

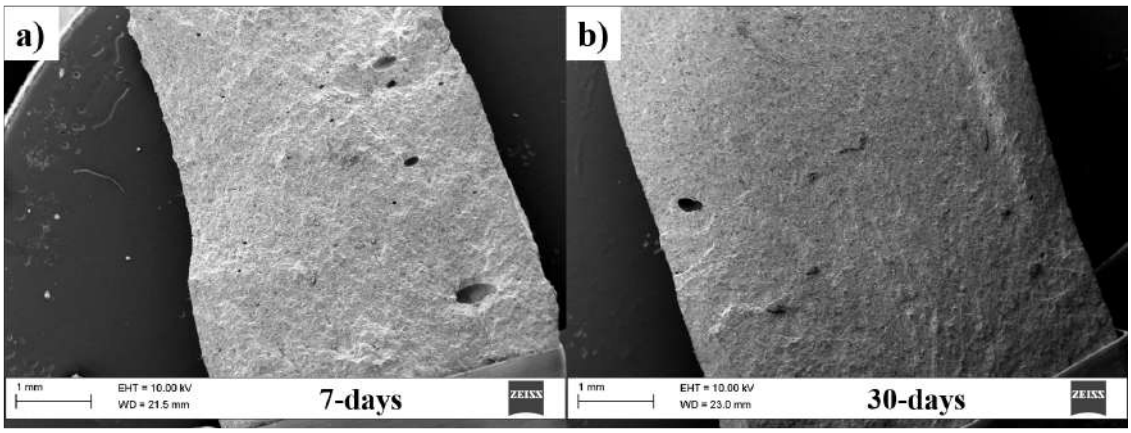

Figure 5.34: SEM micrographs of the inner-surface of control at magnification of x40 after **a)** 7 and **b)** 30 days. The surface appeared smooth with few pores/voids.

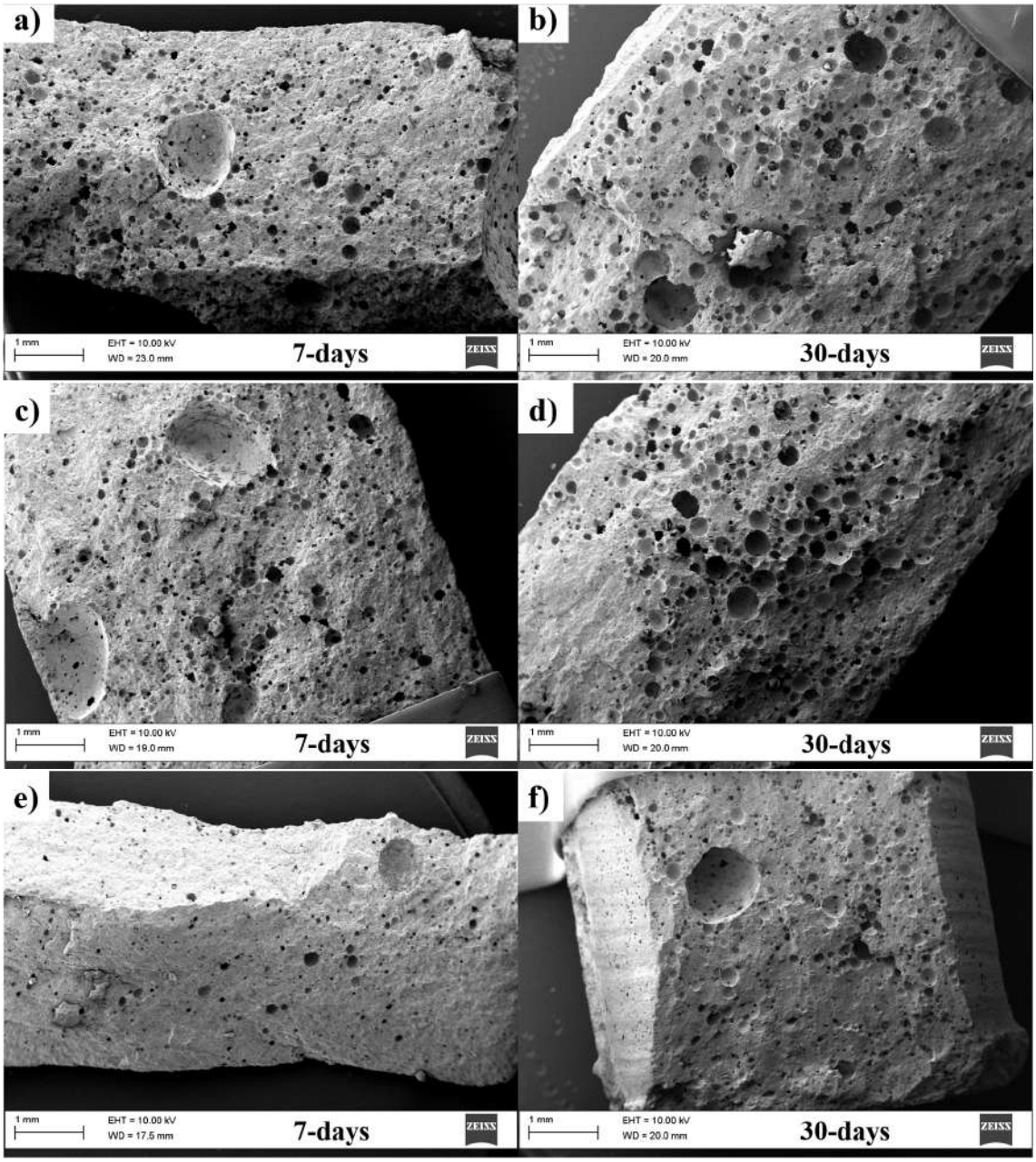

Figure 5.35: SEM micrographs of the inner-surface of the foamed cement at PLRs of 4.0 g/ml (a and b), 4.5 g/ml (c and d) and 5.0 g/ml (e and f) after 7 and 30 days. The FG induced the formation of large spherical pores. The increase in the PLR reduced the number of large pores, although majority of pores were still interconnected by smaller pores.

The frequency of pore size distribution of the control and the foamed cements at different PLRs and storage times were calculated based upon image analysis of six SEM images per group (Figure 5.36). The control PC showed low frequency of the pores from 50 to 200 μm. In comparison, all the foamed cements regardless of which PLR was used, indicated a hierarchical pore size distribution from 50 to 800 μm with the centring peak around 50 to 100 μm. Moreover, the frequency of pores larger than 50 μm was maintained as the hydration time increased. Although the pores with diameters of greater than 400 μm were more noticeable at a PLR of 4.0 g/ml compared with the other PLRs.

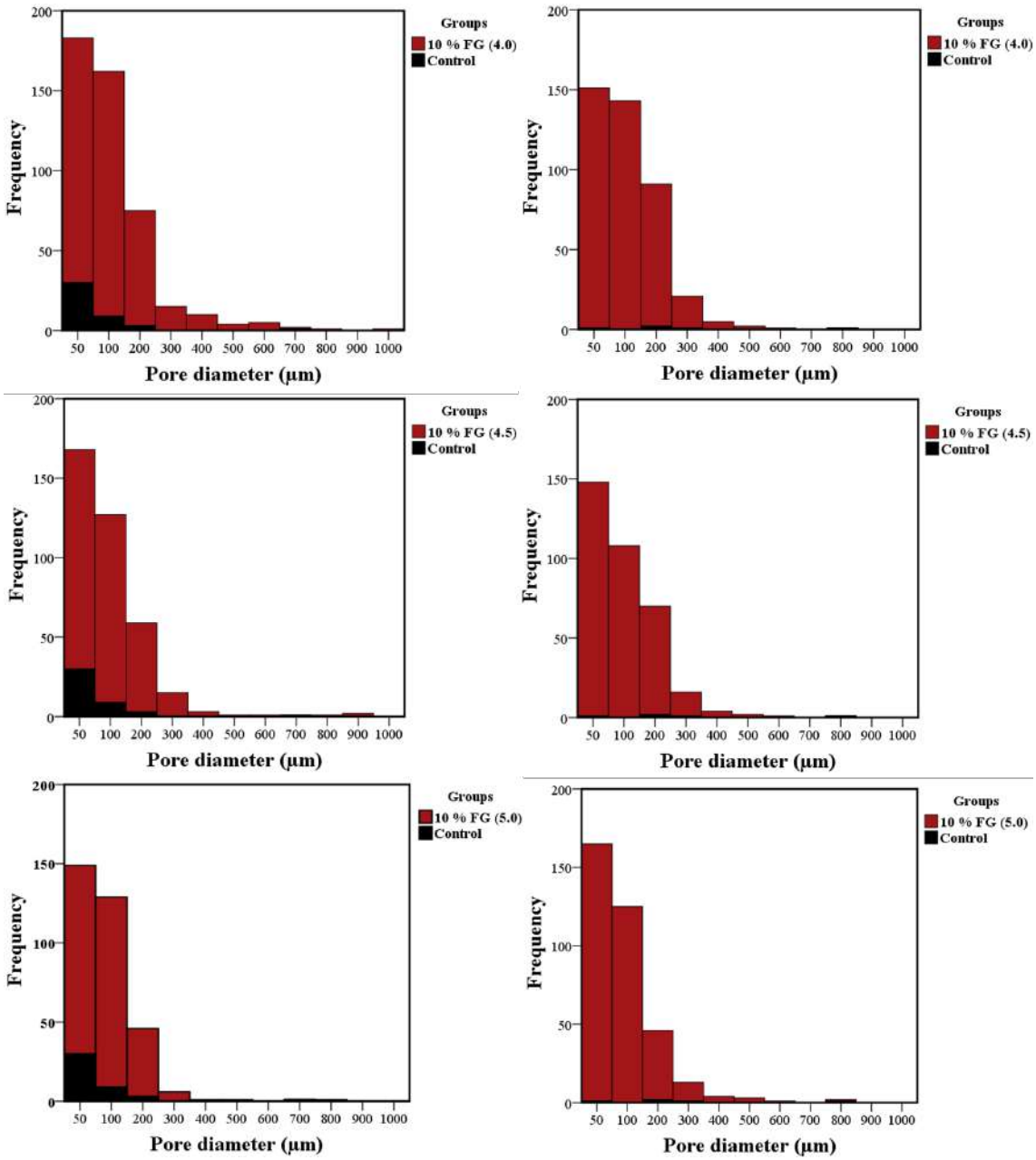

Figure 5.36: Frequency of the pore size distribution of the control and the foamed cements at different PLRs after 7 days (left) and 30 days (right). The foamed cement at 4.0 g/ml showed a noticeable frequency of pores larger than 300 μm compared with others after 7 days. Whilst, the foamed cements maintained the hierarchical pore size distribution over 30 days compared with the control.

5.1.16 Effect of casting methods on the geometry of pores

Injection of the foamed pastes 2.5 min after mixing at the lowest PLR (4.0 g/ml) and the highest PLR (5.0 g/ml) were shown to maintain the geometry of pores compared with when the cement was cast using spatula (Figure 5.37). In the both methods, spherical pores with certain degree of interconnectivity were generated from the foaming process. Furthermore, the total relative porosity of foamed cement was very similar in the both methods.

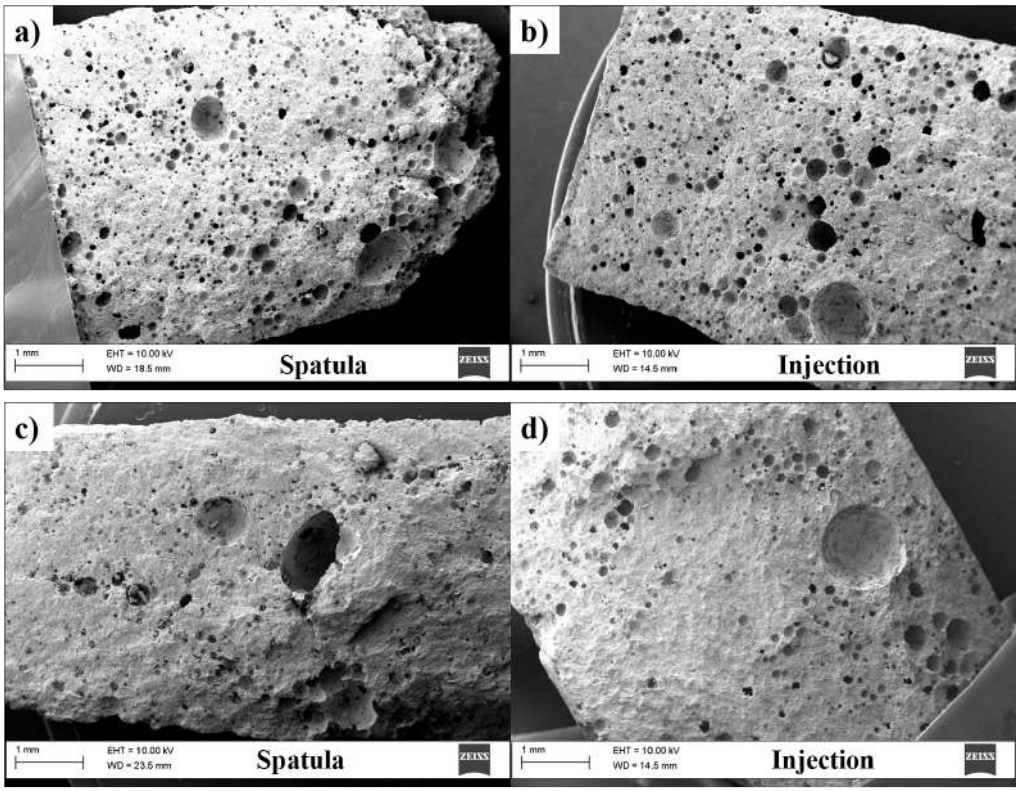

Figure 5.37: SEM micrographs of the foamed cement at PLRs of 4.0 g/ml (a and b) and 5.0 g/ml (c and d) using different casting methods. Both injection and casting of cement using spatula maintained the spherical pores.

5.1.17 Pores size distribution of interconnected pores using MIP

The pore size distribution of interconnected pores for the foamed cements were determined against the unmodified PC (control) using MIP (Figure 5.38). The control cement showed a unimodal pore size distribution centred between 0.01-0.1 μm. Meanwhile, the foamed cements showed a multimodal pore size distribution between 0.01-0.1 μm, 0.5-2 μm and 10-60 μm. It appeared that increasing the PLR reduced the proportion of interconnected pores larger than 10 μm compared with the lower PLR.

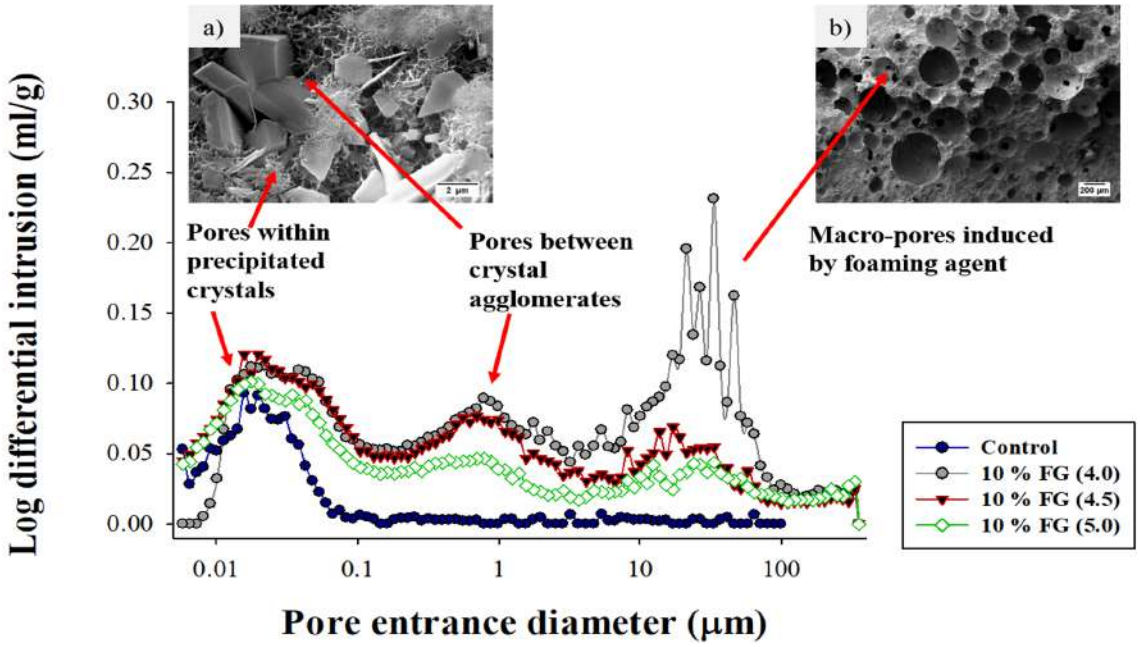

Figure 5.38: Pore size distribution of open pores for the control and the foamed cements. The intrinsic porosity ranging from 0.01 to 2 μm corresponded with the pores within and/or between the precipitated crystals as shown in SEM image (a). The interconnected pores within large macropores were shown to be larger than 10 μm as shown in SEM image (b).

5.1.18 Phase composition analysis using XRD

Considering all the samples contained 20 wt% bismuth oxide, the triplet peak centred at $2\theta = 27^{o}$ was used to normalise all the XRD data (Figure 5.39). After 7 days, the main crystalline phases found from the XRD patterns of the control PC and the foamed cements were calcium hydroxide, bismuth oxide and calcite. C-S-H could not be detected by XRD due to its amorphous structure. Within foamed cements, there was a positive correlation between increasing the PLR and the calcium hydroxide formation.

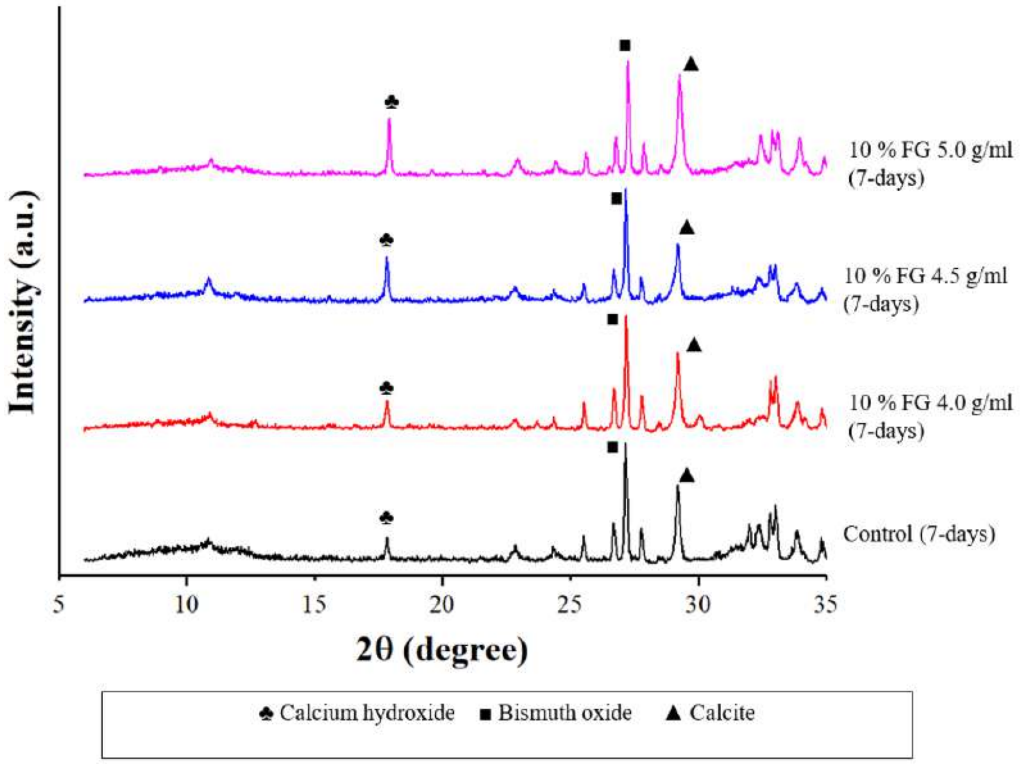

Figure 5.39: XRD patterns of the control and the foamed cements at different PLRs after 7 days. Within foamed cements, the intensity of calcium hydroxide increased with the increase in the PLR compared with the control.

After 30 days of hydration, all cements still indicated the typical peaks for PC including calcium hydroxide peak at 2θ = 18° as shown in Figure 5.40. Meanwhile, the peak corresponding with the calcite at 2θ = 29.4° was lower compared with the 7-days XRD patterns.

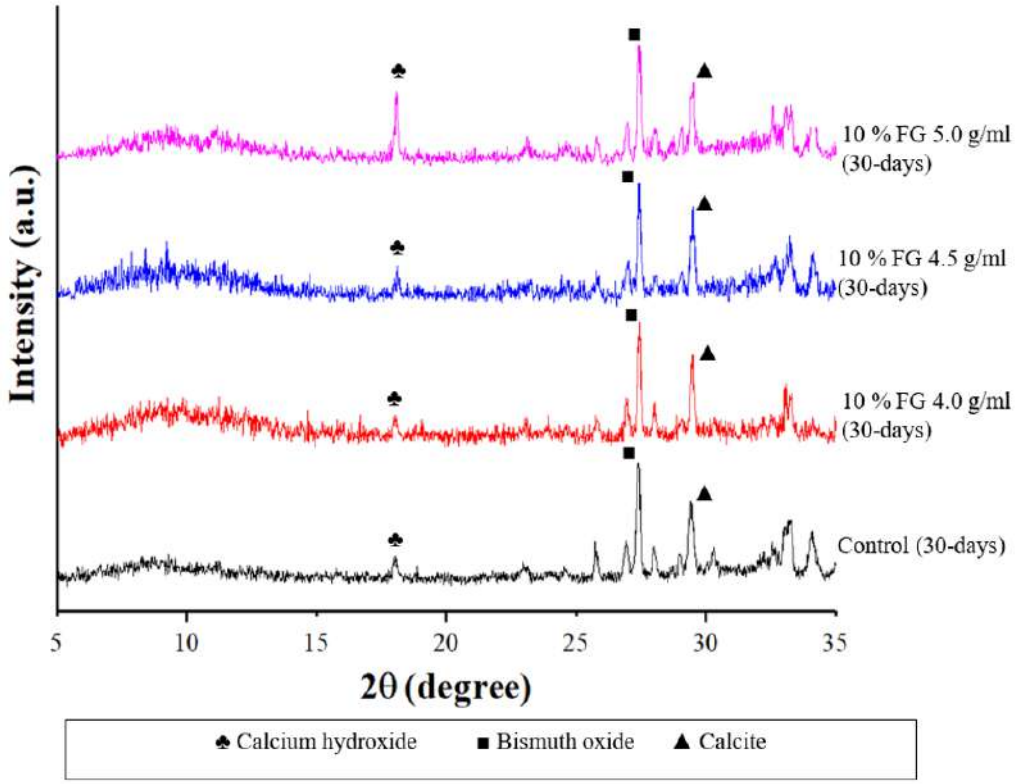

Figure 5.40: XRD patterns of the control and the foamed cements at different PLRs after 30 days. All groups showed the peak corresponded with calcium hydroxide. Meanwhile the peak for calcite decreased considerably when compared with 7-days patterns.

5.2 Discussion

5.2.1 Liquid foam characterisation

5.2.1.1 Foamability

A higher foaming capability was identified for polysorbate 80 solution compared with gelatine possibly due to the greater efficiency of low MW foaming agents in reducing the surface energy than high MW [15, 168]. The foamability remained almost constant for the range of concentrations used in this study (Figure 5.1) which correlated with previous studies [15, 16]. This is potentially due to surfactants having a critical micelle concentration (CMC), which is described as the concentration above which micelles form across the interface [168]. And as the concentration of polysorbate 80 in the present study exceeded the CMC of 1.3 $x10^{-1}$ wt%, it means that the surface has become fully saturated, hence the foamability remained constant.

The CMC value for gelatine has not been determined and previous studies reported that above a concentration of 1.5 wt%, the foamability remained constant, which was also the case in the present study (Figure 5.1) [16]. Surprisingly, all previous studies fabricated foamed CPCs using 20 wt% FG which differed from the present study [15, 16, 118, 119, 131]. This difference may have arisen from earlier magnetic shakers being unable to foam a very viscous gelatine solution compared with a domestic mixer which oscillates more rapidly (11000 rpm) than the magnetic shakers (1200 rpm).

5.2.1.2 Foam stability

The increase in the foam stability of gelatine compared with polysorbate 80 (Figure 5.2) correlated with previous studies since high MW foaming agents allowed the continuous phase of the foam to have a high viscosity [15, 16, 118, 119, 131]. As a result, both gravitational drainage of liquid and bubble coalescence were limited, thus increasing the stability of the foam [15, 16]. In addition, proteins such as gelatine could have created a viscoelastic film by intermolecular covalent disulphide bonds to surround the entrapped air and improved the stability of the foam compared with polysorbate 80 [16].

5.2.2 Effect of foaming agents on the setting time and injectability of PC

5.2.2.1 Setting time

It appeared that both concentration of foaming agents and PLR played key roles in the setting time of the PC. As expected, a reduction in the initial setting time of PC containing 1 % FG occurred due to using high PLRs (Figure 5.3) [119]. The delay in the initial setting time of PC containing 10-20 % FG may have occurred for two reasons: either the foam was not used as the only liquid phase to mix with the powder phase, so the foam phase could have introduced extra water into the model system and lowered the PLR. Or the increase in the viscosity of the cement with increasing gelatine content possibly interfered with the dissolution of calcium-silicate phases by preventing the diffusion of ions which

was previously shown to retard the final setting time of CPCs [119]. Thereby, at the same PLR, increasing the concentration of gelatine to 10 wt% should have lengthened the setting time result, which did not occur. This is potentially because the setting time measurements were carried out at room temperature, allowing the gelation of the gelatine to take place. This could have inhibited the Gilmore needle from penetrating the surface, resulting in the setting time being reduced (Figure 5.2), which was also found in previous study [119].

Non-ionic and hydrophilic surfactants including polysorbate 80 have been shown to be more effective in retarding the setting time of bone cements by inhibiting the hydration of the cement (Figure 5.4) [118, 169]. The negative influence of FP on the setting time of PC with increasing concentration was in accordance with a previous study on CPCs [118]. The exact underlying mechanism is not clear, but one possible explanation could be that the disruption of the foam (arising from the low foam stability of polysorbate 80 immediately after it was mixed with water) which could have introduced a significant amount of water into the PC model system, and delayed the setting and hardening of the PC.

Other than varying the concentration of foaming agents to accelerate the setting time, the effect of altering the PLR was examined also, as a long setting time would be undesirable regarding longer hospitalisation time and higher cost for healthcare [7, 8, 10]. Nevertheless, some researchers believe that a longer setting time of injectable bone cement could be acceptable as it does not have to set fully prior to wound closure as long

as the cement maintains its integrity [15]. In the present study, as expected increasing the PLR to 5.0 g/ml accelerated the setting reaction by reducing the amount of liquid phase which increased the rate of precipitation and thus, hardening of the PC [10, 59]. This allowed a setting time of 25 min even upon addition of 10 % FG. The obtained setting time value was very similar to the setting time of PMMA (20 min) [6, 10].

The alternative method to reduce the setting time could have been increasing the calcium chloride concentration to 10 wt% as it accelerated the setting time of PC according to the results presented in chapter 3 (Figure 3.1). However, increasing the concentration of calcium chloride was shown to reduce the compressive strength of the cement (Figure 3.7) as well which would be undesirable.

5.2.2.2 Injectability

Cements containing 10 % FG exhibited a very high injectability (Figure 5.5) and excellent cohesion (Figure 5.26) even at high PLRs and therefore, incorporation of 10 wt% calcium chloride could have exerted additional liquefying effect and caused the paste to seep out. High injectability and excellent cohesion are considered as important requirements for bone cements for PVP applications [5, 6, 10]. The improvement in handling properties of the foamed PC compared with the control could have been attributed to the increase in the viscosity of the liquid phase [15, 16]. This prevented powder segregation and maintained a homogeneous extrusion of the cement paste without the risk of phase-separation [16]. Owing to the gelation of FG, the foamed cement maintained its integrity

after injection into the hollow space which may suggest that the foamed cement ensured the early stabilisation of cement without leaking out of the vertebral body [15, 16].

The efficacy of FP in dispersing cement particles has been reported to rely on numerous factors including composition of cement, mixing condition, concentration of sulphate in the cement and type/concentration of surfactant [169, 170, 171]. The carboxyl groups present within the backbone of polysorbate 80 are responsible for its adsorption on the cement surface [171, 172]. Besides, the presence of calcium chloride in this PC model system promoted faster consumption of the gypsum which previously was shown to allow the adsorption of polymer surfactant onto the cement [169, 172]. The result (Figure 5.6) also indicated the important influence of surfactant concentration, which led to phase-separation of the paste and limited its usage with this novel PC. Considering all these factors, addition of 10 % FG at its highest foam stability demonstrated the most suitable properties for PVP application.

5.2.3 Characterisation of the PC setting reaction in the presence of gelatine

5.2.3.1 Setting reaction of cement

A previous FTIR study on foamed CPC reported partial leaching of the gelatine from CPCs after 12 days of setting [119]. However, in the present study the amide I and II bands for gelatine (Figure 5.27) overlapped with the standard PC bands (Figure 5.28) making it

difficult to definitively conclude the extent of gelatine leaching after 7 days. In addition, the FTIR study implied that the peak corresponded with C-S-H; the main strengthening phase did not develop for the foamed PC after 2 h of setting, which correlated with the setting time data [6, 60]. These observations contrasted with the previous study where no difference was identified between FTIR spectra of foamed and control CPCs [119]. The difference in interaction of gelatine with cement in terms of the retardation of PC dissolution compared with CPCs may provide a possible explanation.

The XRD spectra for both storage times (Figure 5.39-40) indicated no significant difference since the development of calcium hydroxide as the by-product of C-S-H formation was observed for both control and foamed cements. This indicated that addition of gelatine did not interfere with the setting reaction after 7 days and the inhibitory effect of gelatine on the setting of the PC was more likely to be temporary. The microstructural analysis (Figure 5.33) also revealed no detrimental effect of gelatine on the formation of hydration phases after 7 days, whilst increasing the PLR of the foamed cement promoted more calcium hydroxide formation that correlated with the XRD spectrum. It is important to note that C-S-H gel could not be detected by XRD due to its amorphous structure in agreement with Camilleri *et al* [152], thus identification of calcium hydroxide could be possibly used to indirectly measure the formation of C-S-H.

5.2.4 Porosity and mechanical properties of foamed cement

5.2.4.1 Porosity studies

Porosity data showed that (Figure 5.8, 10 and 12) surfactant (gelatine) even at high PLRs successfully stabilised the foam at the water-air interface by reducing the surface energies needed to create bubbles [15, 119]. However, the total porosity of this novel PC was remarkably lower compared with the previous studies where a total porosity of 64-73 % for CPCs was reported [16, 119]. This difference arose since PCs could not be used at low PLRs of 1.25-2.50 g/ml in a similar manner to CPCs, due to a long setting time and phase-separation of the paste [5, 6, 60]. In addition, higher gelatine concentrations along with increased amounts of powder could have delayed the foam maturation process [15, 16, 119]. The delay may have been caused by the increased viscosity and the shear stress applied during the mixing stage which disrupted bubble coalescence and lowered the number and size of pores [15]. Although there is no consensus on how much porosity is desirable, the present study demonstrated that for the first time a novel self-setting porous PC was developed which maintained spherical pores over 30 days. At the same time, the precipitation of the hydration phases over time have filled the nano-micron sized pores which explained the reduction in the intrinsic porosity of cement over time (Figure 5.9).

5.2.4.2 Pore size distribution of foamed PC

A decrease in total porosity was expected with production of irregular pore geometry as bubbles were forced out of the syringe which could have destroyed the bubbles partially. Interestingly, the total porosity and pore geometry (Figure 5.37) were maintained for the foamed cement even 2.5 min after injection. From SEM micrographs it was evident that both methods of casting induced large spherical pores possibly due to high foam stability of gelatine which overcame the cohesive force upon the setting reaction of the cement [16, 119]. For this reason, the current method to fabricate porous cement could be applied for PVP where the bone cement is injected through a needle.

Many studies reported a minimum pore size of 100 μm for bone ingrowth with an optimum size of 100-400 μm [89, 90, 91, 173]. The SEM and image analysis of the present study clearly indicated that the foamed PC at PLRs of 4.0-4.5 g/ml possessed plenty of large pores in the range of 100-400 μm (Figure 5.36-7). Large pores can be interconnected by micropores or coalescence of adjacent bubbles which increases the surface area available for fluid transport thus, facilitating the survival of cells within the bulk of the cement [15, 173]. When interpreting the data from MIP (Figure 5.38), it is important to remember that MIP only measures the entrance pore size which is the interconnections between pores [16, 174]. For the foamed PC at the lowest PLR, 14 % of open pores were centred around 30 μm and this value decreased to 10 % and 8 % for 4.5 g/ml and 5.0 g/ml respectively. This may have suggested that at the lowest PLR the foamed PC showed the most promising properties to favour bone ingrowth. A recent

in vivo study by Bohner *et al.* [173] indicated that within 3 weeks, mineralised tissue within micropores as small as 1 μm was formed. This mineralised tissue was only shown to form when the pores were interconnected by pores larger than 1 μm, therefore, the obtained results in the present study showed plenty of interconnected pores large enough to accommodate vascularisation and nutrient transport.

5.2.4.3 Mechanical properties

The relationship between relative porosity and compressive strength of the cement is inversely logarithmic according to Griffith's theory [101, 102, 175]. The increase in total porosity of the foamed cement resulted in the loss in strength as expected (Figure 5.8,10 and 12). Many factors are known to influence strength such as homogeneity of the cements matrix, particle size, porosity, critical flaw size, soaking media and PLR [175].

The hydration of PC can continue up to 30 days where 80 % of the hydration is completed [59, 60], thus the compressive strength of the cement would also be expected to increase, which did occur in the present study (Figure 5.8,10 and 12) even in the presence of gelatine. This finding is quite important since all the previous studies only considered the early mechanical properties (7-12 days) of foamed CPCs [16, 119, 131, 174]. Thereby, addition of gelatine was shown to not interfere with the normal hydration of PC in the long-term which makes it a suitable porogen for PC-based cements. Furthermore, increasing the PLR of the foamed cement positively improved the hydration rate of the cement by accelerating the formation of main strengthening phase; C-S-H [6, 60]. This

highlights that the properties of foamed cement can be readily optimised for a specific application.

The lower compressive strengths values compared with previous studies was unexpected as a higher PLR was used to produce the foamed cements in the present study [16, 119, 131, 174]. This difference could have arisen from the difference in the particle sizes of the starting material and method of introducing the foam to the system which introduced a considerable amount of water. Previous studies reported a median particles size of 5.4-7.3 μm for foamed CPCs [16, 118, 119, 131], which has shown to increase the hydration rate and improve the early strength compared with the coarser cements [176, 177, 178]. PC is a mixture of clinkers, and the particle size has been reported to be in the range of 5 to 90 μm, which is already higher than CPCs [179]. Therefore, the influence of particle size appeared to overpower the effect of PLR in this study and needs to be addressed in further studies.

5.2.4.4 Effect of storage media and regime on the strength of PC

The soaking environment significantly affected the strength of both the control and foamed cements. No difference in the compressive strength of controls stored in different media was expected, however the strength was remarkably improved in PBS or PBS/FCS. Many studies reported that mixing of the cement with serum reduced the mechanical properties of MTA and CPCs by inhibition of the precipitation of hydration phases [5, 134, 175, 180, 181, 182]. However, in the present study the cement was only exposed to serum

containing media once it was set which limited the interactions of proteins with the bulk material. In addition, bodily fluid contains many biomolecules such as enzymes (alkaline phosphatase), vitamins and ions etc. which further complicate the interactions between the body and the biomaterial [134, 180]. In fact, interactions of other biomolecules in serum may have accelerated the hydration of cement and limited proteins interactions for PC system with a very low porosity (11-14 %).

A higher compressive strength for foamed cements stored in PBS was expected, yet the compressive strengths values for samples stored in DW were higher than the other media in accordance with previous study [119]. This could have occurred as a consequence of the lower solubility of PC in water which limited the leaching of gelatine, so that it acted as an agglutinant to PC crystals and enhanced the strength of the cement [119]. On the other hand, immersion of samples in PBS containing solutions could have slowed down the precipitation of hydration phases due to interactions of calcium and silicate ions with other ions in PBS, and thus increased the dissolution of cement (solubility) [175]. This might have led to increase dissolution of gelatine, hence loss of more gelatine which reduced the mechanical strength of the cement by increasing the porosity according to previous studies [119, 132, 183]. Therefore, increasing the solubility of porous cement could have overcome the effect of serum components on the hydration rate of cements compared with low porosity system. Unfortunately, the leaching of gelatine could not be determined in the present study as the amide bands of gelatine overlapped with PC bands.

Refreshing the media on daily basis reduced the strength of the cement (Figure 5.16)

compared with the static regime. Once the medium was refreshed on daily basis, the precipitated by-products could have been removed, thus the equilibrium may have not been reached and allowed further dissolution of the cement each time the medium was refreshed [184, 185]. For these reasons, solubility and the total porosity were all increased. Despite the adverse effect of the dynamic regime on the setting of the cement, the compressive strength values were still higher than healthy cancellous bone (2-9 MPa) and therefore, potentially suitable for load-bearing applications [22].

5.2.4.5 Investigation of the strength-deteriorating effect of gelatine

Regardless of the immersion media used for the cements, the similar strut densities of all foamed cement and controls (Figure 5.18-19) indicated that the addition of gelatine did not interfere with normal hydration of cement, which correlated with XRD data unlike other porogens such as mannitol and sucrose (Figure 4.10). Studies on the early strength of foamed PC as a function of porosity indicated that the strength-deteriorating effect of gelatine was dependent on the soaking media (Figure 5.14). The partial cross-linking of gelatine when samples were immersed in DW could have acted as a flaw as well. Conversely, when the cement was soaked in PBS-containing solutions, the leaching of gelatine limited its interaction with cement reactants and thus no change in the materials constants (Figure 5.15) [119, 184].

5.2.4.6 Weibull modulus studies

The Weibull modulus values obtained in the present study were within the range of ceramic materials (5-20) [142, 186]. According to the strength-porosity results, the reduction in the reliability of strength (Figure 5.25) upon the addition of gelatine were as expected. However, the reduction in the reliability of the data only became significant when 10 % FG was added to the cement. Despite this, the Weibull modulus values for the foamed cements in the present study were still higher than macroporous CPC [187]. A previous study demonstrated by Seuba *et al.* indicated that for porous ceramics, the Weibull modulus was dependent upon the wall thickness of the pores rather than porosity, whilst the compressive strength was influenced only by porosity [188]. Therefore, the Weibull modulus and compressive strength were shown to be controlled quasi-independently [188]. Furthermore, the influence of porosity on the Weibull modulus of porous ceramic is not entirely understood, due to the difficulties in controlling individual features of porous ceramics which should be addressed in future studies [186, 188].

Cements were more reliable when stored in PBS/FCS than DW. The improvement in the reliability of data could arise from the additional interactions between cement reactants and PBS solution as explained previously. However, no study has investigated the effect of soaking media on the reliability of strength data which makes it difficult to draw a definite conclusion. This perhaps suggests that for a ceramic material, using the mean strength value could be misleading and measuring the Weibull modulus along with strength studies could provide a better understanding.

Comparing the reliability of controls obtained in the present study (Figure 21-2) with results presented by Wynn-Jones *et al.*, indicated that the reliability of strength data was lowered by incorporation of bismuth oxide [6]. Coomaraswamy *et al.* demonstrated that bismuth oxide had a detrimental effect on reliability of PC by increasing the size of flaws [102]. This may suggest that for future studies investigation of other radiopacifying agents for PC-based cement should be considered.

5.2.5 Effect of storage media on the setting of PC

Various studies have reported that the Ca/P ratio of apatite deposits on MTA were greater than 1.67 indicating the formation of carbonated apatite which favours new bone formation [135, 136, 189]. Following previous studies, using complementary techniques such as SEM (Figure 5.31) and FTIR (Figure 5.32) both clearly indicated that the chemical composition of the outer-surface of PC was modified by immersion in physiological fluids [133]. However, the uniformity and Ca/P ratio of these deposits were highly dependent on the chemical composition of the soaking/immersion media [133, 135, 136, 189].

5.2.5.1 Setting of PC in SBF

Kokubo *et al.* [190] suggested that formation of carbonated apatite on any biomaterial soaked in SBF was an indication of *in vivo* bioactivity [133, 190]. However, this suggestion was shown to be invalid as many studies reported no bone integration was evident *in vivo* [133, 191, 192, 193, 194]. A review by Bohner *et al.* [133] also reported a lack of

scientific evidence to accept the suitability of SBF for bioactivity testing, which correlated with the obtained results since very little carbonated apatite deposit was formed compared with serum containing solution [133]. There are two main differences between serum and SBF which limits its use: i) absence of serum proteins which may inhibit or promote apatite formation and ii) addition of TRIS buffer to SBF. Therefore, interpretation of any results obtained from immersion of a material in SBF should be done with caution [133].

5.2.5.2 Setting of PC in presence of proteins

Many studies have reported that PBS promoted the formation of apatite deposits on CPCs and PCs [58, 82, 134, 135, 189]. The outer-surface of PC was shown to become a reactive substrate upon immersion in culture medium. The formed HA on the outer-surface of the PC could have occurred due to the high pH and series of reaction between cements reactants and the storage medium as explained elsewhere by Gandolfi *et al.*, which promoted the formation of carbonated apatite [82].

During PVP procedures, bodily fluid including proteins will be immediately adsorbed on the external surface of the biomaterial. Therefore, addition of 10 % FCS to PBS was important to mimic *in vivo* conditions [195, 196]. Interestingly, in the presence of serum proteins, formation of carbonated apatite was accelerated with a higher Ca/P ratio than identified in samples immersed in PBS. This could have occurred due to the presence of other biomolecules which may have promoted carbonate ions to substitute the phosphate ions during maturation of apatite as well as increasing the nucleation sites for apatite

precipitation.

The strut density of sample stored in PBS/FCS was 2.71 g/cm^3 which was significantly higher than the density identified after storage in DW (Figure 5.18-9). Since the porosity values were similar in both media, the deposition of HA with density of $\approx$ 3.14 g/cm^3 could be the reason for higher density values. Many studies on CPCs indicated that proteins inhibited the formation of HA on brushite cements, [133, 134, 182, 184], whilst, others reported the formation of the HA *in vivo* [195, 196]. Hence, FCS could either inhibit or promote HA formation according to the types and concentration of proteins as well as cement composition [133]. Bohner *et al.* also indicated that immersion of a solid biomaterial into serum could modify the composition of the solution, which can either inhibit or promote apatite formation [133]. The setting of PC increased the local pH of the solution by three pH units which then reduced the HA solubility by 10-100-fold and accelerated apatite formation.

5.2.6 Solubility of PC

The solubility of PC (Figure 5.20) was shown to be much lower compared with reported values in literature mainly due to using higher PLRs in the present study which limited the dissolution of cement [135, 136]. It was shown that the solubility of the samples in PBS/FCS was lowered compared with PBS. This could be attributed to the formation of much thicker carbonated apatite on the outer-surface of the cement which may have acted as a diffusion barrier and limited the ionic exchange between cement and

serum [134, 175]. In addition, FCS contains 50-90 ppm calcium ions compared with PBS solution which could also reduce the solubility of PC in agreement with previous studies [134, 175, 184, 185].

5.3 Summary

To summarise the results of this chapter indicated that by changing the PLRs and content of added FG, it was possible to optimise the material properties to develop a porous self-setting PC with high injectability and sufficient early mechanical strength to stabilise the fractured vertebral body. However, the setting time was doubled which is undesirable for vertebroplasty applications. Hydration of the PC in the presence of proteins promoted formation of carbonated apatite which is important for bone formation at the surface of the biomaterials.

Chapter 6

Conclusions

The sufficient durability and compressive strength of PCs have been the main driving forces in development of this material for medical applications [59, 60]. The major finding of the first chapter was that the PC model system with a combination of 75 wt% PC, 20 wt% bismuth oxide and 5 wt% calcium chloride, demonstrated the optimal setting time, injectability and compressive strength for load-bearing applications regardless of the ageing of the cement over time. The degradation of the cements reactants with storage reduced the reactivity of the cement and prevented sodium citrate additions from causing flash setting of the old batch in contrast to the new batch [14].

The addition of both soluble sugars and sodium bicarbonate to the PC, appeared to adversely influence the material properties of PC with no creation of macropores. However, the mechanism causing these negative effects differed for each porogen. When sugars added to the cement, the setting time increased and cement pastes behaved as liquids, as sugars appeared to adsorb onto the cement surface and poisoned the hydration of the cement [154, 156]. Subsequently, the intrinsic porosity increased due to the increase in the unreacted water within the paste, resulting in a very weak cement, unsuitable for load-bearing applications. The addition of sodium bicarbonate above 5 wt% appeared to

interfere with alkaline setting reaction of the PC and made the paste too dry to work with [161, 197].

When gelatine was added as a protein based foaming agent to the cement, the high viscosity of gelatine allowed a homogeneous extrusion of the cement through the syringe even at high PLRs. Although gelatine possessed a very high foam stability, the coalescence of bubbles still occurred which allowed formation of large spherical pores ranging from 100 to 400 μm after the setting of the cement. These large pores were interconnected by smaller pores typically with diameters larger than 10 μm. The total porosity of the foamed cement could be optimised by changing the PLR of the system. The increase in the porosity of foamed cement appeared to increase the solubility and reduced the compressive strengths to a level higher or comparable with that of healthy cancellous bone. Therefore, this porous injectable PC has the potential to be used for load-bearing applications, although *in vitro* and *in vivo* assessments of this cement is needed to confirm and improve this PC formulation.

Chapter 7

Future work

The investigation of batch stability using XRD indicated a general degradation of cement over time compared with the fresh new batch despite storage of the PC powder in a desiccator. For future work, studying several aged batches over a range of humidities and temperatures could provide a better insight into the ageing process. In the present study, type II Mastercrete Lafarge PC was used due to its high early compressive strength demonstrated by previous research conducted within the Biomaterials Unit of the University of Birmingham [6, 66, 102]. For future studies, investigation of the effect of additives on the other types of PC cement from different sources could allow identification of a new working window for sodium citrate.

Throughout this project a variety of complementary techniques were used to characterise the influence of porogens and foaming agents on the setting of the PC. To completely understand the underlying mechanism of each porogen, using other techniques such as zeta potential and differential scanning calorimetry (DSC) could be beneficial to further explain injectability and the setting reactions. Zeta potential measures the surface charge of the cement during its setting reaction. Such data could be used to further explain injectability studies [6, 198]. DSC measures the enthalpy change during the setting

of the cement. The result of DSC is particularly useful since the hydration of PC contains couple of exothermic peaks within the 2 h of the setting. This can be traced and used to compare the heat profile of modified cements with control to identify any change in the overall energy release of PC [199, 200].

Since the particle size of starting material plays an important role in the ultimate mechanical properties of the set cement, sieving the powder to obtain fine particles without any agglomerates will be recommended to improve the compressive strength of foamed cements. The median particle size of cement can be measured more precisely using laser diffraction techniques for direct comparison with previous studies [22].

In the present study the average pore size was calculated based upon machine learning algorithms previously shown to be an accurate and reliable method to distinguish spherical objects from the surface of a biomaterial [138, 139]. It may be desirable for future studies to reconstruct the 3D model of porous PC using a micro-computed tomography (micro-CT) to analyse the sample in 3D environment [201, 202]. Micro-CT can provide useful information about pore size distribution as well as micro and macroporosity of the porous ceramics. However, the resolution of micro-CT can be problematic if the pores are smaller than the resolution of the machine as the machine cannot detect smaller pores. This technique is also very expensive and time consuming compared with SEM [201, 202].

The ultimate aim of this study was to find a suitable method to induce macroporosity in PC-based cements, and there remains room for improvements. The setting time of 20 min for bone cement is an indication of the appropriate time for closure of the wound

to minimise the hospitalisation time and ensure early stabilisation of the vertebral body. Many factors are involved in changing the setting time of the cement such as PLR, particle size, additives and temperature [10, 15]. From the factors mentioned above, addition of accelerants and increasing the PLR were shown to reduce the setting time of foamed cements to 25 min. However, the porosity and interconnectivity of foamed cements were considerably reduced. Therefore, the addition of other available accelerants (sodium nitrate) or fibres (collagen) should be investigated to reduce the long setting time of the foamed cement at a low PLR.

The compressive strength of different types of bone cement has always been measured as the main mechanical property for vertebroplasty applications. Since PC is a ceramic material, it will be recommended to measure other mechanical properties including bending strengths (three-point bending and biaxial flexural strength), bending modulus and fatigue strength according to ISO 5833:2002 to examine the durability of this novel cement [6, 10, 40].

This has been the first study which successfully fabricated an injectable self-setting porous PC for load-bearing applications. Hence, biological *in vitro* assessment of this novel cement determining cell adhesion, gene expression and synthesis and mineralisation of bone matrix would be important to obtain an indication of biocompatibility.

Chapter 8

Appendix

8.1 EDS analysis

Clinker phase	Chemical formula	Atom	Molecular mass
Alite	$3CaO.SiO_2$	Ca	120
		O	80
		Si	28
		Total =	**228**
Belite	$2CaO.SiO_2$	Ca	80
		O	64
		Si	28
		Total =	**172**
Tricalcium aluminate	$3CaO.Al_2O_3$	Ca	120
		O	96
		Al	54
		Total =	**270**
Tetracalcium aluminoferrite	$4CaO.Al_2O_3Fe_2O_3$	Ca	160
		O	160
		Al	54
		Fe	112
		Total =	**486**
Calcium sulphate anhydrous	$CaSO_4$	Ca	40
		S	32
		O	64
		Total =	**136**
Calcium sulphate hemihydrate	$CaSO_4.H_2O$	Ca	40
		S	32
		O	80
		H	2
		Total =	**154**
Calcium sulphate dihydrate	$CaSO_4.2H_2O$	Ca	40
		S	32
		O	96
		H	4
		Total =	**172**

Hydration phase	Chemical formula	Atom	Molecular mass
Ettringite	$6CaO.\ Al_2O_3.3SO_3.32H_2O$	Ca	240
		O	800
		Al	54
		S	96
		H	64
		Total =	**1254**
Calcium monosulphate	$4CaO.Al_2O_3.SO_3.12H_2O$	Ca	160
		O	**352**
		Al	54
		S	32
		H	24
		Total =	**622**
Calcium aluminate hydrate	$4CaO.Al_2O_3.13H_2O$	Ca	160
		O	320
		Al	54
		H	26
		Total =	**560**
C-S-H	$3CaO.SiO_2.8H_2O$	Ca	120
		O	240
		Si	28
		H	16
		Total =	**376**

Theoretical ratio for clinker and hydration phases											
Clinker phases	**Ca/O**	**Ca/Si**	**O/Si**	**Ca/Al**	**O/Al**	**Ca/Fe**	**O/Fe**	**Al/Fe**	**Ca/S**	**O/S**	**S/Al**
Alite	1.50	4.29	2.86								
Belite	1.25	2.86	2.29								
Tricalcium aluminate	1.22			2.22	1.78						
Tetracalcium aluminoferrite	1.00			2.96	3.00	1.43	1.43	0.48			
Calcium sulphate dihydrate	0.42								1.25	3.00	
Calcium sulphate hemihydrate	0.50								1.25	2.50	
Calcium sulphate anhydrous	0.63								1.43	2.29	
Hydration phases											
ettringite	0.30			4.75	14.81				2.50	8.33	1.78
Calcium monosulphate	0.46			2.90	6.52				5.00	11.00	0.59
C-S-H	0.51	4.29	8.57								
Calcium aluminate hydrate	0.51			2.90	5.92						

EDS of the new batch of PC

Element	Average wt%
O	47.01
Na	0.13
Mg	0.63
Al	1.99
Si	7.04
S	0.55
K	0.48
Ca	40.27
Fe	1.89

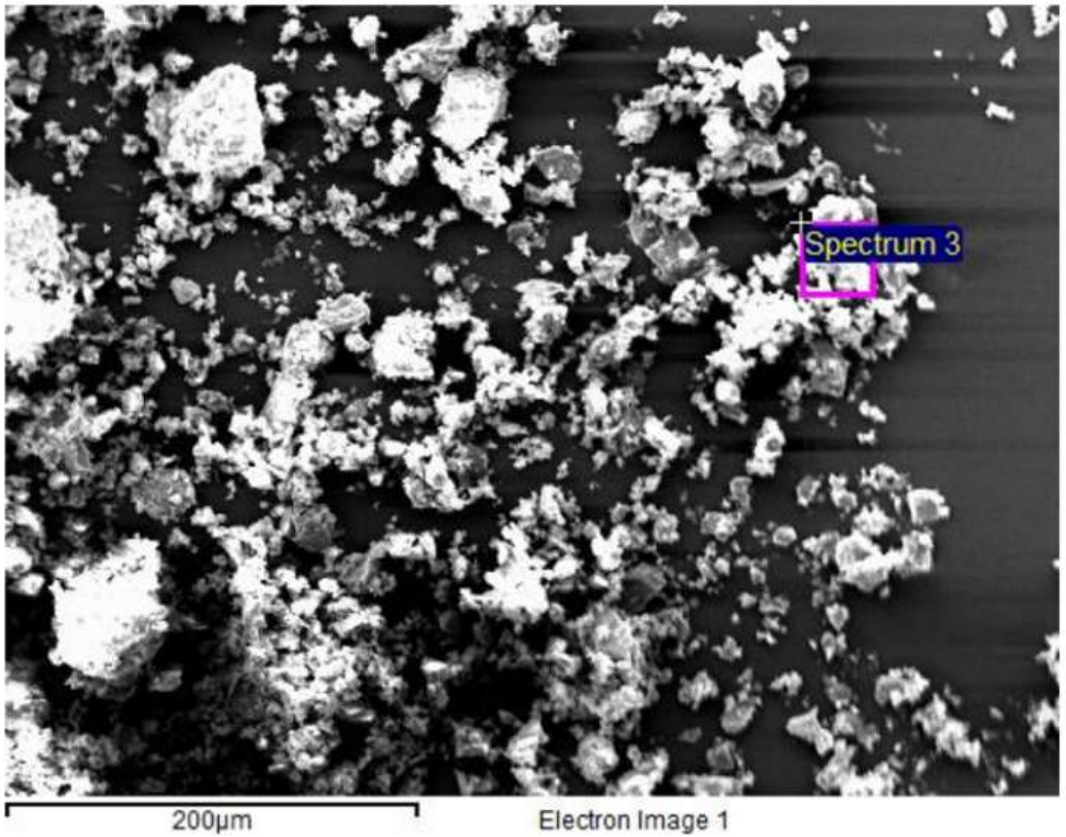

Figure 8.1: SEM image of the new batch powder with corresponding EDS analysis.

Observed ratio for the new batch of PC (wt%)											
	Ca/O	Ca/Si	O/Si	Ca/Al	O/Al	Ca/Fe	O/Fe	Al/Fe	Ca/S	O/S	S/Al
	0.85	5.72	6.68	20.24	23.62	21.31	23.97	1.06	73.22	85.47	0.28
Percentage difference between observed and theoretical ratios											
Clinker phases	Ca/O	Ca/Si	O/Si	Ca/Al	O/Al	Ca/Fe	O/Fe	Al/Fe	Ca/S	O/S	S/Al
Alite	43.33	-33.00	-134.00								
Belite	32.00	-100.00	-192.00								
Tricalcium aluminate	30.33			-811.71	-1226.97						
Tetracalcium aluminoferrite	15.00			-583.78	-687.33	-1390.21	-1576.22	-120.83			
calcium sulphate dihydrate	-102.38								-5757.60	-2749.00	
calcium sulphate hemihydrate	-70.00								-5757.60	-3318.8	
calcium sulphate anhydrous	-34.92								-5020.28	-3632.31	
Hydration phases											
ettringite	-183.33			-326.10	-59.49				-2828.80	-926.05	84.27
Calcium monosulphate	-84.78			-597.93	-262.27				-1364.40	-677.00	52.54
C-S-H	-66.67	-33.00	22.00								
Calcium aluminate hydrate	-66.67			-597.931	-298.99						

EDS of the old batch of PC

Element	Average wt%
O	51.22
Na	0.27
Mg	0.69
Al	1.90
Si	6.03
S	1.50
K	0.93
Ca	35.83
Fe	1.63

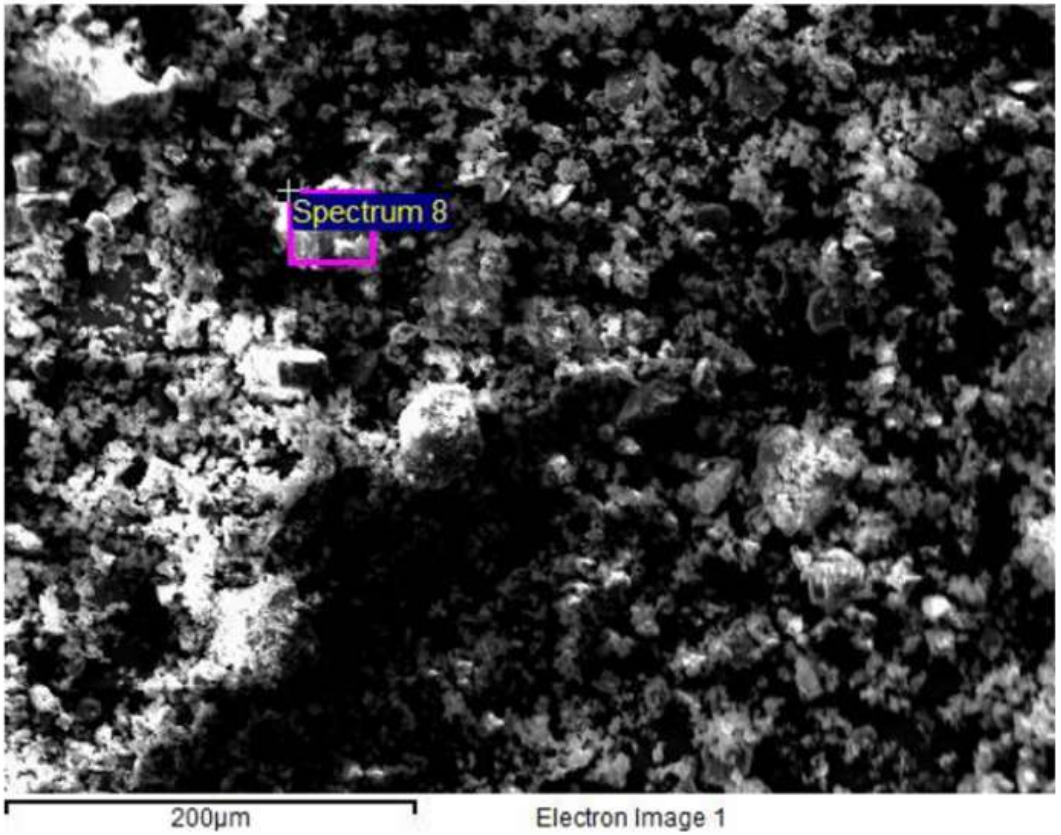

Figure 8.2: SEM image of the old batch powder with corresponding EDS analysis.

Observed ratio for the old batch of PC (wt%)											
	Ca/O	Ca/Si	O/Si	Ca/Al	O/Al	Ca/Fe	O/Fe	Al/Fe	Ca/S	O/S	S/Al
	0.7	5.94	8.49	18.86	26.96	22.12	31.62	1.17	23.89	34.15	0.79
Percentage difference between observed and theoretical ratios											
Clinker phases	Ca/O	Ca/Si	O/Si	Ca/Al	O/Al	Ca/Fe	O/Fe	Al/Fe	Ca/S	O/S	S/Al
Alite	53.33	-38.46	-196.85								
Belite	44.00	-107.69	-270.74								
Tricalcium aluminate	42.62			-749.55	-1414.61						
Tetracalcium aluminoferrite	30.00			-537.16	-798.67	-1446.85	-2111.19	-143.75			
calcium sulphate dihydrate	-66.67								-1811.20	-1038.33	
calcium sulphate hemihydrate	-40.00								-1811.20	-1266.00	
calcium sulphate anhydrous	-11.11								-1570.63	-1391.27	
Hydration phases											
ettringite	-133.33			-297.05	-82.04				-855.60	-309.96	55.62
Calcium monosulphate	-52.17			-550.34	-313.50				-377.80	-210.45	-33.90
C-S-H	-37.25	-38.46	0.93								
Calcium aluminate hydrate	-37.25			-550.34	-355.41						

8.2 Effect of static and dynamic regimes on material properties

8.2.1 Compressive strength

Statistical analysis of data, NS = non significant.

7 days hydration in PBS/FCS	
Groups	**Static vs. Dynamic**
Control	$p < 0.05$
5 % FG	$p < 0.05$
10 % FG (4.0)	$p < 0.05$
10 % FG (4.5)	NS
10 % FG (5.0)	$p < 0.05$

30 days hydration in PBS/FCS	
Groups	**Static vs. Dynamic**
Control	$p < 0.05$
5 % FG	$p < 0.05$
10 % FG (4.0)	$p < 0.05$
10 % FG (4.5)	$p < 0.05$
10 % FG (5.0)	$p < 0.05$

7 days hydration in PBS	
Groups	**Static vs. Dynamic**
Control	NS
5 % FG	$p < 0.05$
10 % FG (4.0)	$p < 0.05$
10 % FG (4.5)	NS
10 % FG (5.0)	$p < 0.05$

30 days hydration in PBS	
Groups	**Static vs. Dynamic**
Control	NS
5 % FG	$p < 0.05$
10 % FG (4.0)	$p < 0.05$
10 % FG (4.5)	$p < 0.05$
10 % FG (5.0)	$p < 0.05$

8.2.2 Relative porosity

7 days hydration in PBS/FCS	
Groups	**Static vs. Dynamic**
Control	NS
5 % FG	NS
10 % FG (4.0)	NS
10 % FG (4.5)	NS
10 % FG (5.0)	$p < 0.05$

30 days hydration in PBS/FCS	
Groups	**Static vs. Dynamic**
Control	NS
5 % FG	$p < 0.05$
10 % FG (4.0)	NS
10 % FG (4.5)	$p < 0.05$
10 % FG (5.0)	$p < 0.05$

7 days hydration in PBS	
Groups	**Static vs. Dynamic**
Control	$p < 0.05$
5 % FG	$p < 0.05$
10 % FG (4.0)	$p < 0.05$
10 % FG (4.5)	$p < 0.05$
10 % FG (5.0)	$p < 0.05$

30 days hydration in PBS	
Groups	**Static vs. Dynamic**
Control	NS
5 % FG	NS
10 % FG (4.0)	$p < 0.05$
10 % FG (4.5)	$p < 0.05$
10 % FG (5.0)	$p < 0.05$

8.3 Effect of hydration media on solubility

8.3.1 PBS vs. PBS/FCS

	Hydration day	PBS vs. PBS/FCS
Control	1-day	$p < 0.05$
	3-day	$p < 0.05$
	5-day	$p < 0.05$
	7-day	$p < 0.05$
	14-day	$p < 0.05$
	30-day	$p < 0.05$

	Hydration day	PBS vs. PBS/FCS
10 % FG (4.0)	1-day	NS
	3-day	NS
	5-day	NS
	7-day	NS
	14-day	$p < 0.05$
	30-day	$p < 0.05$

	Hydration day	PBS vs. PBS/FCS
10 % FG (4.5)	1-day	NS
	3-day	$p < 0.05$
	5-day	NS
	7-day	NS
	14-day	$p < 0.05$
	30-day	$p < 0.05$

	Hydration day	PBS vs. PBS/FCS
10 % FG (5.0)	1-day	NS
	3-day	NS
	5-day	$p < 0.05$
	7-day	NS
	14-day	$p < 0.05$
	30-day	$p < 0.05$

8.3.2 Solubility of samples in PBS

Solubility in PBS- 1-day

	Control	10 % FG (4.0)	10 % FG (4.5)	10 % FG (5.0)
Control		$p < 0.05$	$p < 0.05$	NS
10 % FG (4.0)			NS	$p < 0.05$
10 % FG (4.5)				$p < 0.05$
10 % FG (5.0)				

Solubility in PBS- 3-day

	Control	10 % FG (4.0)	10 % FG (4.5)	10 % FG (5.0)
Control		NS	$P < 0.05$	NS
10 % FG (4.0)			NS	NS
10 % FG (4.5)				NS
10 % FG (5.0)				

Solubility in PBS- 5-day

	Control	10 % FG (4.0)	10 % FG (4.5)	10 % FG (5.0)
Control		NS	NS	NS
10 % FG (4.0)			NS	NS
10 % FG (4.5)				NS
10 % FG (5.0)				

Solubility in PBS- 7-day

	Control	10 % FG (4.0)	10 % FG (4.5)	10 % FG (5.0)
Control		$P < 0.05$	$P < 0.05$	$P < 0.05$
10 % FG (4.0)			NS	NS
10 % FG (4.5)				NS
10 % FG (5.0)				

Solubility in PBS- 14-day

	Control	10 % FG (4.0)	10 % FG (4.5)	10 % FG (5.0)
Control		$P < 0.05$	$P < 0.05$	$P < 0.05$
10 % FG (4.0)			NS	NS
10 % FG (4.5)				NS
10 % FG (5.0)				

Solubility in PBS- 30-day

	Control	10 % FG (4.0)	10 % FG (4.5)	10 % FG (5.0)
Control		$P < 0.05$	$P < 0.05$	NS
10 % FG (4.0)			$P < 0.05$	$P < 0.05$
10 % FG (4.5)				NS
10 % FG (5.0)				

8.3.3 Solubility of samples in PBS/FCS

Solubility in PBS/FCS- 1-day

	Control	10 % FG (4.0)	10 % FG (4.5)	10 % FG (5.0)
Control		P < 0.05	P < 0.05	P < 0.05
10 % FG (4.0)			NS	P < 0.05
10 % FG (4.5)				P < 0.05
10 % FG (5.0)				

Solubility in PBS/FCS- 3-day

	Control	10 % FG (4.0)	10 % FG (4.5)	10 % FG (5.0)
Control		P < 0.05	P < 0.05	P < 0.05
10 % FG (4.0)			NS	NS
10 % FG (4.5)				NS
10 % FG (5.0)				

Solubility in PBS/FCS- 5-day

	Control	10 % FG (4.0)	10 % FG (4.5)	10 % FG (5.0)
Control		P < 0.05	P < 0.05	P < 0.05
10 % FG (4.0)			P < 0.05	P < 0.05
10 % FG (4.5)				P < 0.05
10 % FG (5.0)				

Solubility in PBS/FCS- 7-day

	Control	10 % FG (4.0)	10 % FG (4.5)	10 % FG (5.0)
Control		P < 0.05	P < 0.05	P < 0.05
10 % FG (4.0)			NS	NS
10 % FG (4.5)				NS
10 % FG (5.0)				

Solubility in PBS/FCS- 14-day

	Control	10 % FG (4.0)	10 % FG (4.5)	10 % FG (5.0)
Control		P < 0.05	P < 0.05	P < 0.05
10 % FG (4.0)			NS	NS
10 % FG (4.5)				NS
10 % FG (5.0)				

Solubility in PBS/FCS- 30-day

	Control	10 % FG (4.0)	10 % FG (4.5)	10 % FG (5.0)
Control		P < 0.05	P < 0.05	NS
10 % FG (4.0)			P < 0.05	P < 0.05
10 % FG (4.5)				NS
10 % FG (5.0)				

8.4 SEM analysis of the scraped off deposit

8.4.1 EDS analysis of the outer-surface of samples stored in DW and PBS/FCS

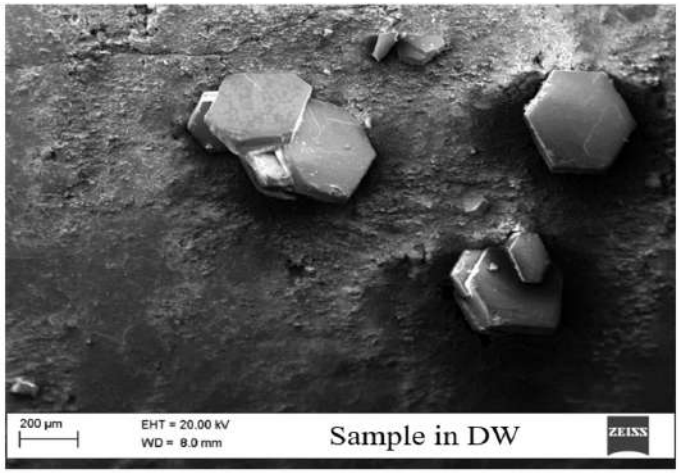

Element	Weight%	Atomic%
C K	5.49	10.72
O K	38.41	56.33
Al K	0.40	0.34
Si K	0.00	0.00
Cl K	0.00	0.00
Ca K	55.71	32.61
Totals	100.00	

Figure 8.3: SEM image of the sample stored in DW with corresponding EDS analysis.

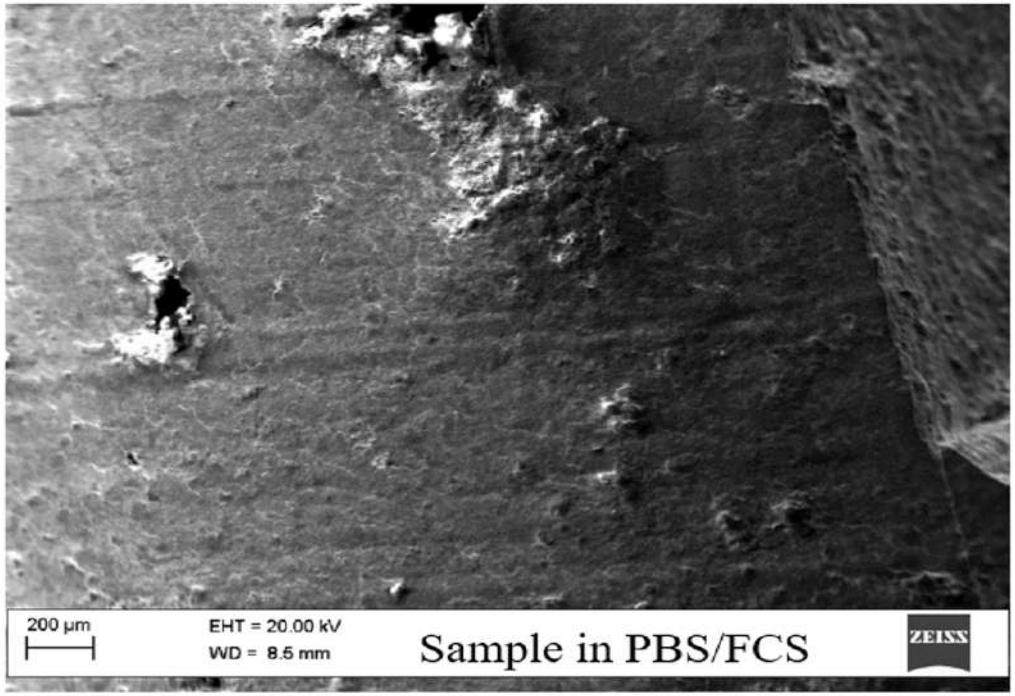

Element	Weight%	Atomic%
C K	11.63	20.03
O K	43.68	56.46
Na K	0.43	0.39
Al K	0.40	0.30
Si K	1.17	0.86
P K	6.73	4.49
Ca K	33.36	17.21
Bi M	2.61	0.26
Totals	100.00	

Figure 8.4: SEM image of the sample stored in PBS/FCS with corresponding EDS analysis.

8.4.2 EDS analysis of scraped off powder in different media

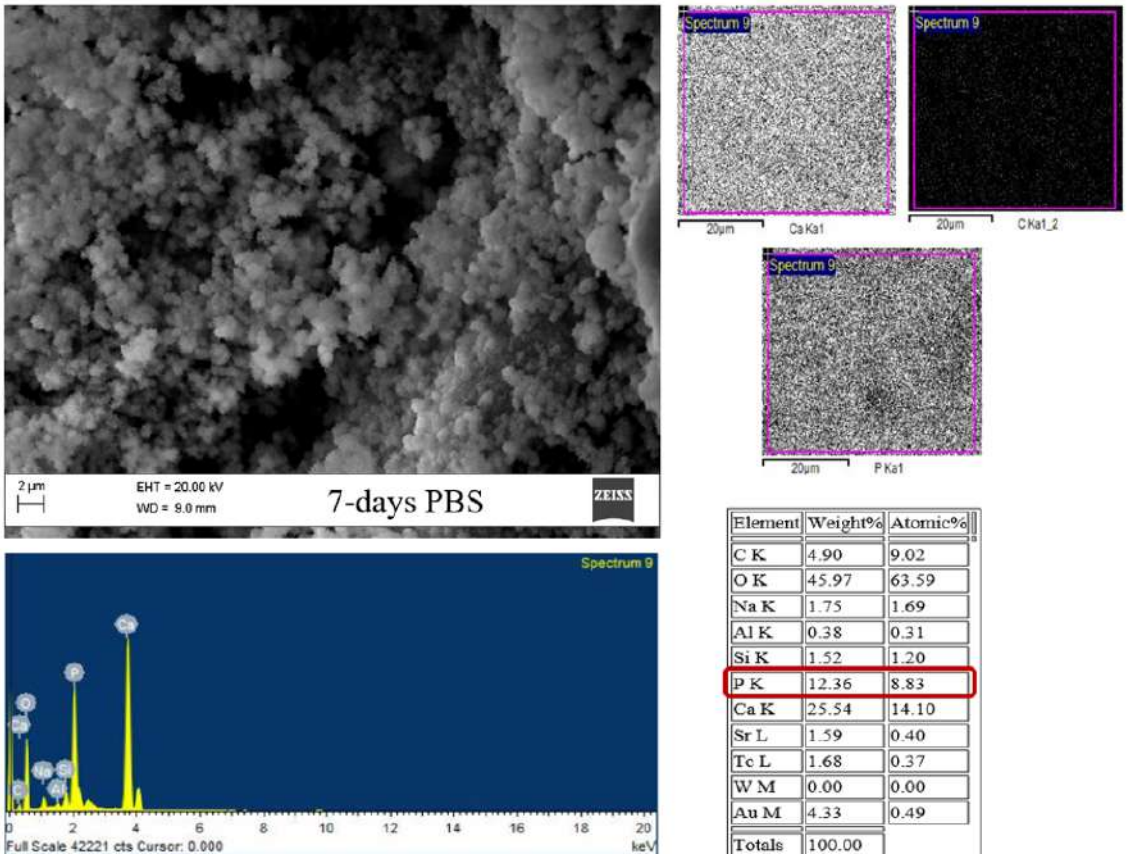

Element	Weight%	Atomic%
C K	4.90	9.02
O K	45.97	63.59
Na K	1.75	1.69
Al K	0.38	0.31
Si K	1.52	1.20
P K	12.36	8.83
Ca K	25.54	14.10
Sr L	1.59	0.40
Tc L	1.68	0.37
W M	0.00	0.00
Au M	4.33	0.49
Totals	100.00	

Figure 8.5: SEM image of the scraped off deposit from the sample stored in PBS for 7 days, followed by the EDS analysis and the elemental mapping of the deposit.

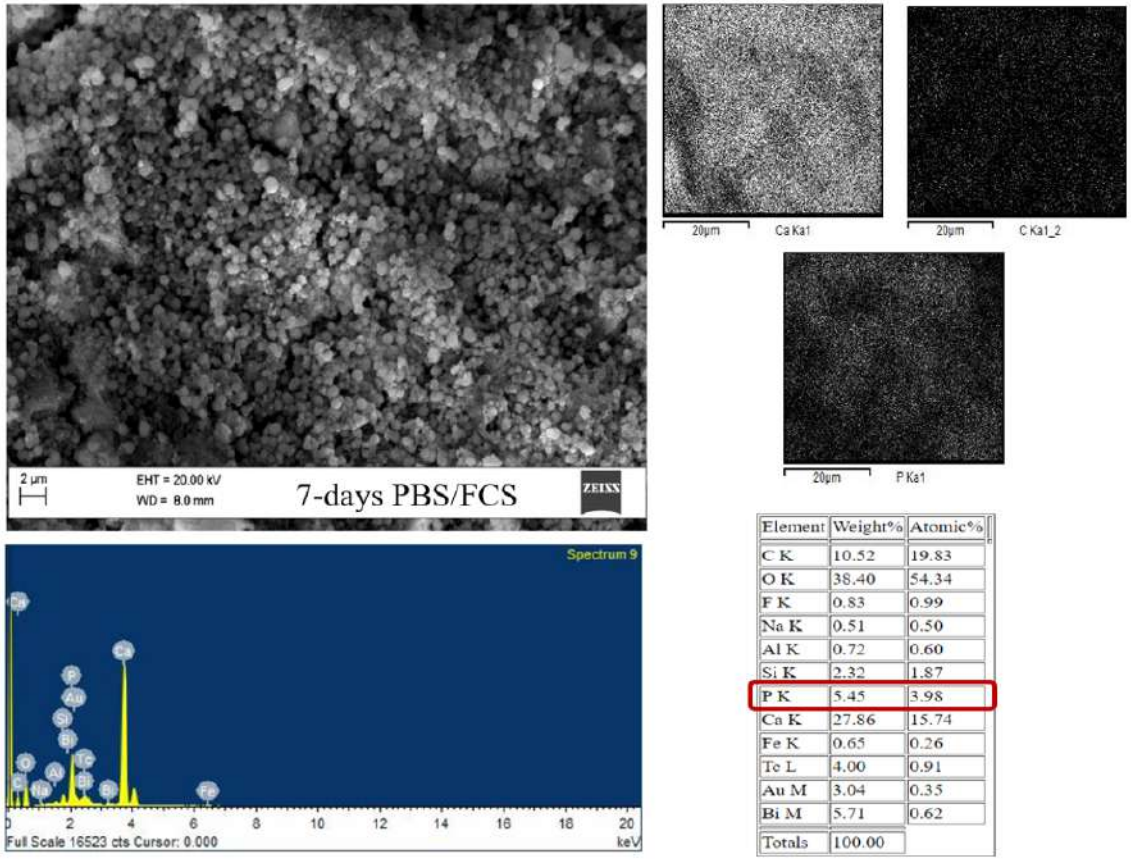

Element	Weight%	Atomic%
C K	10.52	19.83
O K	38.40	54.34
F K	0.83	0.99
Na K	0.51	0.50
Al K	0.72	0.60
Si K	2.32	1.87
P K	5.45	3.98
Ca K	27.86	15.74
Fe K	0.65	0.26
Te L	4.00	0.91
Au M	3.04	0.35
Bi M	5.71	0.62
Totals	100.00	

Figure 8.6: SEM image of the scraped off deposit from the sample stored in PBS/FCS for 7 days, followed by the EDS analysis and the elemental mapping of the deposit.

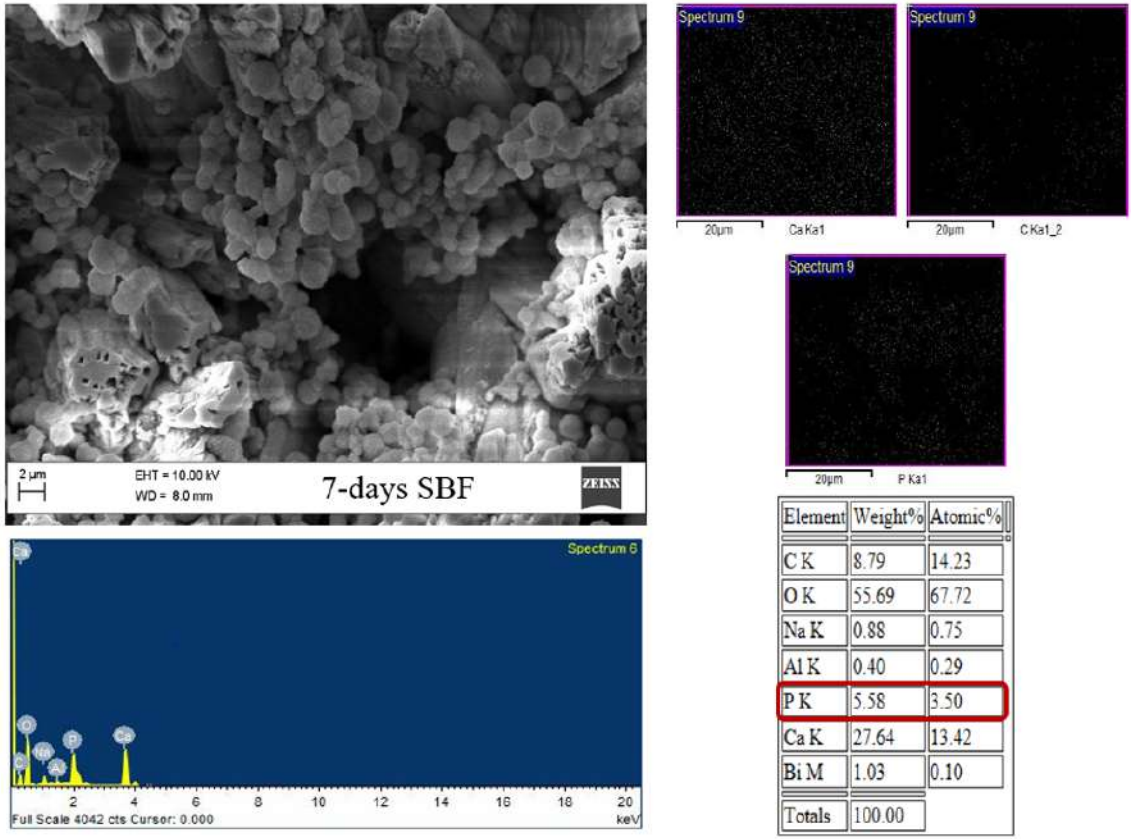

Element	Weight%	Atomic%
C K	8.79	14.23
O K	55.69	67.72
Na K	0.88	0.75
Al K	0.40	0.29
P K	5.58	3.50
Ca K	27.64	13.42
Bi M	1.03	0.10
Totals	100.00	

Figure 8.7: SEM image of the scraped off deposit from the sample stored in SBF for 7 days, followed by the EDS analysis and the elemental mapping of the deposit.

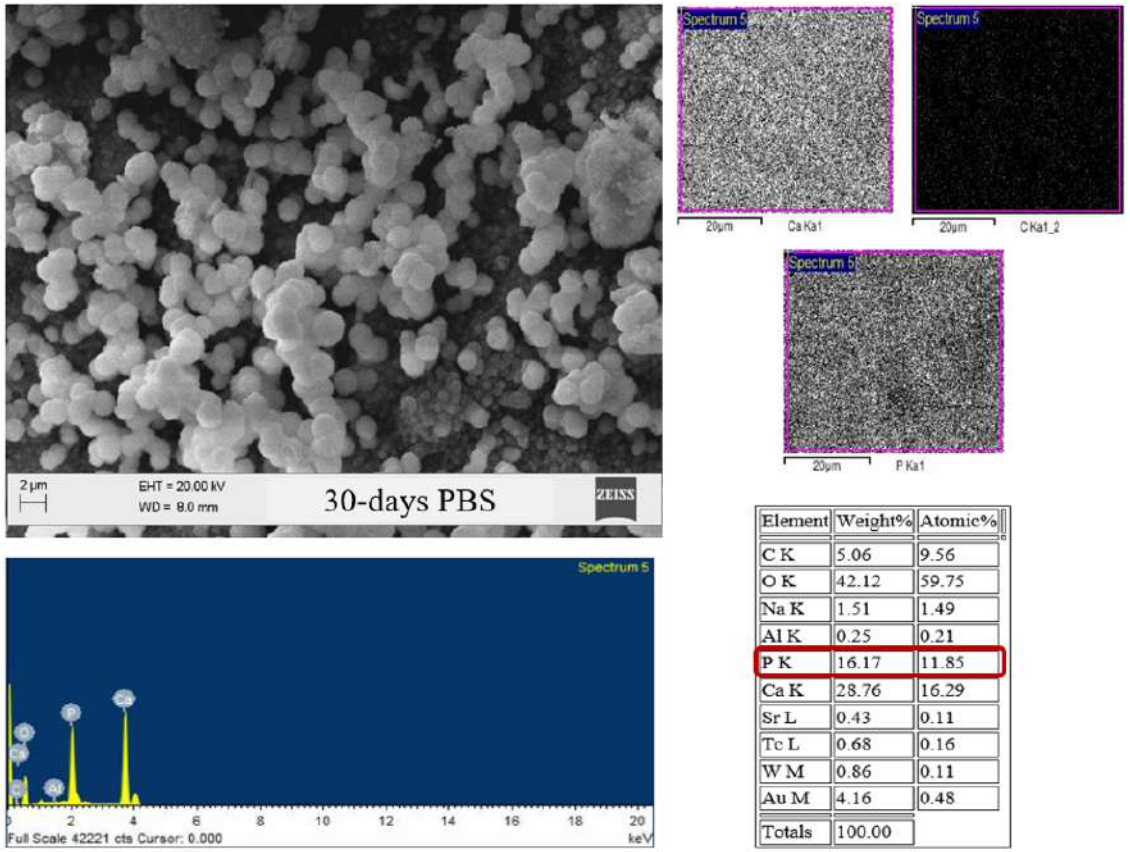

Element	Weight%	Atomic%
C K	5.06	9.56
O K	42.12	59.75
Na K	1.51	1.49
Al K	0.25	0.21
P K	16.17	11.85
Ca K	28.76	16.29
Sr L	0.43	0.11
Tc L	0.68	0.16
W M	0.86	0.11
Au M	4.16	0.48
Totals	100.00	

Figure 8.8: SEM image of the scraped off deposit from the sample stored in PBS for 30 days, followed by the EDS analysis and the elemental mapping of the deposit.

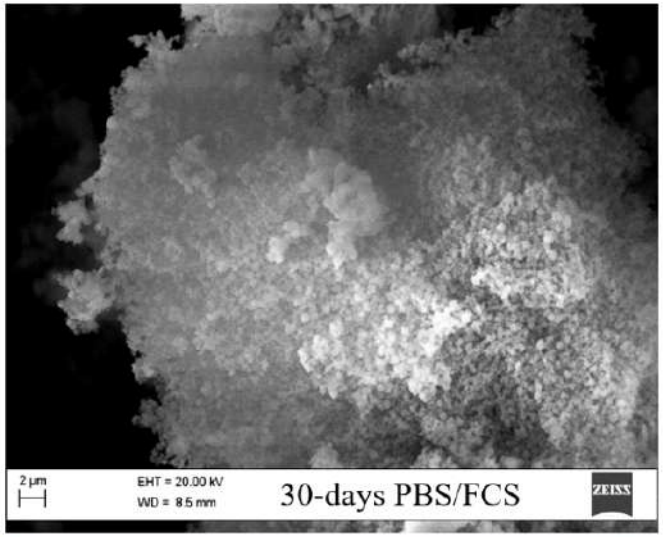

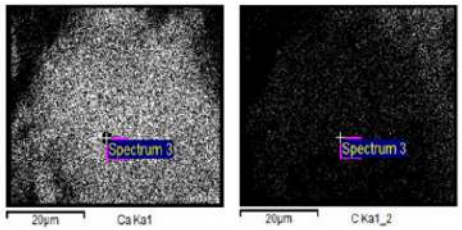

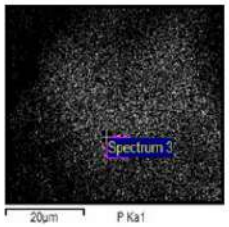

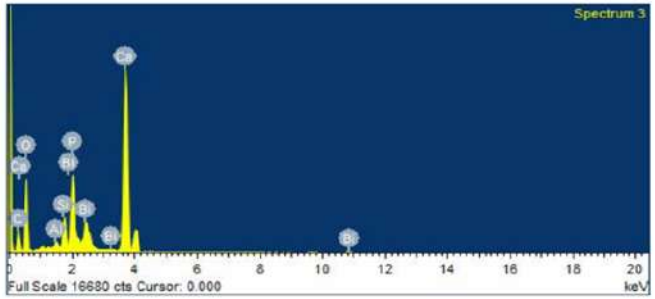

Element	Weight%	Atomic%
C K	11.90	20.56
O K	44.08	57.21
F K	1.45	1.59
Na K	0.38	0.34
Al K	0.42	0.32
Si K	2.28	1.68
P K	6.64	4.45
Ca K	24.82	12.86
Fe K	0.14	0.05
Tc L	1.18	0.25
Au M	1.89	0.20
Bi M	4.81	0.48
Totals	100.00	

Figure 8.9: SEM image of the scraped off deposit from the sample stored in PBS/FCS for 30 days, followed by the EDS analysis and the elemental mapping of the deposit.

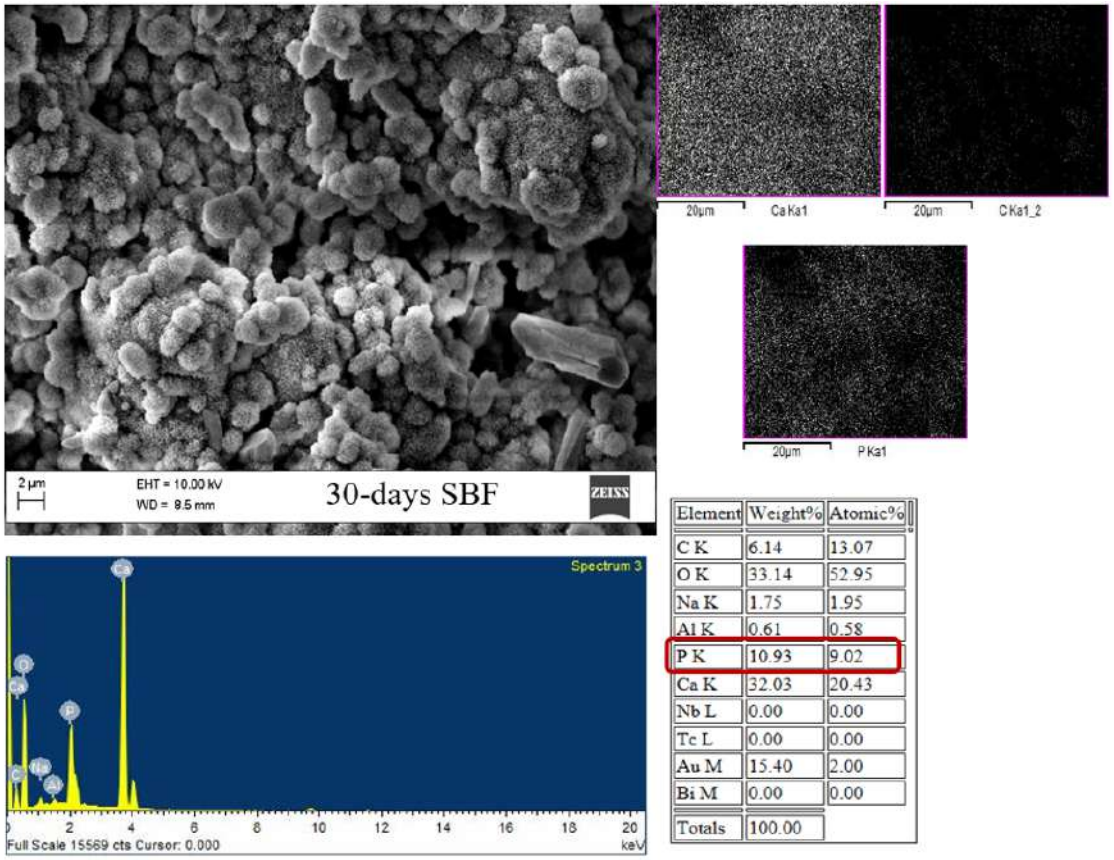

Element	Weight%	Atomic%
C K	6.14	13.07
O K	33.14	52.95
Na K	1.75	1.95
Al K	0.61	0.58
P K	10.93	9.02
Ca K	32.03	20.43
Nb L	0.00	0.00
Tc L	0.00	0.00
Au M	15.40	2.00
Bi M	0.00	0.00
Totals	100.00	

Figure 8.10: SEM image of the scraped off deposit from the sample stored in SBF for 30 days, followed by the EDS analysis and the elemental mapping of the deposit.

Bibliography

[1] Hench LL. Biomaterials. Science. 1980;208(4446):826–831.

[2] Ratner BD, Hoffman AS, Schoen FJ, Lemons JE. Biomaterials science: an introduction to materials in medicine. 3rd ed. xxv-xxviii. Oxford: Academic press; 2013.

[3] Roemhildt ML. Calcium phosphate compatible bone cement: characterization, bonding properties and tissue response [P.h.D Thesis]. Iowa state university; 2002.

[4] Tortora G, Derrickson B. Principles of anatomy and physiology. 13th ed. 182-186. USA: John Wiley & Sons; 2008.

[5] Moetazedian A. Influence of serum proteins and ions on compressive strength, setting time and relative porosity of novel Portland cement in percutaneous vertebroplasty [Thesis]. University of Birmingham; 2016.

[6] Wynn-Jones GD. Development of a Portland cement based for vertebroplasty [P.h.D Thesis]. University of Birmingham; 2013.

[7] McCall T, Cole C, Dailey A. Vertebroplasty and kyphoplasty: A comparative review of efficacy and adverse events. Curr Rev Musculoskelet Med. 2008;1(1):17–23.

[8] Alexandru D, So W. Evaluation and Management of Vertebral Compression Fractures. Perm J. 2012;16(4):46–51.

[9] Deb S. Orthopaedic bone cements. 1st ed. 3-11. Cambridge: Woodhead; 2008.

[10] Lewis G. Injectable bone cements for use in vertebroplasty and kyphoplasty: State-of-the-art review. J Biomed Mater Res B. 2006;76(2):456–468.

[11] Yang L, Gao C, Wei D, Yang H, Chen T. Nanotechnology for treating osteoporotic vertebral fractures. Int J Nanomed. 2015;10:5139–5157.

[12] Camilleri J. Mineral Trioxide Aggregate in Dentistry: from preparation to application. 1st ed. 1-17. Berlin: Springer; 2014.

[13] Wynn-Jones GD, Shelton RM, Hofmann MP. Development of Portland cement for orthopedic applications, establishing injectability and decreasing setting times. J Biomed Mater Res B. 2012;100B(8):2213–221.

[14] Wynn-Jones GD, Shelton RM, Hofmann MP. Injectable citrate-modified Portland cement for use in vertebroplasty. J Biomed Mater Res B. 2014;102B(8):1799–1808.

[15] Netti P. Injectable biomedical foams for bone regeneration. In: Ginebra M, Montufar E, editors. Biomedical foams for tissue engineering applications. Cambridge: Woodhead; 2014. p. 281–312.

[16] Montufar EB, Traykova T, Planell JA, Ginebra MP. Comparison of a low molecular weight and a macromolecular surfactant as foaming agents for injectable self setting hydroxyapatite foams: Polysorbate 80 versus gelatine. Mater Sci Eng C. 2011;31(7):1498–1504.

[17] Boskey AL, Coleman R. Ageing and bone. J Dent Res. 2010;89(12):1333–1348.

[18] Hadjidakis DJ, Androulakis II. Bone remodelling. Ann N Y Acad Sci. 2006;1092:385–396.

[19] Clarke B. Normal bone anatomy and physiology. Clin J Am Soc Nephrol. 2008;3(3):S131–S139.

[20] Mescher AL. Junqueira's basic histology text and atlas. 14th ed. 138-145. Indiana: Mc-Graw-Hill; 2016.

[21] Berkhout J, Stone JA, Verhamme KM, Danhof M, Post TM. Disease systems analysis of bone mineral density and bone turnover markers in response to alendronate, placebo, and washout in postmenopausal women. CPT Pharmacometrics Syst Pharmacol. 2016;5(12):656–664.

[22] Hofmann MP, Mohammed AR, Perrie Y, Gbureck U, Barralet JE. High-strength resorbable brushite bone cement with controlled drug-releasing capabilities. Acta Biomater. 2009;5(1):43–49.

[23] O'Hara R, Buchanan F, Dunne N. Injectable calcium phosphate cements for spinal

bone repair. In: Dubruel P, Van Vlierbergh S, editors. Biomaterials for Bone Regeneration: Novel Techniques and ApplicationS. Cambridge: Woodhead; 2014. p. 26–61.

[24] Francis RM, Baillie SP, Chuck AI, Crook PR, Dunn N, Fordham JN, et al. Acute and long-term management of patients with vertebral fractures. QJM. 2004;97(2):63–74.

[25] Okazaki T, Saito K. Bone scintigraphy for the diagnosis of the responsible level of osteoporotic vertebral compression fractures in percutaneous balloon kyphoplasty. Clin Neurol Neurosurg. 2017;152:23–27.

[26] Colon-Emeric CS, Saag KG. Osteoporotic fractures in older adults. Best Pract Res Clin Rheumatol. 2006;20(4):695–706.

[27] Zhang YL, Shi LT, Tang PF, Sun ZJ, Wang YH. Correlation analysis of osteoporotic vertebral compression fractures and spinal sagittal imbalance. Orthopade. 2017;46:249–255.

[28] Zhang H, Xu C, Zhang T, Gao Z, T Z. Does percutaneous vertebroplasty or balloon kyphoplasty for osteoporotic vertebral compression fractures increase the incidence of new vertebral fractures? A meta-analysis. Pain Physician. 2017;20(1):E13–E28.

[29] Xie L, Zhao ZG, Zhang SJ, Hu YB. Percutaneous vertebroplasty versus conserva-

tive treatment for osteoporotic vertebral compression fractures: An updated meta-analysis of prospective randomized controlled trials. Int J Surg. 2017;47:25–32.

[30] Sambrook P, Cooper C. Osteoporosis. Lancet. 2006;367(9527):2010–2018.

[31] Galibert P, Deramond H, Rosat P, Le-Gars K. Preliminary note on the treatment of vertebral angioma by percutaneous acrylic vertebroplasty. Neurochirurgie. 1987;33(2):166–168.

[32] Kim J, Park K, Yi S, Shin H, Yoon D, Kim K. Real-time CT fluoroscopy (CTF)-guided vertebroplasty in osteoporotic spine fractures. Yonsei Med J. 2005;46(5):635–642.

[33] Chen LH, Hsieh MK, Liao JC, Lai PL, Niu CC, Fu TS, et al. Repeated percutaneous vertebroplasty for refracture of cemented vertebrae. Arch Orthop Trauma Surg. 2010;131(7):927–933.

[34] Taylor RS, Taylor RJ, Fritzell P. Balloon kyphoplasty and vertebroplasty for vertebral compression fractures- a comparative systematic review of efficacy and safety. Spine. 2006;31(23):2747–2755.

[35] Chen YJ, Chen HY, Lo DF, Chen HT, Hsu HC. Kirschner wire-guided technique for inserting a second needle into inadequately filled vertebrae in vertebroplasty: a technical report. Spine J. 2014;14(12):3025–3029.

[36] Verlann JJ, Oner FC, Dhert W. Anterior spinal column augmentation with injectable bone cements. Biomaterials. 2006;27(3):290–301.

[37] Verlaan JJ, Oner FC, Dhert WJ. Anterior spinal column augmentation with injectable bone cements. Biomaterials. 2006;27(3):290–301.

[38] Provenzano MJ, Murphy KP, Riley LH. Bone cements: Review of their physiochemical and biochemical properties in percutaneous vertebroplasty. AmJNeuroradiol. 2004;25(10):1286–1290.

[39] Heini PF, Berlemann U. Bone substitutes in vertebroplasty. Eur Spine J. 2001;10:S205–S213.

[40] International Standard ISO 5833 Implants for surgery Acrylic resin cements. British Standards Institution; 2002.

[41] Bashoor Zadeh M. Geometric characterisation and simulation of cell-mediated resorption for porous bone substitutes using micro computed tomography and advanced fuzzy method [P.h.D thesis]. Universite de Sherbrooke; 2011.

[42] Shridhar P, Chen Y, Khalil R, Cho SK, Tillman B, Kumta PN, et al. A Review of PMMA Bone Cement and Intra-Cardiac Embolism. Materials. 2016;9(821):1–14.

[43] Vaishya R, Chauhan M, Vaish A. Bone cement. J Clin Orthop Trauma. 2013;4(4):157–163.

[44] Deb S. Mechanical properties of bone cements. In: Dunne N, editor. Orthopaedic bone cements. 1st ed. Cambridge: Woodhead; 2008. p. 233–238.

[45] Arora M, Chan EK, Gupta S, Diwan AD. Polymethylmethacrylate bone cements and additives: A review of the literature. World J Orthop. 2013;4(2):67–74.

[46] Lu JX, Huang ZW, Tropiano P. Human biological reactions at the interface between bone tissue and polymethylmethacrylate cement. J Mater Sci Mater Med. 2002;13(8):803–809.

[47] Yang Z, Chen L, Hao Y, Zang Y, Zhao X, Shi L, et al. Synthesis and Characterization of an Injectable and Hydrophilous Expandable Bone Cement Based on Poly(methyl methacrylate). ACS Appl Mater Interface. 2017;9:40846–40856.

[48] Heini PF, Walchli B, Berlemann U. Percutaneous transpedicular vertebroplasty with PMMA: operative technique and early results. Eur Spine J. 2000;9(5):445–450.

[49] Nouda S, Tomita S, Kin A, Kawahara K, Kinoshita M. Adjacent vertebral body fracture following vertebroplasty with polymethylmethacrylate or calcium phosphate cement: biomechanical evaluation of the cadaveric spine. Spine. 2009;34(24):2613–2618.

[50] Gbureck U, Barralet JE, Spatz K, Grover LM, Thull R. Ionic modification of cal-

cium phosphate cement viscosity. Part I: hypodermic injection and strength improvement of apatite cement. Biomaterials. 2003;25(11):2187–2195.

[51] Barralet JE, Grover LM, Gbureck U. Ionic modification of calcium phosphate cement viscosity. Part II: hypodermic injection and strength improvement of brushite cement. Biomaterials. 2003;25(11):2197–2203.

[52] Bohner M. Reactivity of calcium phosphate cements. J Mater Chem. 2007;17(38):3980–3986.

[53] Ginebra MP, Canal C, Espanol M, Pastorino D, Montufar EB. Calcium phosphate cements as drug delivery materials. Adv Drug Deliv Rev. 2012;64(12):1090–1110.

[54] Barrere F, Van Blitterswijk CA, De Groot K. Bone regeneration: molecular and cellular interactions with calcium phosphate ceramics. Int J Nanomedicine. 2006;1(3):317–332.

[55] Ginebra MP, Traykova T, Planell JA. Calcium phosphate cements as bone drug delivery systems: a review. J Control Release. 2006;113(2):102–110.

[56] Le Ferrec M, Mellier C, Boukhechba F, Le Corroller T, Guenoun D, Fayon F, et al. Design and properties of a novel radiopaque injectable apatitic calcium phosphate cement, suitable for image-guided implantation. JBiomedResB. 2017;00B(00):1–10.

[57] Camiller J, Pit Ford TR. Mineral trioxide aggregate: A review of the constituents and biological properties of the material. Int Endod J. 2006;39(10):747–754.

[58] Darvell BW, Wu RCT. MTAan hydraulic silicate cement: review update and setting reaction. Dent Mater. 2011;27(5):407–422.

[59] Taylor H. Cement chemistry. 2nd ed. 1-125. Slough: Thomas Telford; 2004.

[60] Lea FM. The chemistry of cement and concrete. 2nd ed. 6-90. Oxford: Butterworth-Heinemann; 2003.

[61] Altan H, Tosun G. The setting mechanism of mineral trioxide aggregate. J Istanbul Univ Fac Dent. 2016;50(1):65–72.

[62] Dubina E. The phenomenon of cement ageing on moist air: Surface chemistry, mechanisms and effects on admixture performance [P.h.D thesis]. Technischen Universitt Mnchen; 2012.

[63] Aligizaki KK. Pore structure of cement-based materials: Testing, interpretation and requirements. 1st ed. 5-10. New York: CRC Press; 2006.

[64] Cheung J, Jeknavorian A, Robert L, Silva D. Impact of admixtures on the hydration kinetics of Portland cement. Cem Concr Res. 2011;41(12):1289–1309.

[65] Moore AE, Taylor H. Crystal structure of ettringite. Acta Cryst. 1970;26:386–393.

[66] O'Beirne JL. Development and characterisation of a Portland cement-based dental root filling material [P.h.D thesis]. University of Birmingham; 2010.

[67] Torabinejad M, Hong CU, McDonald F, Pitt Ford TR. Physical and chemical properties of a new root-end filling materiaL. J Endod. 1995;21(7):349–353.

[68] Liu W, Chang J. In vitro evaluation of gentamicin release from a bioactive tricalcium silicate bone cement. Mater Sci Eng. 2009;29(8):2486–2492.

[69] Sarkar N, Caicedo R, Ritwik R, Moiseyeva R, Kwashima I. Physiochemical basis of the biological properties of mineral trioxide aggregate,. J Endod. 2005;31(2):97–100.

[70] Rathinam E, Rajasekharan S, Chitturi RT, Martens L, De Coster P. Gene expression profiling and molecular signaling of dental pulp cells in response to tricalcium silicate cements: A systematic review. J Endod. 2015;41(11):1805–1817.

[71] Yaltirik M, Ozbas H, Bilgic B, Issever H. Reactions of connective tissue to mineral trioxide aggregate and amalgam. J endod. 2004;30(2):95–99.

[72] Lee SJ, Monsef M, Torabinejad M. Sealing ability of a mineral trioxide aggregate for repair of lateral root perforations. J Endod. 1993;19(11):541–544.

[73] Mente J, Leo M, Panagidis D, Saure D, Pfefferle T. Treatment outcome of mineral trioxide aggregate: Repair of root perforations-long-term results. J Endod. 2014;40(6):790–796.

[74] Williams DF. On the mechanisms of biocompatibility. Biomaterials. 2008;29(20):2941–2953.

[75] Ding SJ, Kao CT, Chen CL, Shie MY, Huang TH. Evaluation of human osteosarcoma cel line genotoxicity effects of mineral trioxide agregate and calcium silicate cements. J Endod. 2010;36(7):1158–1162.

[76] Huang TH, Ding SJ, Hsu TC, Kao CT. Effect of mineral trioxide aggregate (MTA) extracts on mitogen-activated protein kinase activity in human osteosarcoma cell line (U2OS). Biomaterials. 2003;24(22):3909–3913.

[77] Haglund R, He J, Jarvis J, Safavi KE, Spangberg LS, Zhu Q. Effects of root-end filling materials on fibroblasts and macrophages in vitro. Oral Surg Oral Med Oral Pathol Oral Radiol Endod. 2003;95(6):739–745.

[78] Nakayama A, Ogiso B, Tanabe N, Takeichi O, Matsuzaka K, Inoue T. Behaviour of bone marrow osteoblast-like cells on mineral trioxide aggregate: Morphology and expression of type I collagen and bone-related protein mRNAs. Int Endod J. 2005;38(4):203–210.

[79] Saidon J, He J, Zhu Q, Safavi K, Spangberg LS. Cell and tissue reactions to mineral trioxide aggregate and Portland cement. Oral Surg Oral Med Oral Pathol Oral Radiol Endod. 2003;95(4):483–489.

[80] Camilleri J, Montesin FE, Di Silvio L, Pitt Ford TR. The chemical constitution and biocompatibility of accelerated Portland cement for endodontic use. Int Endod J. 2005;38(11):834–842.

[81] Camilleri J, Monstesin FE, Papaioannou S, McDonald F, Pitt Ford TR. Biocompatibility of two commercial forms of mineral trioxide aggregate. Int Endod J. 2004;37(10):699–704.

[82] Gandolfi M, Taddei P, Tinti A, Prati C. Apatite-forming ability (bioactivity) of ProRoot MTA. Int Endod J. 2010;43(10):917–929.

[83] Holland R, De Souza V, Murata SS, J NM, Bernabe PFE, Otoboni Filho JA, et al. Reaction of rat connective tissue to implanted dentine tube filled with mineral trioxide aggregate, Portland cement or calcium hydroxide. Braz Dent J. 2001;12(1):3–8.

[84] Holland R, De Souza V, Murata SS, J NM, Bernabe PFE, Otoboni Filho JA, et al. Reaction of rat connective tissue to implanted dentine tubes filled with a white mineral trioxide aggregate. Braz Dent J. 2002;13(1):23–26.

[85] Torabinejad M, Chivian N. Clinical applications of mineral trioxide aggregate. J Endod. 1999;25(3):197–205.

[86] Lai PL, Chu IM, Chen LH, Chen WJ. Chemical and physical properties of bone cement for vertebroplasty. Biomed J. 2013;36(4):162–167.

[87] Prati C, Gandolfi MG. Calcium silicate bioactive cements: Biological perspectives and clinical applications. Dent Mater. 2015;31(4):351–370.

[88] Parirokh M, Torabinejad M. Mineral trioxide aggregate: A comprehensive litera-

ture review–part III: clinical applications, drawbacks, and mechanism of action. J Endod. 2010;36(3):400–413.

[89] Kasten P, Beyen I, Niemeyer P, Luginbuhl R, Bohner M, Ritcher W. Porosity and pore size of beta-tricalcium phosphate scaffold can influence protein production and osteogenic differentiation of human mesenchymal stem cells: An in vitro and in vivo study. Acta Biomater. 2008;4(6):1904–1915.

[90] Chang B, Song W, Han T, Yan J, Li F, Zhao L, et al. Influence of pore size of porous titanium fabricated by vacuum diffusion bonding of titanium meshes on cell penetration and bone ingrowth. Acta Biomater. 2016;33:311–321.

[91] Von Doernberg MC, Von Rechenberg B, Bohner M, Grunenfelder S, van Lenthe GH, Muller R. In vivo behavior of calcium phosphate scaffolds with four different pore sizes. Biomaterials. 2006;27(30):5186–5198.

[92] Hing KA. Bone repair in the twenty-first century: biology, chemistry or engineering? Philos Trans A Math Phys Eng Sci. 2004;362(1825):2821–2850.

[93] Kruyt MC, de Bruijn JD, Wilson CE, Oner FC, van Blitterswijk CA, Verbout AJ, et al. Viable osteogenic cells are obligatory for tissue engineered ectopic bone formation in goats. Tissue Eng. 2003;9(2):327–336.

[94] Karageorgiou V, Kaplan D. Porosity of 3D biomaterial scaffolds and osteogenesis. Biomaterials. 2005;26(27):5474–5491.

[95] Roy TD, Simon JL, Ricci JL, Rekow ED, Thompson VP, Parsons JR. Performance of degradable composite bone repair products made via three-dimensional fabrication techniques. J Biomed Mater Res A. 2003;66(2):283–291.

[96] Klenke FM, Liu Y, Yuan H, Hunziker EB, Siebenrock KA, Hofstetter W. Impact of pore size on the vascularization and osseointegration of ceramic bone substitutes in vivo. J Biomed Mater Res A. 2008;85(3):777–786.

[97] Jones AC, H AC, Hutmacher DW, Milthorpe BK, Sheppard AP, Knackstedt MA. The correlation of pore morphology, interconnectivity and physical properties of 3D ceramic scaffolds with bone ingrowth. Biomaterials. 2009;30(7):1440–1451.

[98] Hing KA. Bioceramic bone graft substitutes: Influence of porosity and chemistry. Int J Appl Ceram Tec. 2005;2(3):184–199.

[99] Kuboki Y, Jin Q, Takita H. Geometry of carriers controlling phenotypic expression in BMP-induced osteogenesis and chondrogenesis. J Bone Joint Surg Am. 2001;83-A:105–115.

[100] Gauthier O, Bouler JM, Aguado E, Pilet P, Daculsi G. Macroporous biphasic calcium phosphate ceramics: influence of macropore diameter and macroporosity percentage on bone ingrowth. Biomaterials. 1998;19(1-3):133–139.

[101] Takahashi T, Yamamoto M, Loku K, Goto S. Relationship between compres-

sive strength and pore structure of hardened cement pastes. Adv Cem Res. 1997;9(33):25–30.

[102] Coomaraswamy K, lumley P, M H. Effect of bismuth oxide radioopacifier content on the material properties of an endodontic Portland cement-based (MTA-like) system. J Endod. 2007;33(3):295–298.

[103] Ginebra M, Espanol M, Montufar EB, Perez R, Mestres G. New processing approaches in calcium phosphate cements and their applications in regenerative medicine. Acta Biomater. 2010;6(8):2863–2873.

[104] Cama G, Barberis F, Botter R, Cirillo P, Capurro M, Quarto R, et al. Preparation and properties of macroporous brushite bone cements. Acta Biomater. 2009;5(6):2161–2168.

[105] Markovic M, Takagi S, Chow LC. Formation of macropores in calcium phosphate cement through the use of mannitol crystals. Key Eng Mater. 2001;192-195:773–776.

[106] Takagi S, Chow LC. Formation of macropores in calcium phosphate cement implants. J Mater Sci Mater Med. 2001;12(2):135–139.

[107] Xu HHK, Quinn JB. Calcium phosphate cement containing resorbable fibers for short-term reinforcement and macroporosity. Biomaterials. 2002;23(1):193–202.

[108] Xu HH, Weir MD, Burguera EF, Fraser AM. Injectable and macroporous calcium phosphate cement scaffold. Biomaterials. 2006;27(24):4279–4287.

[109] Xu HHK, Weir MD, Simon CG. Injectable and strong nano-apatite scaffolds for cell/growth factor delivery and bone regeneration. Dent Mater. 2008;24(9):1212–1222.

[110] Link DP, van den Dolder J, van den Beucken JJ, Wolke JG, Mikos AG, Jansen JA. Bone response and mechanical strength of rabbit femoral defects fi lled with injectable CaP cements containing TGF- 1 loaded gelatin microparticles. Biomaterials. 2008;29(6):675–682.

[111] Bohner M. Calcium phosphate emulsions: possible applications. Key Eng Mater. 2001;192-195:765–768.

[112] Bohner M, van Lenthe GH, Grnenfelder S, Hirsiger W, Evison R, Mller R. Synthesis and characterization of porous -tricalcium phosphate blocks. Biomaterials. 2005;26(31):6099–6105.

[113] Charriere E, Lemaitre J, Zysset P. Hydroxyapatite cement scaffolds with controlled macroporosity: Fabrication protocol and mechanical properties. Biomaterials. 2003;24(3):809–817.

[114] Li X, Li D, Lu B, Tang Y, Wang L. Design and fabrication of CAP scaffolds by indirect solid free form fabrication. Rapid Prototyping J. 2005;11(5):312–318.

[115] Del Real RP, Wolke JGC, Vallet-Regi M, Jansen JA. A new method to produce macropores in calcium phosphate cements. Biomaterials. 2002;23(17):3673–3680.

[116] Del Real RP, Ooms E, Wolke JGC, Vallet-reg M, Jansen JA. In vivo bone response to porous calcium phosphate cement. J Biomed Mater Res A. 2003;1(65):30–36.

[117] Almirall A, Larrecq G, Delgado JA, Martinez S, Planell JA, Ginebra MP. Fabrication of low temperature macroporous hydroxyapatite scaffolds by foaming and hydrolysis of an -TCP paste. Biomaterials. 2004;25(17):3671–3680.

[118] Unosson J, Montufar EB, Engqvist H, Ginebra M, Persson C. Brushite foams the effect of Tween® 80 and Pluronic® F-127 on foam porosity and mechanical properties. J Biomed Mater Res B. 2016;104(1):67–77.

[119] Montufar EB, Traykova T, Etienne S, Luigi A, Santin M, Planell JA, et al. Self-hardening calcium deficient hydroxyapatite/gelatine foams for bone regeneration. J Mater Sci Mater Med. 2010;21(3):863–869.

[120] Gbureck U, Hlzel T, Klammert U, Wrzler K, Mller FA, Barralet JE. Resorbable dicalcium phosphate bone substitutes prepared by 3D powder printing. Adv Funct Mater. 2007;17(18):3940–3945.

[121] Gbureck U, Hlzel T, Doillon CJ, Mller FA, Barralet JE. Direct printing of bioceramic implants with spatially localized angiogenic factors. Adv Mater. 2007;19(17):795–800.

[122] Xu HK, Quinn JB, Takagi S, Chow LC, Eichmiller FC. Strong and macroporous calcium phosphate cement: Effects of porosity and fiber reinforcement on mechanical properties. J Biomed Mater Res. 2001;57(3):457–466.

[123] Tang M, Weir MD, Xu HHK. Mannitol-containing macroporous calcium phosphate cement encapsulating human umbilical cord stem cells. J Tissue Eng Regen Med. 2012;6(3):214–224.

[124] Kai D, Li D, Zhu X, Zhang L, H F, Zhang X. Addition of sodium hyaluronate and the effect on the performance of the injectable calcium phosphate cement. J Mater Sci Mater Med. 2009;20(8):1595–1602.

[125] Cimatti B, Engel EE, Nogueira-Barbosa MH, Frighetto PD, Volpon JB. Physical and mechanical characterisation of a porous cement for metaphyseal bone repair. Acta Ortop Bras. 2015;23(4):197–201.

[126] Higuita-Castro N, Gallego-Perez D, Pelaez-Vargas A, Garca Quiroz F, Posada OM, Lopez LE. Reinforced Portland cement porous scaffolds for load-bearing bone tissue engineering applications. 2012. J Biomed Mater Res B;100(2):501–507.

[127] Wang Z, Liu L, Zhou J, Zhou C. Impacts of potassium permanganate (KMnO4) catalyst on properties of hydrogen peroxide (H2O2) foamed porous cement slurry. Constr Build Mater. 2016;111:72–76.

[128] Halliwell B, Clement MV, Long LH. Hydrogen peroxide in the human body. FEBS letters. 2000;486(1):10–13.

[129] Bos MA, van Vliet T. Interfacial rheological properties of adsorbed protein layers and surfactants: A review. Adv Colloid Interf Sci. 2001;91(3):437–471.

[130] Aulton ME. Pharmaceutics. The science of dosage form design. London: Churchill Livingstone; 2002.

[131] Montufar EB, Traykova T, Gil C, Harr I, Almirall A, Aquirre A. Foamed surfactant solution as a template for self-setting injectable hydroxyapatite scaffolds for bone regeneration. Acta Biomater. 2010;6(3):876–885.

[132] Perez RA, Kim HW, Ginebra MP. Polymeric additives to enhance the functional properties of calcium phosphate cements. J Tissue Eng. 2012;3(1):1–20.

[133] Bohner M, Lemaitre J. Can bioactivity be tested in vitro with SBF solution? Biomaterials. 2009;30(12):2175–2179.

[134] Grover LM, Knowles JC, Fleming GJ, Barralet JE. In vitro ageing of brushite calcium phosphate cement. Biomaterials. 2003;24(23):4133–4141.

[135] Gandolfi MG, Siboni F, Polimeni A, Bossu M, Riccitiello F, Rengo S. In vitro screening of the apatite-forming ability, biointeractivity and physical [roperties of a tricalcium silicate material for endodontics and restorative dentistry. Dent J. 2013;1(4):41–60.

[136] Gandolfi MG, Siboni F, Primus CM, Prati C. Ion release, porosity, solubility, and bioactivity of MTA Plus tricalcium silicate. J Endod. 2014;40(10):1632–1637.

[137] Scheidegger AE. General spectral theory for the onset of the instabilities in displacement process in porous media. Pure Appl Geophys. 1960;47(1):41–51.

[138] Vyas N. Imaging dental ultrasonic cavitation and its effects [P.h.D thesis]. University of Birmingham; 2017.

[139] Vyas N, Sammons RL, Addison O, Dehghani H, Walmsley AD. A quantitative method to measure biofilm removal efficiency from complex biomaterial surfaces using SEM and image analysis. Sci Rep. 2016;7(6):1–10.

[140] Rigby SP, Barwick D, Fletcher RS, Riley SN. Interpreting mercury porosimetry data for catalyst supports using semi-empirical alternatives to the Washburn equation. Appl Catal A. 2003;238(2):303–318.

[141] Stutzman PE. Guide for X-ray powder diffracton analysis of Portland cement and clinker. National institute of standards and technology; 1996.

[142] Palin WM, Garry JP, Fleming FJ, Burke T, Marquis PM, Randall RC. The reliability in flexural strength testing of a novel dental composite. J Dent. 2003;31(8):549–557.

[143] Myrdal R. Retarding admixtures for concrete. Concrete innovation centre; 2007.

[144] Cody AM, Leeb RD Hand Codya, Sprya PG. The effects of chemical environment on the nucleation, growth, and stability of ettringite [Ca3Al(OH)6]2(SO4)326H2O. Cem Concr Res. 2004;34(5):869–881.

[145] Rai S, Chaturvedi S, Sing NB. Examination of Portland cement paste hydrated in the presence of malic acid. Cem Concr Res. 2004;34(3):455–462.

[146] Ylemen R, Jaglid U, Panas I. Early hydration and setting of Portland cement monitored by IR, SEM and Vicat techniques. Cem Concr Res. 2009;39(5):433–439.

[147] Habib M, Baroud G, Gitzhofer F, M B. Mechanisms underlying the limited injectability of hydraulic calcium phosphate paste. Acta Biomater. 2008;4(5):1465–1471.

[148] Habib M, Baroud G, Gitzhofer F, Bohner M. Mechanisms underlying the limited injectability of hydraulic calcium phosphate paste. Part II: Particle separation study. Acta Biomater. 2010;6(1):250–256.

[149] Bortoluzzi EA, Broon NJ, Bramante CM, Felippe WT, Tanomaru Filho M, Esberard RM. The influence of calcium chloride on the setting time, solubility, disintegration, and pH of mineral trioxide aggregate and white Portland cement with a radiopacifier. J Endod. 2009;35(4):550–554.

[150] Stepkowska ET, Blanes JM, Franco F, Real C, Perez-Rodriguez JL. Phase transfor-

mation on heating of an aged cement paste. Thermocim Acta. 2004;420(1-2):79–87.

[151] Stepkowska ET, Blanes JM, Real C, Perez-Rodriguez JL. Hydration products in two aged cement pastes. J Therm Anal Calorim. 2005;82(3):731–739.

[152] Camilleri J. Characterization and chemical activity of Portland cement and two experimental cements with potential for use in dentistry. Int Endod J. 2008;41(9):791–799.

[153] Shimogoryo R, Eguro T, Kimura E, Maruta M, Matsuya S, Ishikawa K. Effects of added mannitol on the setting reaction and mechanical strength of apatite cement. Dent Mater J. 2009;28(5):627–633.

[154] Juenger MCG, Jennings HM. New insights into the effects of sugar on the hydration and microstructure of cement pastes. Cem Concr Res. 2002;32(3):393–399.

[155] Mitchell LD, Prica M, Birchall JD. Aspects of Portland cement hydration studied using atomic force microscopy. J Mater Sci. 1996;31(16):4207–4212.

[156] Thomas NL, Birchall JD. The retarding action of sugars on cement hydration. Cem Concr Res. 1983;13:830–842.

[157] Kleinlogel A. Influence on concrete. 222-223. New York: Frederick Ungar Publishing; 1950.

[158] Bruere GM. Set-retarding effects of sugars in portland cement pastes. Nature. 1966;212(5061):502–503.

[159] Young JF. A review of the mechanisms of set-retardation in portland cement pastes containing organic admixtures. Cem Concr Res. 1972;2(4):415–433.

[160] Ramachandran VS, Feldman RF, Beaudoin JJ. Concrete science. London: Heyden; 1981.

[161] Reddy VV, Rao HS, Jayaveera KN. Influence of strong alkaline substances (sodium carbonate and sodium bicarbonate) in mixing water on strength and setting properties of concrete. Indian J Eng Mater Sci. 2006;13(2):123–128.

[162] Pham ST. Modifications on microporosity and physical properties of cement mortar caused by carbonation: Comparison of experimental methods. Adv Mater Sci Eng. 2013;2013.

[163] Lou FJ, He L, Pan Z, Duan WH, Zhao XL, Collins F. Effect of very fine particles on workability and strength of concrete made dune sand. Constr Build Mater. 2013;47:131–137.

[164] Nazari A, Riahi S, Riahi S, Shamekhi SF, Khademno A. An investigation on the strength and workability of cement based concrete performance by using ZrO2 nanoparticles. J Am Sci. 2010;6(4):29–33.

[165] Komatsu R, Makida K, Tsukamoto K. In-situ observation of ettringite crystals. J Cryst Growth. 2009;311(3):1005–1008.

[166] Luke K, Luke G. Effect of sucrose on retardation of Portland cement. Adv Cem Res. 2000;12(1):9–18.

[167] Cody RD, Cody AM, Spry PG, Lee H. Reduction of concrete deterioration by ettringite using crystal growth inhibition technique [Report]; 2001.

[168] Sain-Jalmes A, Peugeot ML, Ferraz H, Langevin D. Differences between protein and surfactant foams: Microscopic properties, stability and coarsening. Colloids Surf A Physicochem Eng Asp. 2005;263(1):219–225.

[169] Negim E, Kozhamzharovia L, J K, Bekbayeva L, C W. Effects of surfactants on the properties of mortar containing styrene/methacrylate superplasticiser. Sci World J. 2014;2014:1–11.

[170] Merlin F, Guitouni H, Mouhoubi H, Mariot S, Vallee F, Van Damme H. Adsorption and heterocoagulation of nonionic surfactants and latex particles on cement hydrates. J Colloid Interface Sci. 2005;281(1):1–10.

[171] Aggarwal LK, Thapliyal PC, Karade SR. Properties of polymer-modified mortars using epoxy and acrylic emulsions. Constr Build Mater. 2007;21(2):379–383.

[172] Ohama Y. Handbook of polymer-modified concrete and mortars. USA: Elsevier; 1995.

[173] Bohner M, Baroud G, Bernstein A, Dobelin N, Galea L, Hesse B. Characterization and distribution of mechanically competent mineralized tissue in micropores of beta-tricalcium phosphate bone substitutes. Mater Today. 2017;20(3):106–115.

[174] Perut F, Montufar EB, Ciapetti G, Santin M, Salvage J, Traykova T, et al. Novel soybean/gelatine-based bioactive and injectable hydroxyapatite foam: Material properties and cell response. Acta Biomater. 2011;7(4):1780–1787.

[175] Sheikh Z, Zhang YL, Grover L, Merle GE, Tamimi F, Barralet J. In vitro degradation and in vivo resorption of dicalcium phosphate cement based grafts. Acta Biomater. 2015;26:338–346.

[176] Celik IB. The effects of particle size distribution and surface area upon cement strength development. Powder Technol. 2009;188(3):272–276.

[177] Erdogdu K, Turker P. Effects of fly ash particle size on strength Portland cement fly ash mortars. Cem Concr Res. 1998;28(9):1217–1222.

[178] Mehdipoor I, Khayat KH. Effect of particle-size distribution and specific surface area of different binder systems on packing density and flow characteristics of cement paste. Cem Concr Compos. 2017;78:120–131.

[179] Bentz DP, Garboczi EJ, Haecker CJ, Jensen OM. Effect of cement particle size distribution on performance properties of Portland cement-based materials. Cem Concr Res. 1999;29(10):1663–1671.

[180] Tingey M, Bush P, Levine MS. Analysis of mineral trioxide aggregate surface when set in the presence of fetal bovine serum. J Endod. 2008;34(1):45–49.

[181] Nekoofar MH, Stone DF, Dummer PM. The effect of blood contamination on the compressive strength and surface microstructure of mineral trioxide aggregate. Int Endod J. 2010;43(9):782–791.

[182] Chauhan S, Hofmann M, Shelton R. Effect of protein addition on the setting behaviour of a calcium phosphate cement. Key Eng Mat. 2006;309-311:841–844.

[183] Mouzakis D, Zaoutsos SP, Bouropoulos N, Rokidi S, Papanicolaou G. Influence of artificially-induced porosity on the compressive strength of calcium phosphate bone cements. J Biomater Appl. 2016;31(1):112–120.

[184] Mehrban N, Bowen J, Vorndran E, Gbureck U, Grover LM. Structural changes to resorbable calcium phosphate bioceramic aged in vitro. Colloids Surf B Interfaces. 2013;111:469–478.

[185] Grover LM, Gbureck U, Wright AJ, Tremayne M, Barralet JE. Biologically mediated resorption of brushite cement in vitro. Biomaterials. 2006;27(10):2178–2185.

[186] Roohani-Esfahani SI, Newman P, Zreiqat H. Design and fabrication of 3D printed scaffolds with a mechanical strength comparable to cortical bone to repair large bone defects. Sci Rep. 2016;6(19468):1–8.

[187] Barralet JE, Grover T L nad Gaunt, Wright AJ, Gibson IR. Preparation of

macroporous calcium phosphate cement tissue engineering scaffold. Biomaterials. 2002;23(15):3063–3072.

[188] Seuba J, Deville S, Guizard C, Stevenson AJ. The effect of wall thickness distribution on mechanical reliability and strength in unidirectional porous ceramics. Sci Technol Adv Mater. 2016;17(1):128–135.

[189] Yamamoto S, Han L, Okiji T. Evaluation of the Ca ion release, pH and surface apatite formation of a prototype tricalcium silicate cement. Int Endod J. 2017;2:e73–e82.

[190] Kokubo T, Takadama H. How useful is SBF in predicting in vivo bone bioactivity? Biomaterials. 2006;27(15):2907–2915.

[191] Walsh WR, Morberg P, Yu Y, Yang JL, Haggard W, Sheath PC, et al. Response of a calcium sulfate bone graft substitute in a confined cancellous defect. Clin Orthop. 2003;406:228–236.

[192] Theiss F, Apelt D, Brand B, Kutter A, Zlinszky K, Bohner M, et al. Biocompatibility and resorption of a brushite calcium phosphate cement. Biomaterials. 2005;26(21):4383–4394.

[193] Apelt D, Theiss F, El-Warrak AO, Zlinszky K, Bettschart-Wolfisberger R, Bohner M, et al. In vivo behavior of three different injectable hydraulic calcium phosphate cements. Biomaterials. 2004;25(7-8):1439–1451.

[194] Ohura K, Bohner M, Hardouin P, Lemaitre J, Pasquier G, Flautre B. Resorption of, and bone formation from, new beta-tricalcium phosphate-monocalcium phosphate cements: an in vivo study. J Biomed Mater Res. 1996;30(2):193–200.

[195] Tamimi F, Sheikh Z, Barralet JE. Dicalcium phosphate cements: Brushite and monetite. Acta Biomater. 2012;8(2):474–487.

[196] Maria SM, Prukner C, Sheikh Z, Mueller F, Barralet JE, Komarova SV. Reproducible quantification of osteoclastic activity: Characterisation of a biomimetic calcium phosphate assay. J Biomed Mater Res B Appl Biomater. 2014;102(5):903–9012.

[197] Janotka I. Hydration of the cement paste with Na2CO3 addition. Ceram Silik. 2001;45(1):16–23.

[198] Gbureck U, Probst J, Thull R. Surface properties of calcium phosphate particles for self setting bone cements. Biomol Eng. 2002;19(2-6):51–55.

[199] Yang JM. Polymerisation of acrylic bone cement using differential scanning calorimetry. Biomaterials. 1997;18(19):1293–1298.

[200] Maffezzoli A. Polymerisation kinetics of acrylic bone cements by differential scanning calorimetry. J Therm Anal. 1996;47(1):35–49.

[201] Du Plessis A, Olawuyi BJ, Boshoff WP, Le Roux SG. Simple and fast porosity

analysis of concrete using X-ray computed tomography. Mater Struct. 2014;49(1-2):553–562.

[202] Cox BD. Assessment of a three-dimensional measurement technique for porosity evaluation of PMMA bone cement. J Mater Sci Mater Med. 2006;17(6):553–557.